Ion Flux Regulates Inflammasome Signaling

by

Jordan Robin Yaron

A Dissertation Presented in Partial Fulfillment
of the Requirements for the Degree
Doctor of Philosophy

Approved April 2015 by the
Graduate Supervisory Committee:

Deirdre R. Meldrum, Chair
Joseph N. Blattman
Honor L. Glenn

ARIZONA STATE UNIVERSITY

May 2015

ABSTRACT

The NLR family, pyrin domain-containing 3 (NLRP3) inflammasome is essential for the innate immune response to danger signals. Importantly, the NLRP3 inflammasome responds to structurally and functionally dissimilar stimuli. It is currently unknown how the NLRP3 inflammasome responds to such diverse triggers. This dissertation investigates the role of ion flux in regulating the NLRP3 inflammasome. Project 1 explores the relationship between potassium efflux and Syk tyrosine kinase. The results reveal that Syk activity is upstream of mitochondrial oxidative signaling and is crucial for inflammasome assembly, pro-inflammatory cytokine processing, and caspase-1-dependent pyroptotic cell death. Dynamic potassium imaging and molecular analysis revealed that Syk is downstream of, and regulated by, potassium efflux. Project 1 reveals the first identified intermediate regulator of inflammasome activity regulated by potassium efflux. Project 2 focuses on $P2X_7$ purinergic receptor-dependent ion flux in regulating the inflammasome. Dynamic potassium imaging revealed an ATP dose-dependent efflux of potassium driven by $P2X_7$. Surprisingly, ATP induced mitochondrial potassium mobilization, suggesting a mitochondrial detection of purinergic ion flux. ATP-induced potassium and calcium flux was found to regulate mitochondrial oxidative signaling upstream of inflammasome assembly. First-ever multiplexed imaging of potassium and calcium dynamics revealed that potassium efflux is necessary for calcium influx. These results suggest that ATP-induced potassium efflux regulates the inflammasome by calcium influx-dependent mitochondrial oxidative signaling. Project 2 defines a coordinated cation flux dependent on the efflux of potassium and upstream of mitochondrial oxidative signaling in inflammasome regulation. Lastly, this dissertation contributes two methods that will be useful for investigating inflammasome biology: an optimized pipeline for single cell transcriptional analysis, and a mouse macrophage cell line expressing a genetically encoded intracellular ATP sensor. This dissertation contributes to understanding the fundamental role of ion flux in regulation of the NLRP3 inflammasome and identifies potassium flux and Syk as potential targets to modulate inflammation.

DEDICATION

To Val, your love and affection have provided me an endless source of encouragement

and

In loving memory of my Bobie, Blanche Robin,
who instilled in me the greatest respect for the pursuit of knowledge

ACKNOWLEDGEMENTS

I would first like to acknowledge my dissertation committee, Dr. Deirdre R. Meldrum, Dr. Joseph N. Blattman and Dr. Honor L. Glenn, for their support and guidance. I would like to give a special thanks to Dr. Glenn for her (apparent) willingness to be a constant sounding board for my often-manic ramblings as I talk myself through experimental conclusions.

I am very lucky to have had the resources of the Center for Biosignatures Discovery Automation (CBDA) available to me during my dissertation work. Dr. Meldrum's strong leadership of, and vision for, CBDA made my interest in studying inflammasome biology a possibility. Also, the ceaseless efforts of Christine Willett, Carol Glaub and Jeffrey Robinson away from the bench kept CBDA running smoothly and made my life much easier than it might have been.

I want to acknowledge the two excellent undergraduate students whom I've had the pleasure of mentoring, Colleen Ziegler and Mounica Rao. They both have the excellent attitudes and skilled bench hands that exemplify the sort of scientist I always hope to work with.

During the course of my dissertation work I had the great honor of working and studying alongside Dr. Kevin Timms, Dr. Bo Wang, Dr. Jia Zeng, Dr. Saeed Merza, Dr. Vivek Nandakumar, Taraka Sai Pavan Grandhi, Brian Johnson, Rey Allen, Jakrey Myers, Jesse Clayton, Fred Lee and Kristen Lee. I also gained immeasurable insight from working with Dr. Yanqing Tian, Dr. Fengyu Su, Dr. Liqiang Zhang, Dr. Xiangxing Kong, Dr. Roger Johnson, Dr. Kimberley Bussey, Dr. Thai Tran, Dr. Dmitry Derkach, Dr. Weimin Gao, Dr. Laimonas Kelbauskas, Dr. Joseph Chao, Dr. Andrew Hatch, Dr. Shashanka Ashili, Dr. Andrey Loskutov, Sandhya Gangaraju, Nanna Hansen, Juan Vela and the rest of my CBDA and Biological Design PhD family. I consider each of these talented scientists and engineers not only colleagues and mentors, but also good friends.

I am fortunate to have started my research career working with Dr. Cody Youngbull. His fascination with the hidden world around us sparked an intellectual fire within me that I hope will never die.

My early studies on inflammasome biology were helped greatly by the advice and guidance of Dr. Brad Cookson and Dr. Wendy Loomis at the University of Washington. Their friendship and mentorship are priceless assets.

I could not have succeeded without the support of the administration of the Biological Design Graduate Program: Dr. Stephen Johnston, Dr. JoAnn Williams, Dr. Anthony Garcia, Maria Hanlin and Laura Hawes.

In my almost 10 years at Arizona State University I have had many amazing professors and instructors, but I would like to give special acknowledgement to Dr. Marco Mangone, Dr. Robby Roberson, Dr. Doug Chandler, Dr. Thomas Martin, Dr. Page Baluch and David Lowry.

I had the unbelievable luck of also working alongside Valerie Harris, whom I fell in love with the moment she interrupted my confocal microscopy experiment during a lab tour. Our relationship is, and will remain, my greatest discovery.

Lastly, I want to thank my family for their support and encouragement.

TABLE OF CONTENTS

Page

CHAPTER Page

LIST OF FIGURES

Figure Page

LIST OF TABLES

CHAPTER 1: INTRODUCTION

The innate immune system protects the host against acute insult by rapidly responding to external and internal danger signals. To do this, professional immune cells detect signatures of danger and engage an amplifying inflammatory cascade, resulting in an infiltration of additional immune cells to the site of damage or infection. Aulus Cornelius Celsus first defined the clinical manifestations of the inflammatory response in his 1st century AD treatise *De Medicina* as the four cardinal signs of inflammation: *calor* (heat), *rubor* (redness), *tumor* (swelling) and *dolor* (pain) (Medzhitov 2010). These signs were modified almost two millennia later by Rudolph Virchow in late 1858 to include *functio laesa* (loss of function) (Medzhitov 2010). It wasn't until the late 1940s when the mechanism of the inflammatory response to infection started to garner attention that refinement of the definition of inflammation began (Dinarello 1984). The symptoms of inflammation were originally, and controversially, attributed to putative factors produced during the acute phase of infection such as endogenous pyrogen and lymphocyte activating factor (Dinarello 1984). This was more generally classified as interleukin-1 (IL-1) later, and was thought to possibly consist of multiple soluble factors (Dinarello 1984). IL-1 as a specific, master pro-inflammatory cytokine was not molecularly identified as the cause of these effects until 1984 and the subsequently purified interleukin-1β (IL-1β) has since been implicated as the molecular driver in an expanding category of infectious and sterile pathologies (Auron et al. 1984; Dinarello 1984; March et al. 1985).

This chapter describes the history, structure and function of inflammasomes, and the cellular machinery responsible for translating the detection of sterile and pathogenic stimuli into pro-inflammatory IL-1 signaling. Also described is the current understanding of how inflammasomes are regulated, as it is still unknown how the same pathway can detect the massive and diverse array of stimuli associated with IL-1 signaling. Further, the phenotypic outcomes of inflammasome activation is described, including the cell fate decisions of orchestrating cells as well as the cells receiving the end-point signals. The discussion of phenotypes associated with IL-1 signaling is continued by describing the clinical relevance to the host, including both stimulus-associated activation and genetic dysregulation of the

inflammasome. The chapter concludes with a description of open questions in inflammasome biology investigated during the course of this dissertation work and the specific contributions of this work.

1.1. DISCOVERY OF THE INFLAMMASOMES

Macrophages are central to engaging the pro-inflammatory response of the innate immune system. Macrophages are bone marrow-derived professional phagocytes that engulf and digest pathogens, particles and debris from the tissues in which they reside. Functionally, macrophages contribute to host survival in two ways: (1) enabling pathogen clearance by promoting inflammation and (2) mediating tissue repair by suppressing inflammation. Classically activated, or M1 macrophages are polarized by exposure to cytokines such as interferon gamma (IFNγ), tumor necrosis factor (TNF) or bacterial components such as lipopolysaccharide (LPS) (Mosser and Edwards 2008). M1 macrophages promote inflammation by the production and release of cytokines such as IL-1β, IL-12 and TNF as well as reactive oxygen (ROS) and nitrogen (RNS) species (Mosser and Edwards 2008). Alternatively activated, or M2, macrophages are polarized by exposure to IL-4, IL-10, IL-13 and TGFβ (Mosser and Edwards 2008). M2 macrophages are anti-inflammatory and promote tissue growth, extracellular matrix repair and angiogenesis by production and release of IL-4, IL-10, transforming growth factor beta (TGFβ), vascular endothelial growth factor (VEGF) and matrix metallopeptidase 9 (MMP9) (Mosser and Edwards 2008).

Essential to mounting an appropriate response to potentially dangerous stimuli is the ability for classically activated macrophages to integrate diverse signals into a generalized inflammatory response. The method that macrophages canonically engage to unify these diverse signals is the assembly and activation of the inflammasome, a multi-protein caspase-1-activating platform that results in, among other pro-inflammatory molecules, the maturation and release of IL-1β.

The processing and release of IL-1β under various chronic and acute pathological conditions has been a topic of intense investigation since its molecular identification in 1984.

Early work identified the lack of a secretion signal sequence in IL-1β, raising questions about the peculiarity of its processing pathway (March et al. 1985). Subsequently, it was found that the processing of immature IL-1β to bioactive IL-1β was due to the activity of a uniquely specific protease, though the identity of the protease remained unknown (Black, Kronheim, and Sleath 1989; Kostura et al. 1989). In 1992, the purification and cloning of the protease responsible for IL-1β maturation was achieved and the protease identified was called the interleukin-1β-converting enzyme (ICE) (Cerretti et al. 1992; Thornberry et al. 1992). While early work demonstrated the need for perturbation of cellular homeostasis by treatment with external stimuli such as ATP or the pore-forming toxin nigericin, the mechanism by which ICE was activated remained unknown (Hogquist et al. 1991; Perregaux and Gabel 1994). Later, when ICE and related aspartic acid-targeting cysteine proteases were renamed “caspase” to reflect their homologous structure and function, the interleukin-1β-converting enzyme became known as caspase-1 (Alnemri et al. 1996).

Apoptosis, a form of benign cell death, has been an intensely researched cellular phenomena since its discovery in 1972 and has important roles in development, tissue maintenance and cancer (Kerr, Wyllie, and Currie 1972). Interestingly, research on apoptosis was influenced by the attention directed towards IL-1 biology in the late 1980s and early 1990s when the identity of the cleavage site for the key apoptotic enzyme, caspase-3 (then called apopain or CPP32), was discovered while searching for additional intracellular substrates for caspase-1 cleavage (Nicholson et al. 1995). This seminal finding underscores the close relationship between apoptosis and caspase-1/IL-1 research. This exchange of ideas between apoptosis and IL-1 research occurred again after the discovery of the apoptosis activating factor (APAF)-1 apoptosome, a caspase-9-activating multi-protein platform critical for intrinsic caspase-3-dependent apoptosis (P. Li et al. 1997; Zou et al. 1999).

The molecular characterization of the apoptosome proved crucial for informing the discovery of a caspase-1-activating, and consequently IL-1β-processing, platform. The APAF-1 apoptosome coordinates the concentrated localization of pro-caspase-9 via homotypic interactions in the APAF-1 and pro-caspase-9 caspase recruitment domains (CARD) thereby

mediating autoproteolytic cleavage of the caspase-9 pro-domain and resulting in activation of bioactive caspase-9 (Hofmann, Bucher, and Tschopp 1997; P. Li et al. 1997; Zou et al. 1999). Active caspase-9 then mediates the downstream activation of caspase-3 and the ultimate completion of apoptosis (Zou et al. 1999).

Around the same time as the discovery of the APAF-1 apoptosome there was an abundance of novel proteins and protein domains identified in mammals and plants with putative relationships to both apoptosis and inflammation. Essential among these discoveries are the pyrin (PYD) and caspase recruitment (CARD) domains, the adapter protein apoptosis-associated speck-like protein containing a CARD domain (ASC, also called PYCARD as it contains both PYD and CARD domains), the NACHT nucleotide binding domain (NBD), and a number of members of the nucleotide oligomerization domain (NOD)-like family of receptors (Hofmann, Bucher, and Tschopp 1997; Masumoto et al. 1999; Bertin and DiStefano 2000; Koonin and Aravind 2000; Z.L. Chu et al. 2001; Hlaing et al. 2001).

In a landmark 2002 paper, the lab of Jurg Tschopp described the assembly of a multi-protein complex for caspase-1 activation and IL-1β processing that they termed the inflammasome, which shares remarkable similarities to the assembly mechanism for the APAF-1 apoptosome (Martinon, Burns, and Tschopp 2002). In a series of cell-free and cell-based experiments, they identified the overall structure of the NLRP1 inflammasome as (1) a central, sensor protein (in their case the protein NALP1; now called NLRP1), (2) the adapter protein ASC or a CARD domain on the sensor protein itself, and (3) the inflammatory caspases 1 and 5 (Martinon, Burns, and Tschopp 2002). Critically, they showed that depletion of ASC prohibited caspase-1 activation and IL-1β maturation in response to LPS, providing the first demonstration that inflammasomes are the machinery necessary for innate immune responses by IL-1 signaling (Martinon, Burns, and Tschopp 2002).

1.2. INFLAMMSOME STRUCTURE AND FUNCTION

1.2.1. NLRs

Inflammasomes are classified by their sensor protein. With the exception of the absent in melanoma (AIM)-2 inflammasome, canonical inflammasomes all contain a protein from the nucleotide-binding domain (NBD, or nucleotide-binding and oligomerization domain [NOD]) and leucine-rich repeat (LRR) containing (NLR) gene family (Ting et al. 2008). In some cases NLR has also been used as an acronym for nucleotide oligomerization domain (NOD)-like receptors (G. Chen et al. 2009). Within this family of gene products, further distinction is stratified by the identity of the N-terminal domains with the two dominant groups of inflammasomes from the NLR family, CARD-containing (NLRC) and NLR family, PYD-containing (NLRP) classifications (Ting et al. 2008). NLRs belong to a larger multi-group family of receptors called pattern recognition receptors (PRRs) that detect microbial and host-derived molecular patterns (Schroder and Tschopp 2010; Takeuchi and Akira 2010). The properties off PRRs and their relationship to inflammasome regulation will be discussed further in section 1.3.1.

Overall, NLRC and NLRP proteins exhibit a high degree of domain similarities. As indicated by the gene names, both contain NBDs and LRRs and are primarily distinguished by the presence of either a CARD or PYD domain. Additionally, specific changes within an internal NBD-associated domain (NAD) have been shown to be essential for ligand detection and, consequently, confer specificity among the structurally similar family of inflammasome sensors (Tenthorey et al. 2014). A graphical overview of the most commonly studied NLRs is provided in **Figure 1-1** and a representation of how the NLRP3 inflammasome assembles is given in **Figure 1-2**.

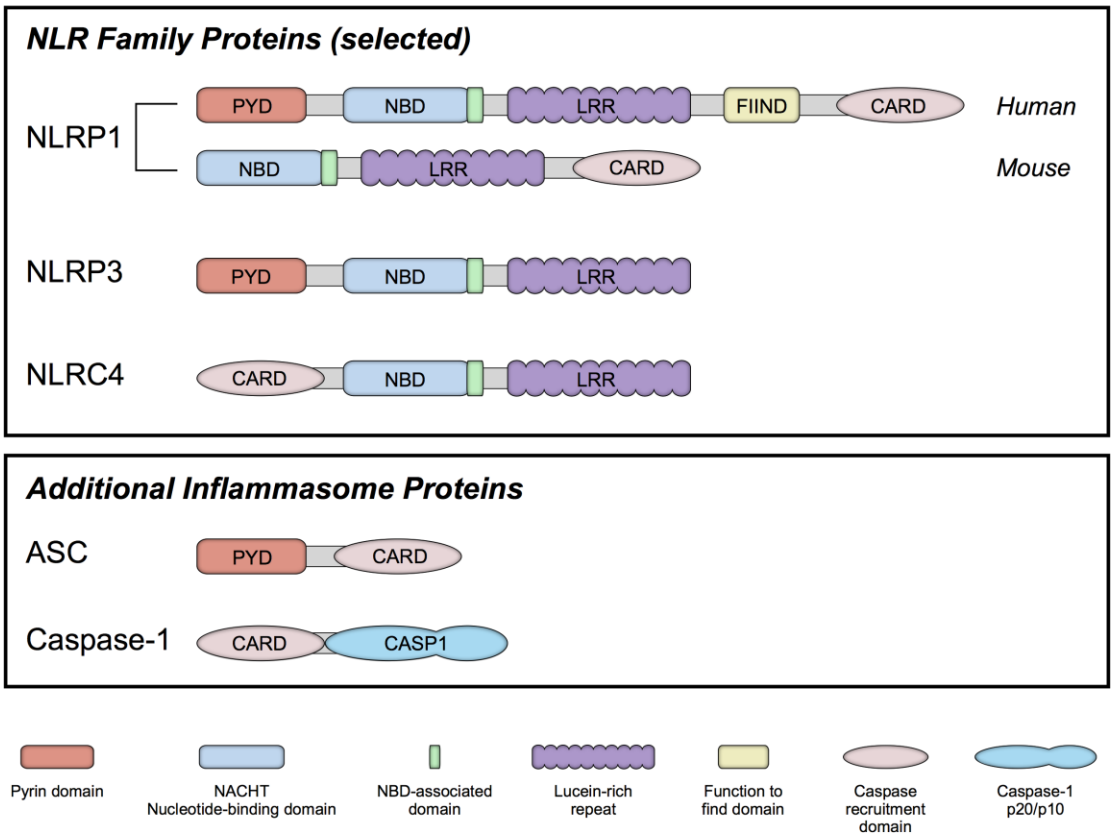

Figure 1-1. Graphical overview of selected inflammasome components. Monocyte-derived cells are capable of assembling a variety of inflammasomes depending on the activating stimulus. Shown here are selected examples of NLR family inflammasome sensors as well as the components ASC (also called Pycard) and Caspase-1. Domain display and order are the primary differences between each NLR sensor protein, while specific sequence variation in the NAD domains confer specificity to selected ligands.

1.2.2. Caspase-1

Caspase-1 is the inflammatory enzyme responsible for canonical processing of the pro-inflammatory cytokines IL-1β and IL-18. It is synthesized as a 45 kilo-Dalton (kD) inactive pro-enzyme containing an N-terminal CARD found in the cytosol of cells from the myeloid lineage (Thornberry et al. 1992; Poyet et al. 2001) (**Figure 1-1**). Pro-caspase-1 is recruited to active inflammasome complexes by CARD-CARD interactions, where it is autoproteolytically cleaved to produce the active enzyme caspase-1 (Martinon, Burns, and Tschopp 2002) (**Figure 1-2**). Cleavage of caspase-1 may be detected by the presence of 10 kD (p10) and 20 kD (p20) fragments by immunoblotting (Thornberry et al. 1992). Experimentally, activated caspase-1 is

detected localized on the inflammasome or released to the cytosol, both of which can be detected by addition of a fluorescent inhibitor prior to stimulation of caspase-1 activation (to detect inflammasome-localized enzyme) or post-stimulation (to detect cytosol-localized enzyme) (Grabarek, Amstad, and Darzynkiewicz 2002). Upon caspase-1-dependent pyroptotic cell death (discussed further in section 1.4.2), activated and pro-form caspase-1 are released and can be detected in culture supernatant (Martinon, Burns, and Tschopp 2002).

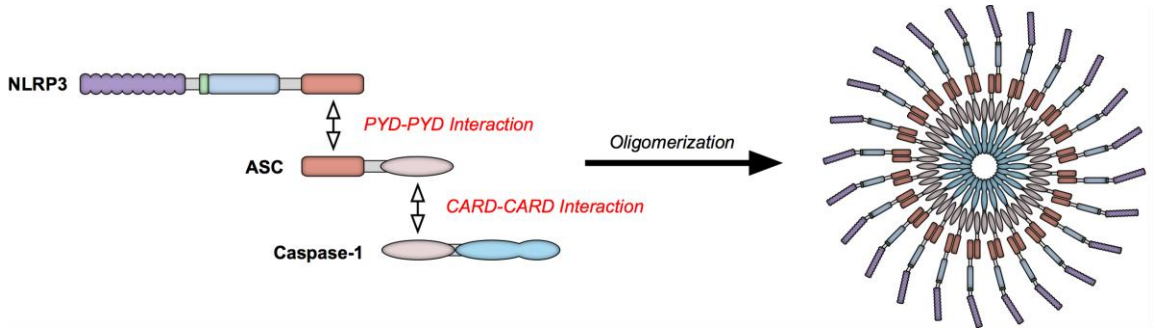

Figure 1-2. Homotypic domain interactions direct NLRP3 inflammasome assembly. PYD domains on NLRP3 and ASC and CARD domains on ASC and Caspase-1 localize by homotypic interactions, resulting in rapid, prion-like assembly of the inflammasome (Cai et al. 2014; Lu et al. 2014). The various components are visualized as concentric rings of homogenous protein by super-resolution microscopy (Man et al. 2014). Close proximity concentration of pro-caspase-1 at the core of the inflammasome results in autocatalytic cleavage and activation.

1.2.3. ASC/PYCARD

Apoptosis-associated speck-like protein containing a caspase recruitment domain (ASC), also called Pycard, is a 22 kD constitutively expressed protein localized to the cytosol and nucleus of monocyte-derived cells (Masumoto et al. 1999; Bertin and DiStefano 2000; Martinon, Hofmann, and Tschopp 2001). ASC contains N-terminal PYD and C-terminal CARD domains (Martinon, Hofmann, and Tschopp 2001) (**Figure 1-1**). The structure of ASC facilitates the recruitment of pro-caspase-1 to inflammasome sensor proteins that do not contain a CARD domain (as in the case of NLRP3), and thus ASC is considered an adapter protein (Martinon, Burns, and Tschopp 2002; Srinivasula et al. 2002). Homotypic interactions between the PYD domains of ASC and the NLR protein facilitate recruitment of cytosolically distributed ASC to a visually punctate focus, while homotypic interactions between the CARD of ASC and the CARD on pro-caspase-1 result

in a similar punctate localization of caspase-1 (Srinivasula et al. 2002; Stehlik et al. 2003) (**Figure 1-2**). Through this recruitment and enriched localization of pro-caspase-1 to the site of inflammasome assembly, autoproteolytic cleavage of pro-caspase-1 to bioactive caspase-1 is possible. The assembly of ASC-dependent inflammasomes has been described to proceed by a prion-like mechanism, facilitating the total enrichment of the cellular complement of each component to a single focus (Cai et al. 2014; Lu et al. 2014). Additionally, ASC is posited to enhance activation of caspase-1 in the NLRP1 inflammasome, which contains it's own CARD domain but also has an N-terminal PYD domain (Martinon, Burns, and Tschopp 2002).

1.2.4. IL-1β and IL-18

Interleukin (IL)-1β and IL-18 are the primary cytokine substrates of caspase-1 activation. IL-1β is an inducible cytokine synthesized as a 34 kD precursor that is subsequently processed to a bioactive 17 kD form (Giri, Lomedico, and Mizel 1985; March et al. 1985; Black et al. 1988). The caspase-1 cleavage site for conversion of precursor IL-1β to mature IL-1β is between Asp116 and Ala117 (Kostura et al. 1989). IL-1β expression is tightly regulated by NF-kappaB (NF-κB) transcriptional activation and it is found at nearly undetectable levels prior to stimulation with an NF-κB inducer such as LPS (Cogswell et al. 1994).

IL-18 (originally called IGIF, or interferon-gamma inducible factor) is synthesized as a 24 kD precursor that is processed to an 18 kD active form via cleavage by caspase-1 between Asp35 and Asn36 (Gu et al. 1997). In contrast to IL-1β, IL-18 is constitutively expressed in monocyte-derived cells and exhibits no requirement for transcriptional upregulation in order to be available for processing and release (Puren, Fantuzzi, and Dinarello 1999).

IL-1β and IL-18 share an uncommon structural feature in that they do not contain classical peptide sequences for secretion signaling (March et al. 1985; Okamura et al. 1995). This unconventional structure leads to the conclusion that IL-1β and IL-18 are not processed or released by the standard ER-Golgi pathway (Nickel and Rabouille 2009). Due to the significant role that IL-1β and IL-18 play in mediating innate inflammatory responses, the mechanisms by which these cytokines are processed and secreted are of interest. Various mechanisms have

been proposed, including lysosomal exocytosis, microvesicle secretion, plasma membrane translocation and lytic release (I.I. Singer et al. 1995; MacKenzie et al. 2001; Bergsbaken et al. 2011; Liu et al. 2014). Despite the well-supported data for each of these pathways, the mechanism by which IL-1β and IL-18 are secreted remains controversial (Lopez-Castejon and Brough 2011).

1.3. NLRP3 INFLAMMASOME REGULATION

NLRP3 is the most widely studied of the inflammasomes, largely due to its activation by a diverse range of activating stimuli (Schroder and Tschopp 2010). Because of its robust and varied responsiveness, the NLRP3 inflammasome has become the preferred system for investigating basic regulation and dynamics of inflammasome activation. The remainder of this dissertation focuses on discussion and investigation specifically related to the NLRP3 inflammasome except where specified.

1.3.1. PAMPs and DAMPs

The NLRP3 inflammasome is responsive to a broad diversity of structural and mechanistically dissimilar stimuli (Schroder and Tschopp 2010). NLRP3 activating stimuli generally fall into the categories of pathogen associated molecular patterns (PAMPs) and damage associated molecular patterns (DAMPs). PAMPs and DAMPs contain regions of highly conserved molecular structure that are, in nearly all cases, detected by pattern recognition receptors (PRRs) that are expressed on the plasma membrane of the cell or found intracellularly. The classes of PRRs include Toll-like receptors (TLRs), C-type lectin receptors (CLRs), NOD-like receptors (NLRs), and retinoic acid-inducible gene (RIG)-I-like receptors (RLRs) (Takeuchi and Akira 2010). How the NLRP3 inflammasome can respond to such a varied array of mechanistically dissimilar stimuli is not well understood, but is at least in part explained by the transduction of PAMP and DAMP signals by the diversity of PRRs. An abbreviated survey representing the diversity of activating stimuli, their classification as a PAMP or a DAMP, and the proposed mechanism for each

stimulus implicated in assembly and activation of the NLRP3 inflammasome at the time of this writing are summarized in **Table 1-1**.

Table 1-1. Abbreviated survey of NLRP3-inducing stimuli

Stimulus	Proposed Mechanism	Reference
DAMPs		
ATP	K+ efflux	(Mariathasan et al. 2006)
Cholesterol	Cathepsin B	(Duewell et al. 2010)
MSU crystals	Cathepsin B, K+ efflux	(Muñoz-Planillo et al. 2013)
Amyloid-beta	Cathepsin B	(Halle et al. 2008; Heneka et al. 2013)
Alum	Cathepsin B, K+ efflux	(Hornung et al. 2008; Muñoz-Planillo et al. 2013)
Silica	Cathepsin B, K+ efflux, ROS	(Dostert et al. 2008; Hornung et al. 2008; Muñoz-Planillo et al. 2013)
Asbestos	K+ efflux, ROS	(Dostert et al. 2008)
Carbon nanotubes	Cathepsin B, $P2X_7$ (K+ efflux), ROS	(Palomäki et al. 2011)
mtDNA	Direct NLRP3 activation (?)	(Shimada et al. 2012)
Palmitate	ROS	(Wen et al. 2011)
Histones	ROS	(Allam et al. 2013)
PAMPs (red = whole pathogen)		
Nigericin	K+ efflux	(Mariathasan et al. 2006)
ssRNA	Cathepsin B, ROS	(Allen et al. 2009)
Beta-Glucans	Cathepsin B, K+ efflux, ROS	(Kankkunen et al. 2010)
Hemozoin	Cathepsin B, K+ efflux, ROS	(Tiemi Shio et al. 2009)
Pneumolysin	Cathepsin B, K+ efflux	(McNeela et al. 2010)
Biglycan	$P2X_7$ (K+ efflux), ROS	(Babelova et al. 2009)
N. gonorrhoeae	Cathepsin B	(Duncan et al. 2009)
L. monocytogenes	Cathepsin B, K+ efflux	(Meixenberger et al. 2010)
C. albicans	K+ efflux, ROS	(Gross et al. 2009)
M. tuberculosis	Phagosomal rupture (not Cathepsin B)	(Wong and Jacobs 2011)

Canonically, the NLRP3 inflammasome requires two, discrete stages of treatment before it can be activated. Signal 1 is generally called “priming” and refers to the processes required for establishing an inflammasome-inducible state in the cell. While most PAMPs can act as Signal 1 treatments, priming is most commonly achieved by treatment with LPS, which activates the PRR Toll-like receptor 4 (TLR4) by interactions dependent on LPS-binding protein (LBP) and CD14

(Muta and Takeshige 2001). Activation of TLR4 triggers a myeloid differentiation primary-response protein 88 (MyD88)-dependent intracellular signaling cascade that activates the IκB kinase (IKK), which phosphorylates nuclear factor of kappa light polypeptide gene enhancer in B-cells inhibitor alpha (IκBα), removing inhibition of nuclear factor kappa-light-chain-enhancer of activated B cells (NF-κB), which then translocates to the nucleus (Akira and Takeda 2004). Once in the nucleus, NF-κB mediates transcriptional upregulation of NLRP3 and proIL-1β (Bauernfeind et al. 2009) (**Figure 1-3A**). The necessity for NF-κB activation and transcriptional upregulation prior to inflammasome assembly has been questioned, however, as basal levels of NLRP3 were found sufficient for low, but detectable, levels of caspase-1 activation (Guarda et al. 2011). Recent reports further emphasize that transcriptional upregulation is dispensable for licensing the inflammasome because post-translational priming resulting from as few as 5 minutes of treatment with LPS provides sufficient licensing for robust activation of inflammasome as well as processing and release of constitutively present proIL-18 (Ghonime et al. 2014). It should also be noted that while LPS provides a convenient and controllable stimulus to prime cells and license the inflammasome, under conditions of sterile inflammation where LPS would not be present IL-1α could trigger priming through IL-1 receptor activation and MyD88-dependent signaling, or exposure to tumor necrosis factor (TNF) (Akira and Takeda 2004; C.-J. Chen et al. 2007; Dinarello 2013; Katnelson et al. 2015).

Application of Signal 2 (also called “stimulation” or “activation”) after a period of priming by Signal 1 results in the assembly of the inflammasome, activation of caspase-1 and processing of IL-1β. The type of Signal 2 treatment is thought to trigger a specific intracellular change, as described in **Table 1-1**, which is detected by NLRP3 to result in inflammasome assembly. For example, treatment with the DAMP monosodium urate crystal (MSU) results in lysosomal destabilization and potassium efflux, both of which are thought to engage NLRP3, while viral single-stranded RNA as well as the M2 ion channel from Influenza virus acts as PAMPs triggering ROS and ion flux to activate NLRP3 (Martinon et al. 2006; Allen et al. 2009; Ichinohe, Pang, and Iwasaki 2010). **Figure 1-3B** depicts activation by purinergic signaling, pore-forming toxins and biological particulates. A unifying mechanism describing how the NLRP3 inflammasome can

detect such diverse stimuli has been elusive, but two popular hypotheses have been proposed: ion flux and redox signaling (Lupfer and Kanneganti 2013). These hypotheses are discussed in the following sections.

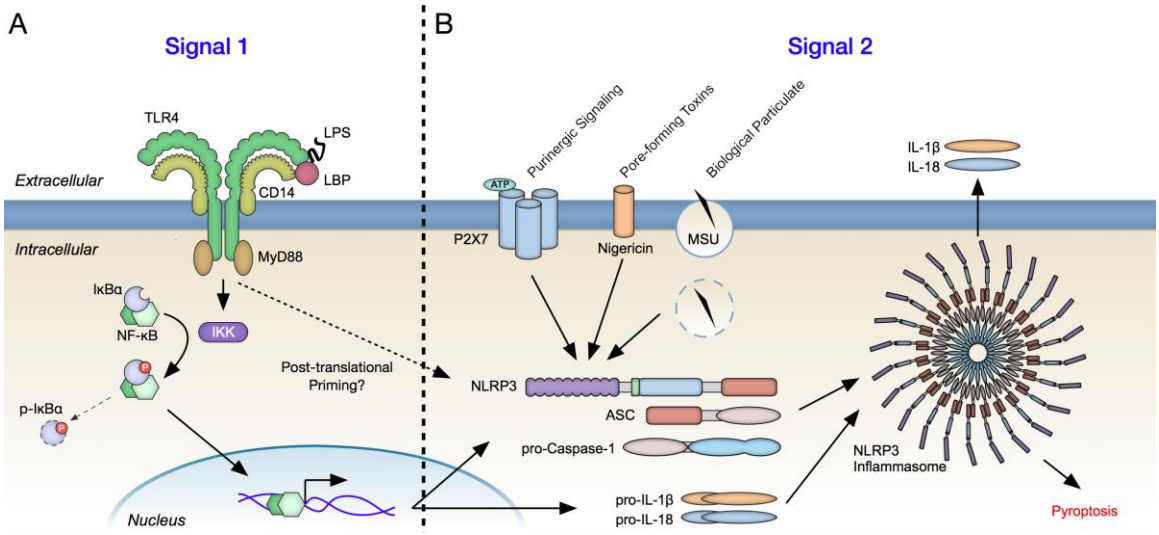

Figure 1-3. Two signals are required for NLRP3 inflammasome activation. (A) Detection of LPS by TLR4, CD14 and LBP result in MyD88-dependent signaling, IKK activation and phosphorylation and destruction of IκBα. Once IκBα is removed, NF-κB translocates to the nucleus, where it transcribes the mRNA coding for pro-IL-1β, pro-IL-18 and other components of the inflammasome. At this time, post-translational priming may also occur. (B) Upon the detection of extracellular ATP at purinergic receptor, or through cellular damage by pore-forming toxins and biological particulate, the individual components of the NLRP3 inflammasome will activate and assemble. The result of NLRP3 inflammasome assembly is processing and secretion of pro-inflammatory cytokines and pyroptotic cell death.

1.3.2. Ion flux

The homeostatic maintenance of electrochemical gradients by asymmetric distribution of ions in compartments and across membranes is essential for cell viability and function (Dubyak 2004). Early work on understanding the regulation of IL-1β indicated that treatment with extracellular ATP or the pore-forming toxin nigericin perturbed cellular potassium and resulted in the robust release of mature IL-1β into culture supernatants (Perregaux and Gabel 1994). This observation was supported by detected efflux of the radioactive potassium analog $^{86}Rb^{+}$ and by inhibition with exchange of sodium chloride for potassium chloride in the medium (Perregaux and Gabel 1994). After characterization of the inflammasome and the identification of a number of NLRP3 inflammasome-inducing agents, subsequent studies further established a link between NLRP3

inflammasome assembly and intracellular potassium depletion by showing inhibition with high concentrations of extracellular potassium (Petrilli et al. 2007). In the context of this relationship, the first pharmacological inhibitor characterized to inhibit the NLRP3 inflammasome was glyburide/glibenclamide, a potassium channel inhibitor commonly used to treat Type-2 diabetes (Lamkanfi et al. 2009). Nigericin is a potassium/proton ionophore that acts in a receptor-independent manner to release potassium-associated concentration gradients across biological membranes, while ATP stimulates the dilation of a cation channel in the $P2X_7$ purinergic receptor (Perregaux and Gabel 1994). Because nigericin is a sufficient stimulus for inflammasome assembly, it may be concluded that potassium efflux, independent of signaling cascades, is a necessary regulating event (Perregaux and Gabel 1994; Petrilli et al. 2007). Indeed, due to the seemingly ubiquitous ability of potassium chloride in the medium to reduce or inhibit inflammasome assembly and function, a recently proposed unifying mechanism placed the role of potassium efflux as the common trigger to bacterial toxins and particulate matter (Muñoz-Planillo et al. 2013). Despite its broad implications, an explanation as to how potassium efflux regulates the assembly of the inflammasome remains unknown.

Intracellular calcium signaling has also been implicated in regulating processing of IL-1β and assembly of the NLRP3 inflammasome (Horng 2014). Initially, early studies postulated that potassium, and not calcium, was the critical regulatory ion for processing and release of IL-1β because treatment with the calcium ionophore A23187 and the intracellular calcium store-releasing agent thapsigargin did not produce mature IL-1β (Walev et al. 1995). However, subsequent experiments found that a rise in intracellular calcium, concomitant with potassium efflux, corresponded with enhanced release of IL-1β that could be inhibited by the intracellular calcium chelator, BAPTA-AM (Brough et al. 2003). Keratinocytes, a non-canonical cell type for production of IL-1β, were found to produce IL-1β when treated with ultraviolet radiation in a cytosolic calcium increase-dependent manner that could also be inhibited by treatment with BAPTA-AM (Feldmeyer et al. 2007). The bacterial PAMP tetanolysin O (TLO), a cholesterol-dependent cytolysin (CDC), was also found to induce assembly of the NLRP3 inflammasome that could be inhibited independently by treatment with BAPTA-AM or extracellular potassium,

suggesting at least a partial requirement for calcium increase in TLO-dependent inflammasome induction (J. Chu et al. 2009). A proposed mechanism by which calcium regulates inflammasome assembly is by induction of calcium overload-induced mitochondrial damage and mitochondrial DNA release-dependent NLRP3 activation (Murakami, Ockinger, Yu, Byles, et al. 2012). These studies implicate a crucial role for cation flux driven by either calcium or potassium in regulation of the NLRP3 inflammasome, though the relationship between these two ions and their independent contributions towards pathway regulation are unclear (Jin and Flavell 2010; Sutterwala, Haasken, and Cassel 2014).

1.3.3. Redox signaling

Redox signaling by reactive oxygen species (ROS) generated by various cellular sources has been implicated in induction of the NLRP3 inflammasome (Harijith, Ebenezer, and Natarajan 2014). Initial studies into the role of reactive oxygen in inflammasome assembly implicated extracellular ATP-triggered nicotinamide adenine dinucleotide phosphate (NADHP) oxidase (NOX) as the cellular source for NLRP3-inducing ROS (Cruz et al. 2007). This evidence was supported by the inhibition of caspase-1 activation by treatment with the NOX inhibitor diphenyleneiodonium chloride (DPI). However, subsequent studies in monocytes from patients with chronic granulomatous disease (CGD), a disease characterized by inactivating mutations in NOX proteins, displayed no loss in activity of the inflammasome as indicated by caspase-1 activation and bioactive IL-1β release after stimulation with prototypical DAMPs, suggesting a more complex role for NADPH oxidase activity (Meissner et al. 2010).

Mitochondrial reactive oxygen species (mROS) constitute the majority of cellular ROS, since it is routinely produced as a byproduct of intracellular ATP synthesis by the electron transport chain, and its generation is increased during mitochondrial dysfunction (Brookes et al. 2004). Blockade of mitophagy/autophagy by 3-methyladenine and mitochondrial uncoupling with rotenone and antimycin A result in mitochondrial dysfunction and mROS generation (Zhou et al. 2011). These treatments were found to trigger the NLRP3 inflammasome, possibly through activation and redistribution of thioredoxin interacting protein (TXNIP) (Zhou et al. 2010; Zhou et

al. 2011). Subsequent studies confirmed that NLRP3 inflammasome induction was depending on mitochondrial dysfunction and mROS generation that could be inhibited by the mitochondrial localized ROS scavenger, MitoTEMPO (Heid et al. 2013). Interestingly, knockdown of the mitochondrial voltage dependent anion channel (VDAC) isotypes 1 and 2, but not 3, suppressed NLRP3 activation (Zhou et al. 2011). VDAC channels are located at the outer mitochondrial membrane and are crucial for the exchange of mitochondrial metabolites and ions to the cytosol and surrounding organelles, as well as generation of ROS (Colombini 2004). These results point to a possible role for mitochondrial sensing of ion levels upstream of inflammasome regulation by reactive oxygen signaling.

1.4. PHENOTYPIC OUTCOMES

1.4.1. Inflammatory signaling

A major consequence of inflammasome assembly is the release of pro-inflammatory cytokines. While the most widely investigated cytokines released are IL-1β and IL-18, release of IL-1α and the nuclear alarmin high mobility group box 1 (HMGB1) are also regulated by the NLRP3 inflammasome (Lamkanfi et al. 2010; Rathinam, Vanaja, and Fitzgerald 2012). Detection of extracellular HMGB1 induces cytokine induction through TLR4 signaling (Ben Lu et al. 2012; Yang et al. 2013). Together, these cytokines orchestrate continued inflammatory response in the presence of pathogenic insult as well as sterile inflammation mediated by biological particulates or tissue damage (G.Y. Chen and Núñez 2010).

In addition to cytokine release, other intracellular components have been implicated in inflammatory signaling both downstream and upstream of NLRP3 inflammasome assembly. The most efficiently released non-cytokine inducer of inflammasome assembly is the intracellular DAMP ATP (Perregaux and Gabel 1994; Laliberte, Eggler, and Gabel 1999; Gombault, Baron, and Couillin 2012). Intracellular ATP may be released by cells dying via caspase-1-dependent cell death (discussed in section 1.4.2) or via pannexin-1 hemichannels (Pelegrin and Surprenant 2006; Piccini et al. 2008; Schenk et al. 2008). Support for autocrine and paracrine activation of the inflammasome by ATP is illustrated by the suppression of IL-1β and IL-18 processing and

release by treatment with apyrase, an enzyme that hydrolyzes extracellular ATP (Piccini et al. 2008). Other examples of non-cytokine signaling in inflammasome regulation include extracellular release of mitochondrial DNA, nucleosomes and assembled inflammasome structures (Nakahira et al. 2010; Q. Zhang et al. 2010; Huang et al. 2011; Shimada et al. 2012; Baroja-Mazo et al. 2014; Kang et al. 2014).

1.4.2. Pyroptosis

Pyroptosis (translated as “to go down in flames” from the Greek roots *pyro* relating to fire and *ptosis* to denote a falling) is a caspase-1-dependent cell death that was initially characterized as distinct from apoptosis in macrophages infected by *Salmonella typhimurium* (Brennan and Cookson 2000; Cookson and Brennan 2001). It was subsequently shown that pyroptosis triggered by *Salmonella* infection is due to flagellin-induced ICE protease-activating factor (IPAF; also called NLRC4) inflammasome activity (Mariathasan et al. 2004; Franchi et al. 2006; Miao et al. 2006). In the case of infection, pyroptotic cell death is thought to prevent pathogen survival by destruction of the host environment and stimulation of neutrophil infiltration (Brodsky and Medzhitov 2011).

Inflammasome assembly and caspase-1 activation do not require stimulation by infection in order to trigger cell death. Early work on the roles of ATP and nigericin, both NLRP3 inflammasome activators, in stimulating IL-1β processing and release also described a morphology for cell lysis that is now considered classical for pyroptosis (Perregaux and Gabel 1994). Specifically, the authors observed a large, round plasma membrane indicative of osmotic lysis and an intact nucleus (Perregaux and Gabel 1994). Other examples of non-infectious pyroptosis via the NLRP3 inflammasome are induction by monosodium urate and silica (Hornung et al. 2008; Hari et al. 2014). The cause for initiation of inflammasome assembly and pyroptosis under these sterile conditions is thought to be triggered by cellular damage through lysosomal destabilization, ROS generation or membrane rupture (Hornung et al. 2008; Hari et al. 2014). While pyroptosis can reduce the virulence of invading pathogens, the exact role of pyroptosis in non-pathogenic inflammasome signaling is not well understood, and in fact may be both

advantageous or deleterious (Zheng, Gardner, and M.C.H. Clarke 2011). This is discussed further in sections 1.4.3 and 1.5.

1.4.3. Microenvironment and systemic response

The initiation of an IL-1-associated systemic febrile response upon endotoxic stimulation with LPS is well established, and mice with IL-1 signaling deficiencies are resistant to potentially lethal LPS-induced shock (P. Li et al. 1995). Upstream of IL-1 processing, a whole mouse study has revealed that LPS-induced fever proceeds through numerous, differential phases driven by TLR4 signaling in hematopoietic and non-hematopoietic cell types (Steiner et al. 2006). In mice with deficient TLR4 signaling, all phases of fever response to LPS injection are suppressed, while in chimeric cells with TLR4-deficient bone marrow but functional TLR4 in somatic cells only the initial phase of fever is suppressed (Steiner et al. 2006). These findings highlight the feedback and redundancy embedded in the systemic inflammatory response, wherein IL-1 signaling is crucial to the efficient initiation of inflammation, but other signaling mechanisms such as prostaglandin E2 (PGE2) signaling in the brain can act downstream of IL-1 signaling (Engström et al. 2012).

Local tissue remodeling or damage has also been attributed to activation of the inflammasome under sterile inflammatory conditions. For example, amyloid-beta deposition in the brain results in activation of the NLRP3 inflammasome through lysosomal destabilization (Halle et al. 2008). The IL-1β release associated with amyloid-beta induced NLRP3 activation has been implicated in the appearance of various Alzheimer's disease-associated etiologies, such as neurofibrillary tangles (Salminen et al. 2008; Heneka et al. 2013). Another example of tissue disruption by NLRP3 activity is obesity-induced inflammation and insulin resistance (Vandanmagsar et al. 2011). The release of ceramides, lipoproteins or other nonmicrobial DAMPS associated with adipose damage potently induced inflammasome activation and ablation of NLRP3 significantly improved insulin signaling and histological scores for inflammation in obese mice (Vandanmagsar et al. 2011). Due to the ability to detect damage-associated signals,

NLRP3 has a central role in sterile, inflammation-associated microenvironment remodeling and pathogenesis.

Immunity acquired by vaccine-induced antibody production is another instance wherein systemic response to inflammation may be crucial. It has been postulated that stimulation of cytokine signaling by induction of the NLRP3 inflammasome with the adjuvant alum can enhance vaccine efficacy (H. Li et al. 2008). This is supported by an impairment of antigen-specific antibody production in post-immunization NLRP3-deficient mice (H. Li et al. 2008). The finding that NLRP3 activity mediates alum adjuvancy provides support for earlier work demonstrating the potential for IL-1 itself to act as a adjuvant (Staruch and Wood 1983; Nencioni et al. 1987). An additional study suggested the ability of alum to promote an adjuvant effect could also be through extracellular release of DNA, suggesting a potential feed-forward signaling loop mediated by NLRP3 detection of DNA as a DAMP (Marichal et al. 2011). Therefore, rational tuning of systemic inflammation driven by the inflammasome may be a route to improve immunogenic responses to vaccination.

1.5. CLINICAL RELEVANCE

1.5.1. Acute and chronic conditions

Several acute clinical conditions have been attributed to NLRP3 inflammasome activity. For example, the destruction of heart tissue during myocardial infarction or ischemia-reperfusion (I/R) injury results in the release of intracellular DAMPs. Detection of these DAMPs by NLRP3 has been implicated in inflammatory tissue damage post-initial injury (Sandanger et al. 2013; Toldo et al. 2014). Deletion of NLRP3 was found to reduce heart tissue damage post I/R injury (Sandanger et al. 2013). Drug design informed by the role of NLRP3 in myocardial infarct injury resulted in the development of a glyburide intermediate that effectively reduced caspase-1 activity and infarct size post I/R injury (Marchetti et al. 2014). Addressing this mechanism has become the topic of pilot clinical trials to reduce injury from myocardial infarction, as inflammasome interventions are becoming increasingly available (Toldo et al. 2014).

Acute lung injury (ALI) is a severe complication of serious illness and affects 10-15% of patients in intensive care units (Goss et al. 2003). Inflammasome-induced IL-18 release was

found to be a critical mediator of ALI experimentally induced by ventilator-induced lung injury (VILI) (Dolinay et al. 2012). This finding was supported by treatment with a neutralizing antibody to IL-18 or genetic deletion of IL-18 or caspase-1, all of which reduced lung injury due to VILI (Dolinay et al. 2012). A possible mechanism for the induction of inflammasome-associated cytokine release in ALI is the release of nuclear contents from damaged cells, such as HMGB1 or histones, both of which are NLRP3 inflammasome-inducing DAMPs and have been associated with ALI (Abrams et al. 2013; Luan et al. 2013; R. Chen et al. 2014).

NLRP3 inflammasome activity has also been implicated in chronic inflammatory conditions. A key example of NLRP3 contributing to chronic pathology is gouty arthritis, often referred to as gout. Gout is a condition caused by local inflammatory responses to deposited monosodium uric acid (MSU) crystals in the synovial fluid of joints (Faires and Mccarty 1962). Additionally, it was demonstrated that uric acid was released as a danger signal from dying cells capable of stimulating dendritic cell maturation (Shi, Evans, and Rock 2003). The molecular mechanism regulating MSU-induced gout was found to be activation and function of the NLRP3 inflammasome (Martinon et al. 2006). Importantly, colchicine, a microtubule assembly inhibitor and clinical treatment for gout, was able to prevent inflammasome assembly and IL-1β processing (Martinon et al. 2006). Based on the identification that IL-1β signaling and inflammasome assembly directed MSU-induced inflammation and gout, the authors postulated that IL-1 receptor blockade would be an effective treatment for gout (Martinon et al. 2006). A subsequent pilot clinical trial demonstrated dramatic efficacy and directly contributed to the use of Anakinra (Kineret), an IL-1 receptor antagonist, and Rilonacept, an IL-1β-inhibiting soluble receptor-Fc fusion protein, in the current treatment regime for gout (So et al. 2007; Terkeltaub et al. 2009).

1.5.2. Genetic autoinflammatory disorders

Mutations in the *MEFV* gene were originally identified as the cause for the autoinflammatory condition Familial Mediterranean Fever (FMF), an chronic condition associated with severe, recurrent systemic inflammation (French FMF Consortium 1997). *MEFV* codes for the protein

Pyrin, which has been shown to inhibit assembly of the inflammasome by interactions with NLRP3, ASC, pro-caspase-1 and pro-IL-1β (Papin et al. 2007). The inability for Pyrin to interact with, and inhibit, components of the inflammasome result in spontaneous activation and resultant IL-1β processing and release (Papin et al. 2007). FMF has been effectively treated with IL-1 receptor antagonists, especially in cases where the application of colchicine, the primary treatment for FMF, showed little improvement (Calligaris et al. 2007).

While mutations in Pyrin result in an indirect dysregulation in inflammasome activation, other genetic autoinflammatory disorders are affected by direct mutation in the gene coding for NLRP3 (also called cryopyrin), collectively known as Cryopyrin-associated periodic syndromes (CAPS) or cryopyrinopathies (Aksentijevich et al. 2007). The CAPS family of autoinflammatory conditions includes familial cold autoinflammatory syndrome (FCAS), Muckle-Wells syndrome (MWS), and neonatal-onset multisystem inflammatory disease (NOMID) (Aksentijevich et al. 2007). FCAS presents with the least severe symptoms, while NOMID is the most severe (Aksentijevich et al. 2007). All CAPS conditions are characterized by autosomal dominant *NLRP3* mutations that cause spontaneous or hypersensitive assembly of the inflammasome and can be either inherited or spontaneous (Aksentijevich et al. 2007). Effective treatment of CAPS conditions can be achieved by either neutralizing released IL-1β with Rilonacept or antagonizing IL-1 receptors with Anakinra (Hoffman et al. 2008; Lepore et al. 2010). Surprisingly, a 22-year old patient with Muckle-Wells syndrome treated with Anakinra was observed to inexplicably recover from pathological deafness caused by the patient's MWS (Mirault et al. 2006). This example supports the therapeutic treatment of inflammasome activity in autoinflammatory conditions and illustrates to the potential complexity of inflammasome-dependent signaling in the clinical symptoms of autoinflammatory conditions.

1.6. OPEN QUESTIONS IN INFLAMMASOME BIOLOGY

The NLRP3 inflammasome has been the subject of intense investigation since its discovery in 2002 (Manji et al. 2002; Martinon, Burns, and Tschopp 2002). Despite elucidation of many factors

driving NLRP3 inflammasome assembly and function, a number of open and actively debated questions remain:

1. **How can the NLRP3 inflammasome respond to such a diverse array of structurally and functionally unrelated insults?** It is unclear how particulate matter, pore-forming toxins, endogenous host danger signals, bacterial structural components, viral genetic factors and osmotic changes can all converge on a single signaling pathway.
2. **What is the role of ion flux upstream of NLRP3 inflammasome activation?** While a number of groups have identified the flux of potassium and calcium at low temporal and spatial resolution as a driving factor in NLRP3 inflammasome assembly, the specific effects of these fluxes are not well understood.
3. **What is the role of mitochondria in NLRP3 inflammasome regulation?** It is currently unclear how the mitochondria participate in NLRP3 inflammasome signaling, and whether it has a soluble transduction role or is merely a stabilizing platform.
4. **What downstream mechanisms in NLRP3 inflammasome signaling are regulated by ion flux?** Most reports identifying the role of ion flux look at the reduction in inflammasome assembly by caspase-1 activation and IL-1β processing and release. The effect of ion flux on specific events upstream of inflammasome assembly are not well characterized.

1.7. THESIS CONTRIBUTIONS

This dissertation addresses a number of fundamental gaps in understanding NLRP3 inflammasome regulation with a focus on the role of cation flux. The primary contributions of this dissertation to the field of inflammasome biology are:

1. The first demonstration of real-time potassium flux measurements downstream of $P2X_7$ receptor activation and nigericin treatment with high spatiotemporal resolution and analyte specificity.

2. The first measurements of correlated, live-cell dynamics of potassium and calcium flux.
3. The identification of Syk tyrosine kinase as a downstream effector of potassium efflux during nigericin-induced inflammasome assembly and pyroptotic cell death.
4. The implication of Syk kinase activity in the generation of mitochondrial reactive oxygen upstream of NLRP3 inflammasome assembly.
5. The identification of a dose-dependent relationship between $P2X_7$ purinergic receptor activation, intracellular potassium efflux and plasma membrane permeability.
6. The identification of a mitochondrial potassium pool mobilization downstream of $P2X_7$ purinergic receptor activation.
7. Establishment of potassium efflux as a regulating step for NLRP3 inflammasome-activating calcium influx during $P2X_7$ purinergic receptor activation.

In addition to clarifying the role for cation flux upstream of NLRP3 activation, this dissertation also describes the development of two methods relevant to the study of single cell signatures of cellular and macrophage heterogeneity:

1. A method for correlated fluorescence microscopy and molecular analysis of live single cells was developed. The method allows for the isolation and observation by fluorescence microscopy of live single cells, coupled with downstream processing and multi-target gene expression analysis by RT-qPCR.
2. A mouse macrophage cell line was generated and characterized expressing a protein-based biosensor for live, kinetic analysis of intracellular ATP.

CHAPTER 2: POTASSIUM EFFLUX DRIVES SYK KINASE-DEPENDENT INFLAMMASOME ASSEMBLY AND PYROPTOSIS

2.1. INTRODUCTION AND BACKGROUND

A prevailing question in NLRP3 inflammasome biology is how a functionally and structurally diverse array of stimuli converges on the same signaling pathway (Sutterwala, Haasken, and Cassel 2014). Multiple reports demonstrate that intracellular potassium efflux is essential for assembly of the inflammasome in response to a diverse array of stimuli (Perregaux and Gabel 1994; Petrilli et al. 2007; Muñoz-Planillo et al. 2013). Notably, potassium efflux was identified as a necessary and sufficient common step in a proposed unifying model for inflammasome assembly in response to bacterial toxins and particulate matter (Muñoz-Planillo et al. 2013). The utilization of an ion flux for initiation of a cell fate decision provides support for the concept of pyroptosis as a "hair-trigger" macrophage suicide with the effect of acting as an early warning system for the host. This is substantiated by the fact that other necessarily rapid biological processes operate by an ion flux-dependent mechanism (Dubyak 2004; Brodsky and Medzhitov 2011). However, despite its established importance, the mechanism whereby maintenance of intracellular potassium concentration regulates the assembly and activity of the inflammasome is still not well understood.

Recent evidence highlights the importance of post-translational signaling in licensing the inflammasome for assembly and downstream outcomes such as cytokine secretion and pyroptosis (Ghonime et al. 2014). This rapid licensing is in contrast to canonical models for inflammasome activation that depend on a sustained, TLR4-dependent, priming period followed by a rapid stimulation period (Akira and Takeda 2004; Lamkanfi and Dixit 2014). This is biologically rational as post-translational signaling occurs more rapidly than *de novo* transcription and translation of effector proteins, thereby enabling a more rapid innate immune response to dangerous stimuli. Further establishing a role for post-translational modifications in regulation of the inflammasome is the discovery of a tyrosine phosphorylation site on the inflammasome adapter protein Apoptosis-associated Speck-like protein containing a Caspase recruitment

domain (ASC) that is described as a molecular switch controlling inflammasome assembly (Hara et al. 2013; Lin et al. 2015). Additionally, phosphorylation of ASC was mediated in large part by spleen tyrosine kinase (Syk), a protein tyrosine kinase that has been shown to be essential for inflammasome-mediate defense against fungi, mycobacteria and malarial hemozoin (Gross et al. 2009; Tiemi Shio et al. 2009; Wong and Jacobs 2011).

As both ion flux and post-translational modifications are rapid signaling mechanisms that have been implicated in regulation of the inflammasome, we sought to determine a potential relationship between these two modes of signaling. It was hypothesized that potassium efflux directs inflammasome assembly and downstream effects via regulation of Syk activation by phosphorylation. This study elucidated a number of characteristics of Syk in the inflammasome pathway: (1) Syk regulates nigericin-induced cell death upstream of inflammasome assembly; (2) Syk activity is necessary for nigericin-induced mitochondrial reactive oxygen species generation; (3) Syk activity is downstream of, and dispensable for, nigericin-induced potassium efflux; (4) potassium efflux regulates Syk activation. This study identifies, for the first time, an intermediate regulator of inflammasome activity and pyroptosis regulated by potassium ion efflux.

2.2. MATERIALS AND METHODS

2.2.1. Reagents

Potassium chloride, LPS (from E. coli O111:B4), paraformaldehyde and BSA for blocking solutions were purchased from Sigma Aldrich (St. Louis, MO, USA). Nigericin was purchased from Invivogen (San Diego, CA, USA) and Cayman (Ann Arbor, MI, USA). OXSI-2 was purchased from Cayman (Ann Arbor, MI, USA). Phosphatase inhibitor cocktail was from Biotool (Houston, TX, USA). Protease inhibitors were from Pierce (Grand Island, NY, USA). Primary antibodies against p-Tyr (sc-7020), Syk (sc-1077) and Caspase-1 (sc-514) were from Santa Cruz Biotechnology (Dallas, TX, USA). Primary antibody against IL-1β (AF-401-NA) was from R&D Systems (Minneapolis, MN, USA). Secondary antibodies, protein ladder and nitrocellulose membranes were from Li-Cor (Lincoln, NE, USA). Mini-PROTEAIN® TGX™ 15-well 4-12% gels were from Bio-Rad (Hercules, CA, USA). Released mouse IL-1β DuoSet (DY401) and ancillary

reagent (DY008) ELISA kits were from R&D Systems (Minneapolis, MN, USA). FAM-FLICA™ Caspase-1 assay kit was from ImmunoChemistry (Bloomington, MN, USA). BCA protein determination kit and premade standards were from Pierce (Grand Island, NY, USA). StrataClean Resin was from Agilent Technologies (Santa Clara, CA, USA). Dynabeads® Protein A for immunoprecipitation and MitoSOX were purchase from Life Technologies (Grand Island, NY, USA). 6× denaturing Laemmli buffer was from Alfa Aesar (Ward Hill, MA, USA). CytoTox96® Non-Radioactive Cytotoxicity Assay for LDH release determination was from Promega (Madison, WI, USA). KS6 intracellular potassium sensor was developed in-house (Center for Biosignatures Discovery Automation, The Biodesign Institute, Arizona State University, Tempe, AZ, USA).

2.2.2. Cell culture

The mouse monocyte/macrophage cell line J774A.1 (ATCC TIB-67™, Manassas, VA, USA) was grown in DMEM (Gibco, Grand Island, NY, USA) supplemented with 10% FBS, 100 U/mL Penicillin G (Gibco, Grand Island, NY, USA) and 100 µg/mL Streptomycin Sulfate (Gibco, Grand Island, NY, USA). Tissue culture flasks were passaged every 3-4 days by scraping and cells were counted for density and viability with a Countess® Automated Cell Counter (Life Technologies, Grand Island, NY, USA) using the Trypan Blue dye exclusion assay.

2.2.3. Lactate Dehydrogenase Release Assay

Released lactate dehydrogenase was measured using the CytoTox 96® Non-Radioactive Cytotoxicity Assay according to manufacturer's instructions. Briefly, cells were seeded in a 96-well tissue culture-treated plate at a concentration of 100,000 cells/well in 200 µL medium and incubated overnight. The following day the medium was exchanged for 100 µL of either fresh medium or medium containing 1 µg/mL LPS and incubation was continued for 4 hours. During the third hour of incubation, inhibitors were added and the plate was returned to the incubator. For stimulation, the complete medium of each well was exchanged for 100 µL of either fresh medium, medium containing 1% Triton X-100 as a maximum release control, or the indicated drugs and/or inhibitors and returned to the incubator for 1 hour. Fifty µL of supernatant was sampled for each

well. The developed assay was measured for absorbance at 492 nm on a Biotek Synergy H4 multi-mode plate reader with Gen5 software.

2.2.4. Immunoprecipitation

Cells were seeded in 6-well tissue culture-treated plates at a concentration of 10^6 cells/well in 2 mL of medium and incubated overnight. The following day, cells were primed in 2 mL fresh medium or medium containing 1 µg/mL LPS and incubated was continued for 4 hours. During the third hour of incubation, inhibitors were added and the plate was returned to the incubator. For stimulation, the complete medium of each well was exchanged for 1.1 mL of either fresh medium or medium containing the indicated drugs and/or inhibitors and returned to the incubator for 15, 30 or 60 minutes. After stimulation, supernatants were collected and resuspended in pre-chilled 1.5 mL microfuge tubes containing complete protease and phosphatase inhibitor cocktails, spun for 5 minutes at 5,000 g in 4 °C and 1 mL of cell-free supernatant was transferred to a clean, pre-chilled 1.5 mL microfuge tube. During centrifugation of the supernatants, the cells still in the plate were lysed with RIPA containing complete protease and phosphatase inhibitor cocktails. Cell free supernatants and lysates were combined in the same 1.5 mL tube and rotated at 4 °C for 30 minutes. After rotation, all samples were centrifuged at 14,000 *g* for 15 minutes at 4 °C. Supernatants were transferred to new tubes and protein content was quantified by BCA assay. Samples were normalized to maximal protein concentration (approximately 1 mg total protein) across all conditions using RIPA.

During the 4 hour LPS priming stage, Protein A-conjugated magnetic beads were rotated at room temperature for 2 hours with 1:50 total Syk capture antibody (#SC-1077) in 5% BSA in TBS containing 0.2% Tween-20. For immunoprecipitation, 1% BSA was added to each protein sample and 40 µL of magnetic beads containing Syk capture antibody were added. Samples were rotated overnight at 4 °C. The following day, the beads were washed 3× with cold RIPA by pull-down using a magnetic bead stand and protein was collected by heating the beads in 50 µL 1× denaturing Laemmli at 95 °C for 10 minutes. Samples were immunoblotted according to the

protocol described in section 2.2.5. Samples were performed by, and experiments were performed, with Mounica Rao.

2.2.5. Immunoblotting

For non-immunoprecipitated protein collection, J774A.1 were seeded in a 6-well tissue culture-treated plate at a concentration of 10^6 cells/well. Cells were primed for 4 hours with 1 µg/mL E. coli O111:B4 LPS in complete DMEM, rinsed with serum-free DMEM, and stimulated with 20 µM nigericin for 30 minutes in 1.1 mL serum-free DMEM. After stimulation, supernatants were collected and concentrated with 10 µL/mL StrataClean Resin by rotating at 4 °C for 1 hour with protease and phosphatase inhibitors. Concentrated supernatant protein was collected from the resin by removing the supernatant and heating in 50 µL 1× denaturing Laemmli at 95 °C for 10 minutes. Cell lysates were collected by directly adding 100 µL 1× hot denaturing Laemmli buffer to each well.

Proteins were heated for 15 minutes at 95 °C before loading 12 µL onto a 15 well 4-12% Mini-PROTEAN TGX gel. Gels were run for 1 hour at 100V in Tris/SDS/Glycine buffer and transferred to 0.2 µm pore nitrocellulose membranes for 1 hour at 100V in Tris/Glycine buffer. Membranes were blocked in 5% BSA in TBS with 0.2% Tween for 1 hour at room temperature. Blocked membranes were probed independently in 5% BSA in TBS containing 0.2% Tween-20 with 1:500 rabbit polyclonal against caspase-1 p10 (#SC-514), 1:1000 goat polyclonal against IL-1β (#AF-401-NA) or multiplexed with 1:500 mouse polyclonal against p-Tyr (#SC-7020) and 1:500 rabbit polyclonal against Syk (#SC-1077) while rotating overnight at 4 °C. Secondary antibodies were applied at 1:15000 in 5% BSA in TBS containing 0.2% Tween-20 with rocking for 1 hour at room temperature. TBS with 0.2% Tween was used for all rinses. Membranes were imaged using a Li-Cor Odyssey CLx infrared scanner on auto exposure with high quality setting. Samples were performed by, and experiments were performed, with Mounica Rao.

2.2.6. ELISA

J774A.1 cells were seeded in 96 well plates at a concentration of 10^5 cells/well and incubated overnight. Cells were primed for 4 hours with 1 µg/mL E. coli O111:B4 LPS and subsequently stimulated for 30 minutes with 20 µM nigericin in 100 µL medium. Where indicated, inhibitors were added 15-20 minutes prior to nigericin stimulation. Supernatants were collected and released IL-1β was evaluated with ELISA using the R&D Systems DuoSet kit according to the manufacturer's protocol. Briefly, high-binding plates were coated overnight with anti-IL-1β capture antibody. The following day, coated plates were blocked with 1% BSA in PBST for 1 hour at room temperature. Washed plates were loaded with 100 µL supernatant samples and incubated overnight at 4 °C. The next day, plates were washed and biotinylated secondary antibody was incubated with the plates for 2 hours. Subsequently, streptavidin-HRP was incubated with samples for 30 minutes and colorimetric development was performed for 20 minutes before addition of a stop solution. Developed plates were read on a Biotek Synergy H4 mutli-mode plate reader with Gen5 software.

2.2.7. Live Cell Potassium and mROS Imaging

For imaging, 10^5 J774A.1 cells were seeded in an 8-chamber Ibidi µ-Slide (Ibidi, Verona, WI, USA) and primed for 4 hours with 1 µg/mL E. coli O111:B4 LPS. Inhibitors were added as indicated for the last 15 minutes of priming. Cells were stimulated with 20 µM nigericin after an initial baseline was taken. Cells were imaged on a Nikon T*i* microscope equipped with a C2si confocal scanner (Nikon Instruments, Melville, NY, USA) and a Tokai Hit stage-top incubator (Tokai Hit Co., Shizuoka, Japan). Excitations lines were 408, 488 and 561 nm and emission was collected using the standard DAPI, FITC and TRITC bandwidths. Objectives used were 20× air 0.75 NA, 60× oil immersion 1.4 NA or 60× water immersion 1.2 NA, all from Nikon.

For potassium imaging, KS6 was diluted 1:1 with 10% w/v Pluronic F127 and added to priming cells at 1:100 dilution. Final concentration of KS6 applied to cells was 5 µM. KS6 was excited at 561 nm and emission was collected in the TRITC channel.

For mROS imaging, cells were stimulated with nigericin as described. 15 minutes after initial stimulation, MitoSOX was added at a final concentration of 5 µM according to manufacturer's protocol, concurrently with 10 µg/mL Hoechst 33342 (Life Technologies, Grand Island, NY, USA) and incubated for an additional 15 minutes prior to imaging. MitoSOX was excited at 488 nm and emission was detected in the TRITC channel while Hoechst 33342 was excited at 408 nm and emission was detected in the DAPI channel.

2.2.8. Caspase-1 FLICA Assay

J774A.1 were seeded at a density of 1-2 x 10^5 per well in 200 µL of complete DMEM and grown overnight. The following day cells were primed for 4 hours with 1 µg/mL E. coli O111:B4 LPS. During the last hour of priming cells were loaded with 1× FAM-YVAD-FMK (Caspase-1 FLICA) and 10 µg/mL Hoechst 33342 in complete medium. Additional inhibitors as described were added during the last 15-20 minutes of priming. Cells were stimulated with 20 µM nigericin for 30 minutes, subsequently washed 2× with warm DMEM and fixed in 2% formaldehyde solution for 10 minutes at room temperature. Formaldehyde solution was made fresh daily from paraformaldehyde powder diluted in PBS. Cells were washed 1× with PBS and submerged in 200 µL mounting medium (90% glycerol with 10X PBS and 0.1% NaN_3). Samples were imaged by laser-scanning confocal microscopy as a series of 0.5 µm z-stacks on a Nikon Ti microscope equipped with a Nikon C2si confocal scanner controlled by the Nikon Elements AR software. Stacks were prepared as maximum intensity projections using ImageJ/FIJI. Caspase-1 FLICA was excited at 488 nm and emission was collected in the FITC channel while Hoechst 33342 was excited at 408 nm and emission was collected in the DAPI channel. Samples were prepared by Mounica Rao.

2.2.9. Statistical Analysis

Data were analyzed in GraphPad Prism version 6.05 (GraphPad, La Jolla, CA, USA) using one-way ANOVA with a Tukey's post-hoc or Fischer's LSD comparison. Results were considered significant if $p < 0.05$.

2.3. RESULTS

2.3.1. Syk is required for proinflammatory cytokine signaling

To evaluate the role of Syk in regulating IL-1β processing and release, NLRP3 inflammasome activity was stimulated in J774A.1 mouse macrophages by treatment with nigericin. Immunoblot analysis revealed a robust production and release into the supernatant of the caspase-1 p10 fragment and mature 17 kD form of IL-1β upon LPS priming and nigericin treatment (**Figure 2-1A**). Both caspase-1 activation and IL-1β processing were dependent on potassium efflux, as treatment with nigericin in the presence of 130 mM KCl completely inhibited both events. Syk activity was also crucial for caspase-1 activation and IL-1β processing as treatment with the Syk inhibitor OXSI-2 resulted in a strong suppression of nigericin-induced processing. In agreement with the immunoblot results, detection of processed and released IL-1β by ELISA showed robust inhibition upon treatment with OXSI-2 (**Figure 2-1B**).

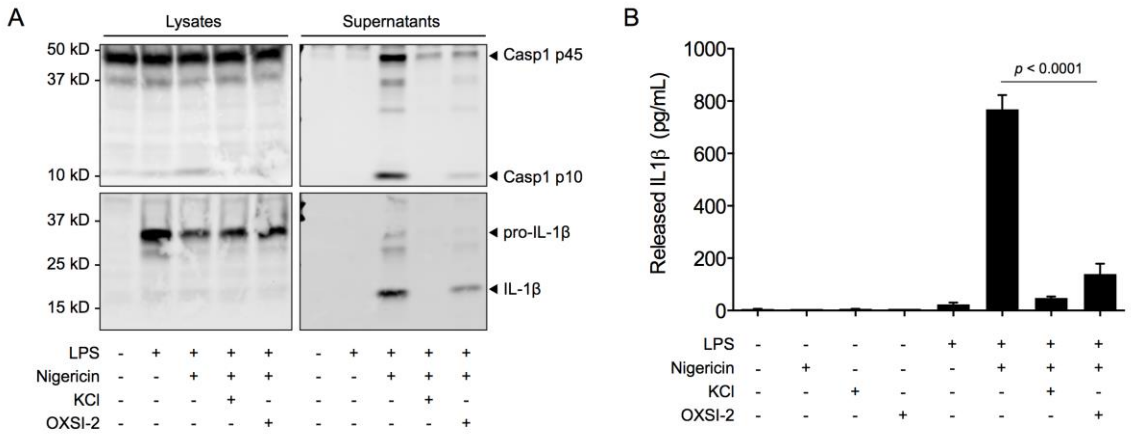

Figure 2-1. Potassium efflux and Syk activity are required for caspase-1 activation and IL-1β processing and release. (A) Immunoblot analysis of caspase-1 and IL-1β in the cell lysates and supernatants of J774A.1 mouse macrophage cells. LPS priming resulted in production of pro-IL-1β, indicating cell priming. Treatment with 20 μM nigericin for 30 minutes resulted in a robust processing and release of the active caspase-1 p10 fragment and mature 17 kD IL-1β in concentrated supernatants. Treatment with 130 mM KCl or 2 μM OXSI-2 resulted in suppression of nigericin-induced caspase-1 activation and IL-1β processing. (B) ELISA evaluation of IL-1β in the supernatants of cells treated as in (A) further supported a requirement for Syk activity in IL-1β release. Nigericin was applied for 60 minutes during ELISA experiments. Bars represent mean and standard error. Statistics were calculated by one-way ANOVA with Tukey's post-hoc comparison. Results represent at least 2 independent experiments.

2.3.2. Syk kinase is essential for nigericin-induced inflammasome assembly

It was next determined whether Syk activity inhibited caspase-1 and IL-1β processing by inhibiting the assembly of the inflammasome complex. Fluorescently tagging activated caspase-1 by pre-exposure with a FAM-conjugated irreversible inhibitor for caspase-1 results in tagging of caspase-1 at the explicit site of activation (i.e., within the inflammasome itself) (Broz et al. 2010). Results show that LPS-primed, nigericin-treated J774A.1 assemble the inflammasome as indicated by single, perinuclear specks of caspase-1 (**Figure 2-2**). As expected, treatment with 130 mM KCl inhibited the assembly of the inflammasome. Importantly, Syk activity was essential for assembly of the NLRP3 inflammasome, as treatment with OXSI-2 resulted in significant suppression of caspase-1 specks. Thus, Syk activity is required for assembly of the inflammasome complex.

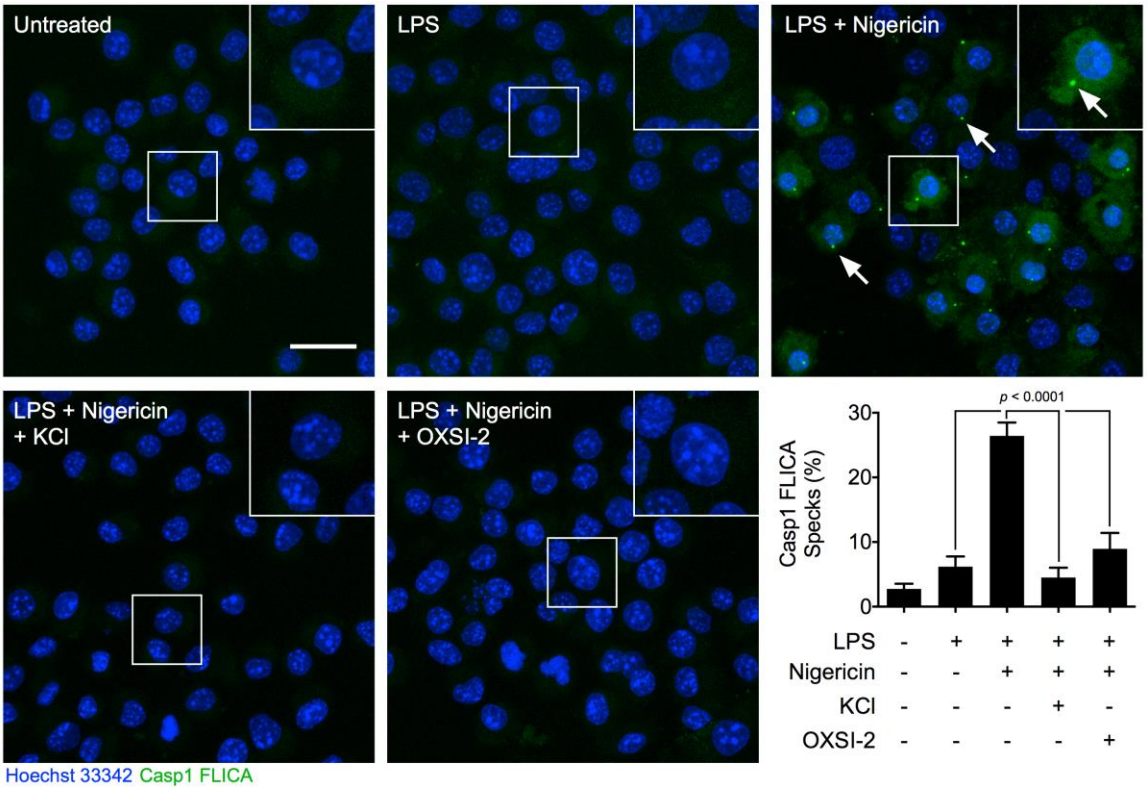

Figure 2-2. Syk activity is required for nigericin-induced inflammasome assembly. J774A.1 mouse macrophage cells were left untreated, primed for 4 hours with 1 µg/mL LPS or primed and stimulated with 20 µM nigericin for 30 minutes. Where indicated, cells were treated with 130 mM KCl or 2 µM OXSI-2 for 15-20 minutes prior to addition of nigericin. Arrows indicate perinuclear caspase-1 specks classical for NLRP3 inflammasome assembly. Bar graph indicates mean and standard error of at least 3 fields from 2 independent experiments evaluated by one-way ANOVA with Tukey's post-hoc comparison. Blue fluorescence is Hoechst 33342 and green fluorescence is caspase-1 FLICA. Scale bar represents 25 µm.

2.3.3. Nigericin-induced pyroptosis is regulated by Syk activity

Because OSXI-2 treatment suppressed inflammasome assembly, it was determined if Syk regulated nigericin-induced pyroptotic cell death as well. As expected, pyroptosis measured by release of lactate dehydrogenase into the medium was found to require both LPS priming and nigericin stimulation to proceed and was dependent on the efflux of potassium, since130 mM KCl suppressed pyroptotic cell death (**Figure 2-3**). Further, treatment with OXSI-2 significantly inhibited nigericin-induced pyroptosis. Therefore, Syk activity is essential for NLRP3 inflammasome assembly, caspase-1 activation and IL-1β processing and release, and progression to caspase-1-dependent pyroptotic cell death.

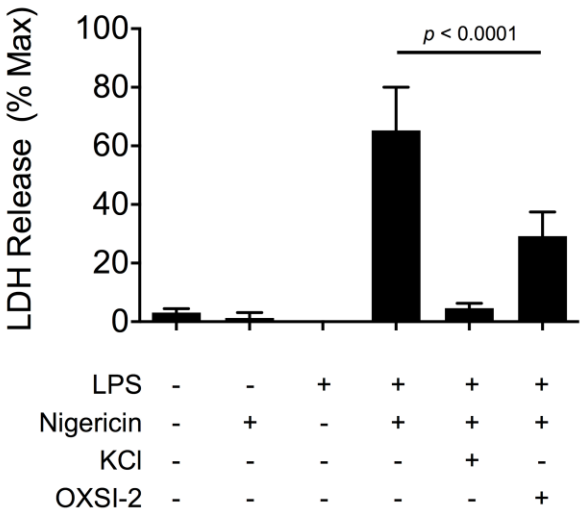

Figure 2-3. Syk activity is required for nigericin-induced pyroptosis. J774A.1 macrophages were left untreated, treated with 20 µM nigericin for 30 minutes, primed for 4 hours with 1 µg/mL LPS or primed with LPS and then subsequently nigericin treated. Where indicated, cells were treated with 130 mM KCl or 2 µM OXSI-2 for 15-20 minutes prior to nigericin treatment. Bars represent mean and standard error of two independent experiments evaluated by one-way ANOVA with Tukey's post-hoc comparison.

2.3.4. Syk activity is necessary for nigericin-induced mitochondrial ROS generation

Mitochondrial destabilization and oxidative signaling has been implicated in triggering the NLRP3 inflammasome. It was determined if treatment with OXSI-2 had a protective effect against mitochondrial ROS generation during nigericin-induced inflammasome activation. Live cell imaging with the reactive oxygen probe MitoSOX revealed that LPS priming with subsequent nigericin treatment resulted in robust oxidation as determined by fluorescence increase of MitoSOX (**Figure 2-4**). Suppression of MitoSOX oxidation upon treatment with 130 mM KCl and OXSI-2 revealed that this process was dependent on potassium efflux and Syk activity. Strong nuclear staining in cells treated with nigericin in the absence of inhibitors was noted. This staining pattern indicates dead cells that have had mitochondria disintegrate and release oxidized MitoSOX probe, which subsequently binds to the DNA in the nucleus (Mukhopadhyay et al. 2007). While these cells indicate the robust pyroptotic consequence of nigericin-induced inflammasome assembly, apparent and substantial non-nuclear signal that was abrogated upon treatment with KCl or OXSI-2. These observations indicate that Syk activity and potassium efflux

regulate events upstream of mitochondrial destabilization and oxidative signaling during nigericin-induced inflammasome activation.

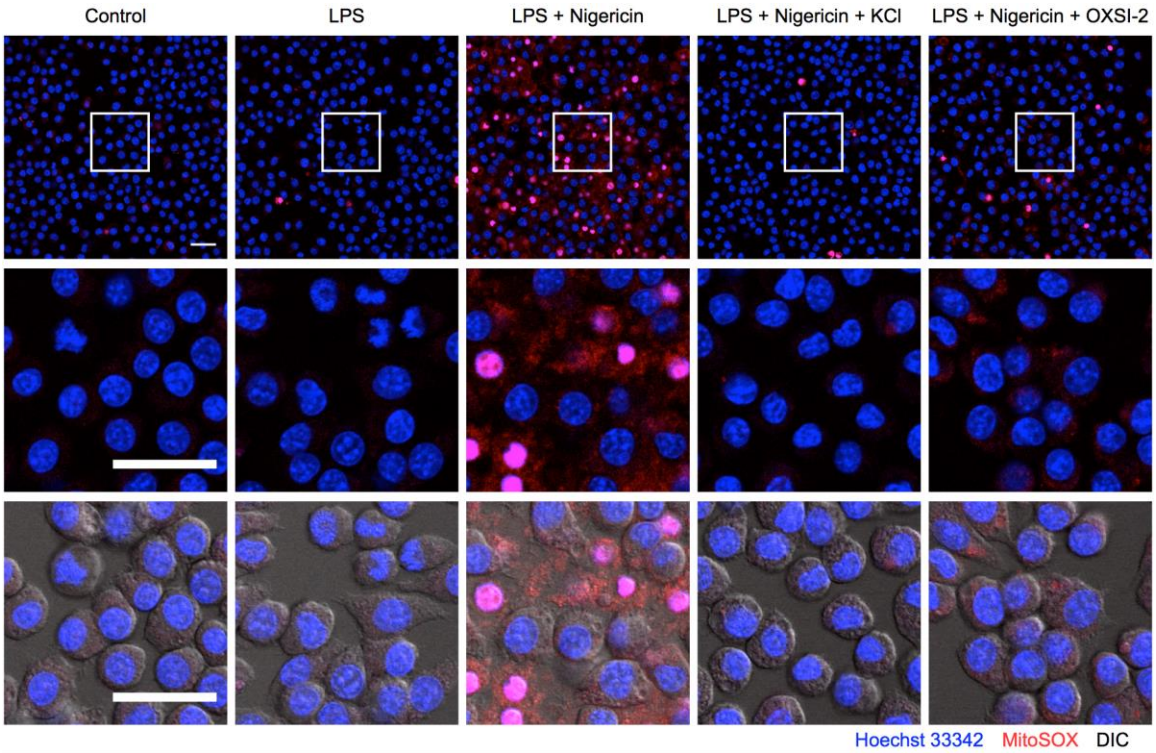

Figure 2-4. Potassium efflux and Syk activity regulate nigericin-induced mitochondrial reactive oxygen species generation. J774A.1 cells were left untreated, primed with 1 µg/mL LPS for 4 hours or primed and then treated with 20 µM nigericin for 30 minutes. Where indicated, cells were treated with 130 mM KCl or 2 µM OXSI-2 for 15-20 minutes prior to nigericin treatment. During the last 15 minutes of nigericin exposure cells were stained with 5 µM MitoSOX and then imaged by confocal microscopy. Results are representative of two independent experiments. Scale bar represents 25 µm.

2.3.5. Syk activity is dispensable for nigericin-induced potassium efflux

A novel intracellular potassium sensor, KS6, for improved real-time imaging of potassium dynamics in live cells was developed (**Figure 2-5A**). KS6 is a visible light intensitometric sensor that exhibits excellent response over a wide potassium concentration range (**Figure 2-5B**). Additionally, it is almost completely selective for potassium over other ions, in contrast to the commercially available sensor, PBFI, that has high cross-selectivity for sodium (data not shown; publication in revision). Further, KS6 is rapidly internalized into live cells and is localized to the mitochondria and the cytosol. Further use and characterization of KS6 is found in Chapter 3.

Live cell imaging of potassium dynamics with KS6 revealed that nigericin-induced potassium efflux was bi-phasic (**Figure 2-5C and D**). The first phase of efflux was gradual and proceeded 5-10 minutes after addition of nigericin to the medium. The second phase was rapid and occurred concurrently with morphology indicative of osmotic lysis as visualized by differential interference microscopy (data not shown). Interestingly, nigericin-treated cells displayed a temporal heterogeneity between the onset of the initial potassium efflux phase and the final loss of potassium during cell lysis. This is in agreement with our previous work with an earlier generation of potassium sensor indicating that potassium efflux and caspase-1 activation as indicated by a fluorogenic probe (which rapidly results in cell death) are temporally distinct (Yaron et al.).

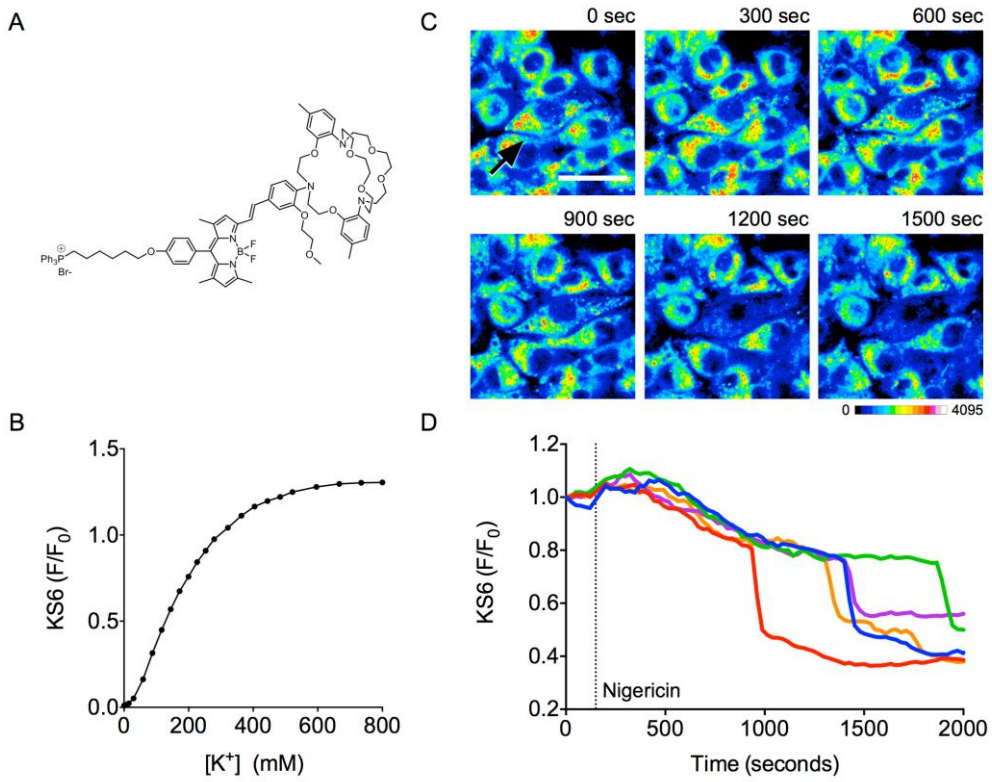

Figure 2-5. Nigericin-induced pyroptosis proceeds by a bi-phasic potassium efflux. (A) Chemical structure of KS6, a live cell intensitometric intracellular potassium sensor. (B) Potassium titration showing emission response of KS6 at 572 nm versus potassium concentration in solution by spectrofluorophotometry. (C) Representative J774A.1 cell (arrow) stained with KS6, then primed for 4 hours with 1 µg/mL LPS and stimulated with 20 µM nigericin followed by continuous imaging. Red indicates high signal intensity and blue indicates low signal intensity. Scale bar represents 25 µm. (D) Single cell potassium traces of example cells exhibiting morphological characteristics of nigericin-induced pyroptosis. Shallow decline in signal indicates the first phase of potassium efflux stimulated by nigericin and sharp decline indicates the second, rapid phase that occurs in parallel with morphology of osmotic lysis.

As both inhibition of potassium efflux with extracellular KCl and inhibition of Syk activity with OXSI-2 resulted in suppression of inflammasome assembly and mROS production, it was next determined if Syk activity had a regulatory role in nigericin-induced potassium efflux. Live cell imaging with KS6 revealed no difference in the kinetics of potassium efflux induced by nigericin treatment in LPS-primed cells with or without Syk inhibition with OXSI-2 (**Figure 2-6**). Taken together, these results indicate that Syk activity occurs upstream of mROS generation, but downstream of potassium efflux during nigericin-induced inflammasome assembly.

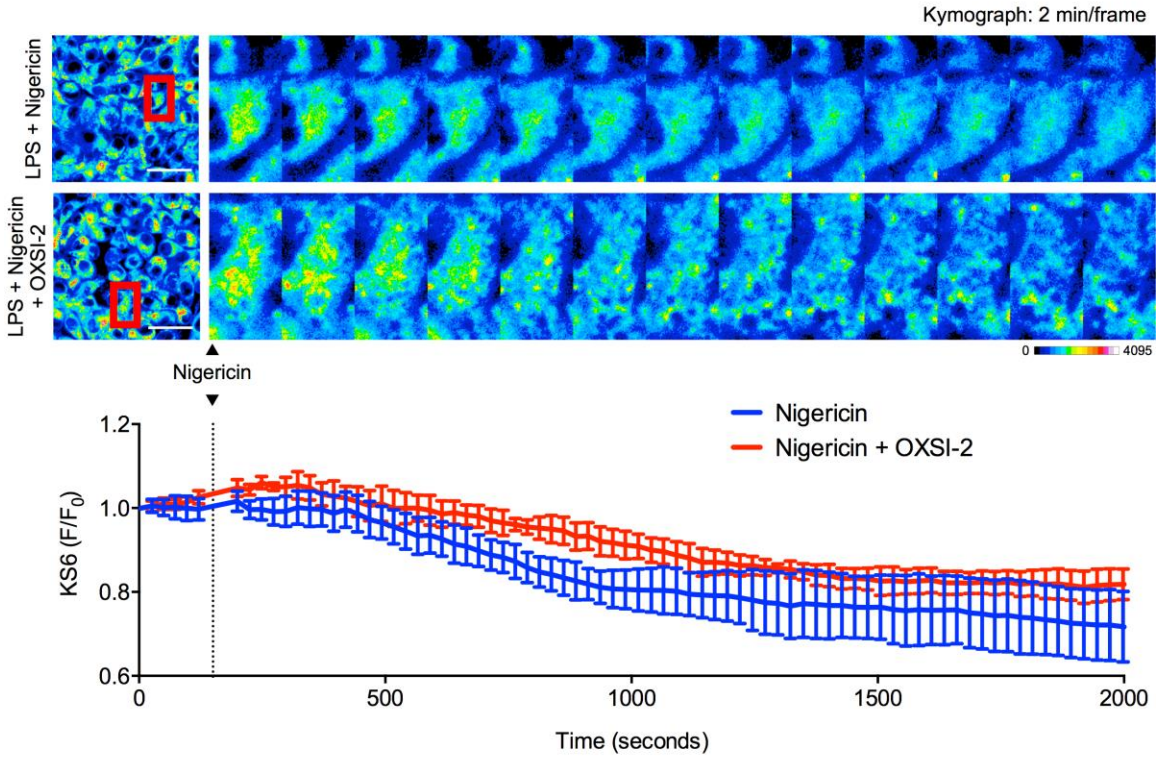

Figure 2-6. Syk activity is dispensable for nigericin-induced potassium efflux. LPS-primed J774A.1 macrophages were loaded with KS6 potassium sensor and stimulated with 20 µM nigericin before continuous imaging by confocal microscopy. Where indicated, cells were treated with 2 µM OXSI-2 for 15-20 minutes prior to nigericin treatment. Red box indicates selected region expanded in kymograph panels. Traces indicated mean and standard deviation of KS6 signal change for 5 cells in a representative field from each condition. Scale bar represents 25 µm. Results are representative of at least two independent experiments.

2.3.6. Potassium efflux is necessary for Syk activation

It was hypothesized that potassium efflux regulates Syk activation during nigericin-induced inflammasome assembly. Quantitative, multiplexed immunoblots of immunoprecipitated Syk probed for total Syk and phospho-tyrosine residues indicated that blockade of potassium efflux with extracellular KCl resulted in a strong suppression of phospho-Syk under conditions that stimulate inflammasome assembly (i.e., LPS priming and nigericin treatment) (**Figure 2-7A**). In agreement with other reports, a time-dependent loss of phospho-Syk signal after the initial stimulus was observed (Hara et al. 2013). Control experiments were performed to determine whether addition of KCl itself was sufficient for suppressing Syk phosphorylation (**Figure 2-7B**). Treatment with nigericin and KCl alone, as well as a combination of nigericin and KCl, was

insufficient for suppressing Syk phosphorylation. These results implicate a need for TLR4-dependent priming with LPS in order to produce conditions wherein Syk phosphorylation is sensitive to potassium efflux. We note that in the J774A.1 macrophage cell line, basal levels of Syk phosphorylation are high (**Figure 2-7A and B**). As this was consistent across all independent experiments, it was concluded that this a characteristic of the J774A.1 cell line and have not been able to find an alternative example in the literature. Indeed, for the conditions used in this experiment, no reports have been published demonstrating basal levels of Syk phosphorylation in un-primed cells (Hara et al. 2013). Two possibilities were postulated regarding the high basal phosphorylation of Syk exhibited by this cell line: (1) apparent phosphorylation is present at sites irrelevant to or inhibitory of inflammasome induction such that aberrant assembly is not triggered; and (2) basal feedback from other kinases in the un-primed cell are toggled concurrently with Syk during LPS priming and post-translationally polarize the cell towards an inflammasome-compatible state.

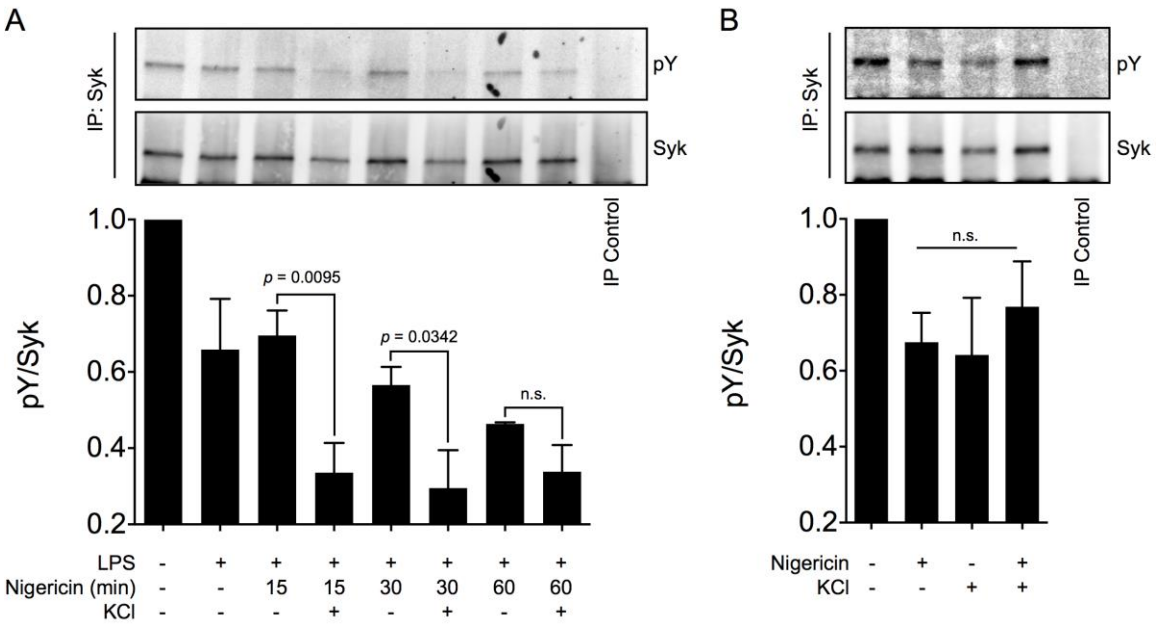

Figure 2-7. Nigericin-induced potassium efflux is required for Syk phosphorylation in LPS-primed J774A.1 cells. (A) J774A.1 mouse macrophages were left untreated or primed for 4 hours with 1 µg/mL LPS before treatment with 20 µM nigericin for the indicated time. 130 mM KCl was added to the medium where indicated. Immunoprecipitation was performed on combined lysates and supernatants with Protein A dynabeads conjugated to total Syk antibody. Multiplexed infrared immunoblots were performed with total Syk and phospho-tyrosine (pY) antibodies. The ratios of pY signal to total Syk were calculated and normalized to untreated controls. (B) J774A.1 cells were left untreated or directly treated with 20 µM nigericin, 130 mM KCl or a combination of both for 15 minutes and processed as described in (A). Values are mean and standard deviation of two independent experiments and *p*-values were calculated using one-way ANOVA with a Fischer's LSD multiple comparison test. IP control indicates total Syk-conjugated Protein A dynabeads left unexposed to collected protein.

2.4. DISCUSSION

Despite significant progress in elucidating mechanisms regulating the NLRP3 inflammasome, an understanding of how functionally and structurally diverse stimuli converge on the same pathway has remained elusive (Sutterwala, Haasken, and Cassel 2014). While most proposed mechanisms for convergent activity of NLRP3 stimuli suggest intermediate regulation by ion flux or oxidative signaling, the mechanism by which these events trigger inflammasome assembly are not well understood (Harijith, Ebenezer, and Natarajan 2014; Horng 2014).

One upstream target for inflammasome regulation is the protein tyrosine kinase Syk. Previous reports have implicated Syk in facilitating NLRP3 inflammasome responses to fungi, mycobacteria, monosodium urate and malarial hemozoin (Gross et al. 2009; Tiemi Shio et al.

2009; Wong and Jacobs 2011). Recent biochemical characterization of Syk activity upstream of the inflammasome identified its role in mediating phosphorylation of a molecular switch on the adapter protein ASC (Hara et al. 2013; Lin et al. 2015). However, the events leading to Syk activation in response to NLRP3 inflammasome stimuli or to what extent it regulates inflammasome activity and pyroptotic cell death have not been identified (Neumann and Ruland 2013; Laudisi, Viganò, and Mortellaro 2014).

The present study focuses on the relationship between potassium ion flux and Syk kinase activity upstream of receptor-independent nigericin induction of the NLRP3 inflammasome. Initial experiments suggested that nigericin-induced NLRP3 inflammasome assembly in LPS-primed J774A.1 mouse macrophage cells was dependent on both potassium efflux and Syk activity. Immunoblot analysis revealed an increase in activated caspase-1 p10 fragment and mature IL-1β in the supernatant of LPS-primed, nigericin-treated cells, both of which were suppressed in the presence of the Syk inhibitor OXSI-2 or 130 mM extracellular KCl. This data was confirmed by the inhibition of IL-1β release as measured by ELISA.

As potassium blockade and OXSI-2 both prevented classical protein processing by the NLRP3 inflammasome, we sought to determine whether this was upstream or downstream of inflammasome assembly. Application of a fluorescent inhibitor of caspase-1 activation (FLICA) revealed a significant production of perinuclear caspase-1 specks in LPS-primed, nigericin-treated cells. Both potassium blockade and OXSI-2 prevented the production of caspase-1 specks as indicated by FLICA labeling, indicating that inhibitory effects were upstream of inflammasome assembly. It was hypothesized that because inhibition of Syk suppressed inflammasome assembly, Syk inhibition might also protect against nigericin-induced pyroptotic cell death. Evaluation of lactate dehydrogenase revealed that Syk played a crucial role in mediating nigericin-induced pyroptosis in LPS-primed J774A.1 cells.

It was next explored whether potassium efflux and Syk regulated mitochondrial ROS generation, since oxidative signaling has been implicated in triggering NLRP3 inflammasome assembly and pyroptosis (Zhou et al. 2010; Harijith, Ebenezer, and Natarajan 2014). Using the mROS probe MitoSOX, it was found that LPS-primed, nigericin-treated cells displayed substantial

MitoSOX oxidation as indicated by an increase in fluorescence. Addition of extracellular KCl or the Syk inhibitor OXSI-2 strongly suppressed MitoSOX fluorescence downstream of nigericin stimulation, suggesting both potassium efflux and Syk activation are upstream of mitochondrial dysfunction. These results contradict the work of Hara et al, that found that inhibition of Syk kinase did not suppress nigericin-induced MitoSOX oxidation (Hara et al. 2013). It is not clear why Hara and colleagues were unable to inhibit mROS generation upon Syk inhibition, but one possibility is methodological differences. In the Hara et al study, LPS-primed peritoneal macrophages were incubated in nigericin and MitoSOX simultaneously for 20 minutes. LPS priming induces TLR4-dependent mROS generation and thus MitoSOX fluorescence will increase as soon as it is added to the cells (Yuan et al. 2013). In the current study, MitoSOX is added after a period of nigericin treatment and an induced increase in mROS may be detectable due to lower background signal from LPS-induced mROS generation alone.

As the effects of potassium blockade and Syk inhibition appeared to closely correlate, it was sought to define a relationship between potassium efflux and Syk activation. KS6, a novel intracellular potassium probe that allows for highly selective, real-time, intensitometric determination of potassium content in live cells, was applied to determine the effects of Syk inhibition on nigericin-induced potassium efflux. Results indicate that Syk inhibition has no effect on the dynamics of nigericin-induced potassium efflux, suggesting that Syk activity is downstream of and dispensable for potassium efflux. Immunoprecipitation of Syk revealed a dynamic phosphorylation pattern downstream of nigericin treatment, with blockade of potassium efflux consistently suppressing Syk phosphorylation under NLRP3 inflammasome-inducing conditions. To confirm that the effects were not due to off-target effects of high extracellular KCl, control experiments were performed in the presence of KCl-supplemented medium without LPS priming and found no effect on Syk phosphorylation. These results suggest that LPS priming toggles Syk to a state that is amenable to inflammasome-promoting activation but requires potassium efflux.

The current study provides the first example of potassium efflux inducing the activation of an intermediate signaling partner in the NLRP3 inflammasome pathway. A model is proposed wherein potassium efflux activates Syk tyrosine kinase by an as-yet unknown mechanism,

resulting in mitochondrial destabilization and mROS generation to trigger the NLRP3 inflammasome and pyroptotic cell death (**Figure 2-8**). Whether Syk directly activates the inflammasome by phosphorylation of ASC, or if an oxidative environment produced by mitochondrial destabilization is required is not clear and warrants further study. Additionally, further application of KS6 to evaluate rapid ion flux dynamics may provide additional information regarding intracellular ionic composition and rapidly responding properties of the NLRP3 signaling pathway. Compan et al proposed that NLRP3 undergoes potassium-dependent conformational changes that are necessary for inflammasome activation during osmotic strength-induced regulatory volume decrease (Compan et al. 2012). It would be interesting to visualize the real-time kinetics of potassium efflux and conformational changes in NLRP3 coupled with pharmacological inhibition or genetic deletion of putative intermediate regulatory partners to determine whether active regulation or passive, ion concentration-dependent processes are involved.

The finding that Syk regulates inflammasome assembly, pro-inflammatory cytokine secretion and pyroptotic cell death is promising for modulating innate immune system-driven inflammatory processes. This is supported by the current popularity of developing therapeutic Syk inhibitors for addressing inflammatory and autoimmune pathologies, many of which are now involved in clinical and pre-clinical trials (Weinblatt et al. 2008; Bajpai 2009; Morales-Torres 2010; Genovese et al. 2011). The novel finding that potassium efflux regulates Syk activation may provide a new avenue for modulating Syk-dependent inflammatory pathologies by targeting channels and processes that regulate ion homeostasis.

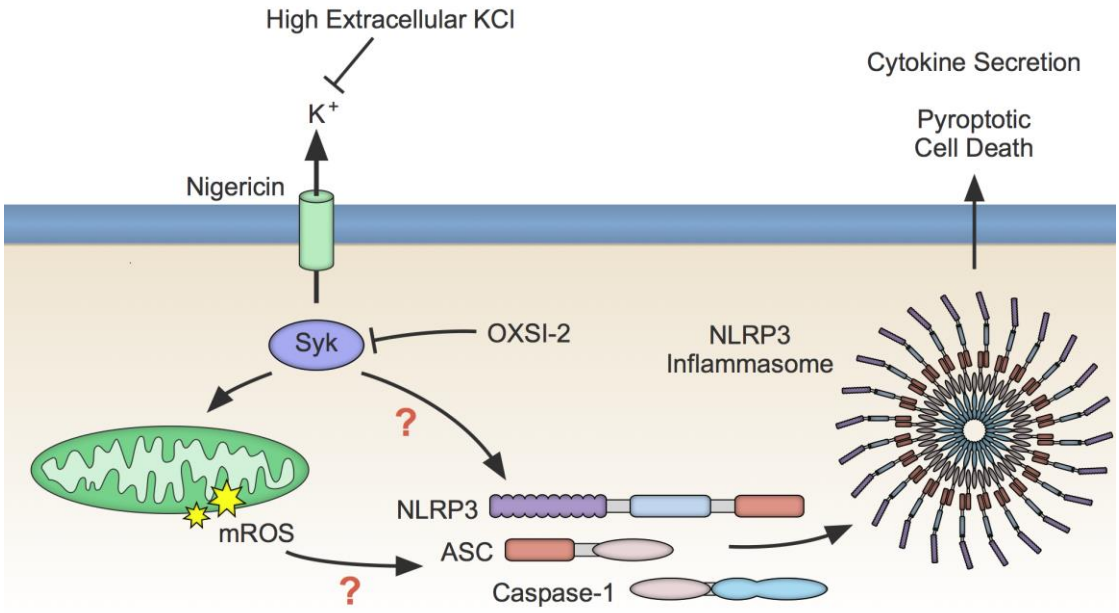

Figure 2-8. Overview of a proposed model for ion flux-driven, Syk-dependent regulation in NLRP3 inflammasome signaling. mROS generation has been implicated in regulating the assembly of the inflammasome. Our results show that potassium efflux and Syk activity are required for mROS generation induced by nigericin treatment. Accordingly, potassium blockade and Syk inhibition prohibit inflammasome assembly, pro-inflammatory cytokine secretion and pyroptotic cell death. Live cell imaging revealed that Syk was downstream and dispensable for nigericin-induced potassium efflux and subsequent analysis found that Syk activity was regulated by depletion of intracellular potassium by nigericin treatment.

CHAPTER 3: K+ REGULATES CA2+ TO DRIVE INFLAMMASOME SIGNALING

3.1. INTRODUCTION AND BACKGROUND

Proposed mechanisms for regulating the activation of the NLRP3 inflammasome pathway are varied and controversial (Sutterwala, Haasken, and Cassel 2014). Among the most popular proposed mechanisms is the flux of cellular ions. The asymmetric distribution of ions in cellular compartments establishes a gradient such that, under conditions of membrane permeability, ions rapidly diffuse across the gradient with little energy input (Dubyak 2004). As such, cells benefit from asymmetric ion distribution to affect rapid processes such as neuronal action potentials (Dubyak 2004). Recent work has implicated potassium flux as the common trigger in regulating NLRP3 inflammasome activity (Muñoz-Planillo et al. 2013). Indeed, it has been understood for over two decades that potassium flux regulates the processing of IL-1β (Perregaux and Gabel 1994; Walev et al. 1995). While potassium is the most commonly studied ion posited to regulated the NLRP3 pathway, calcium flux has gained popularity in recent years because intervention in calcium mobilization has inhibitory effects on inflammasome activity (Lee et al. 2012; Murakami, Ockinger, Yu, Byles, et al. 2012; Horng 2014). Both ions are permeant to the non-specific cation channel formed by plasma membrane expressed $P2X_7$ purinergic receptors, which are activated by external ATP. However, it is currently not known how the two ions relate to each in the context of inflammasome regulation (Horng 2014; Sutterwala, Haasken, and Cassel 2014).

In addition to ion flux, mitochondrial reactive oxygen species (mROS) signaling has been proposed as a critical regulator of NLRP3 activation (Zhou et al. 2011). Mitochondrial dysfunction and loss of mitochondrial membrane potential leads to a rapid increase in mROS production, which has been described to activate the inflammasome through the activity of thioredoxin-interacting protein (TXNIP) (Zhou et al. 2010). In support of this mechanism, most known NLRP3-activating stimuli induce ROS generation and specific mitochondria-targeted ROS scavengers have been shown to inhibit inflammasome assembly (Heid et al. 2013). The existence of a convergent pathway involving ion flux, particularly of potassium, and ROS generation in triggering

the assembly of the inflammasome has been suggested, however such a link has remained elusive (Petrilli et al. 2007; Tschopp 2011).

In this study the hypothesis was tested that $P2X_7$ purinergic receptor activation with extracellular ATP induces mitochondrial ROS generation and this effect is mediated by intracellular and mitochondrial potassium depletion. A novel intracellular potassium sensor was applied to characterize the real-time dynamics of potassium mobilization in the mouse macrophage cell line J774A.1 after stimulation with ATP. By co-localizing the sensor signal to mitochondria using mitochondria-specific dyes, a $P2X_7$-dependent mitochondrial potassium depletion that was sensitive to pharmacological and ionic inhibition was observed. Temporally, mitochondrial potassium mobilization occurred before potassium efflux-dependent mitochondrial ROS generation. Further study identified a critical role for calcium influx upstream of mitochondrial ROS generation, inflammasome assembly and pro-inflammatory cytokine release. The first-ever multiplexed imaging of intracellular potassium and calcium in live cells was performed and found that potassium efflux was required for sustained calcium influx, while calcium chelation had no effect on the kinetics of potassium efflux. It is proposed that mitochondrial ROS generation is a downstream effect of potassium efflux-dependent calcium influx and defines a coordinated, ion flux-driven regulation of the NLRP3 inflammasome via oxidative signaling.

3.2. MATERIALS AND METHODS

3.2.1. Cell culture

The mouse macrophage cell line J774A.1 (TIB-67™) was obtained from ATCC (Manassas, VA, USA) and cultured in DMEM containing 10% FBS, 100 U/mL penicillin and 100 µg/mL streptomycin (Gibco, Grand Island, NY) at 37 °C with 5% CO2 in a humidified atmosphere. Cells were passaged by scraping and viability and density were assessed by Trypan Blue dye exclusion on a Countess® automated cell counter (Life Technologies, Grand Island, NY).

3.2.2. KS6 potassium sensor loading

KS6 (ex/em 561/630 nm) was kept in a 1 mM DMSO stock solution stored at 4 °C. To facilitate consistent dye distribution, stock KS6 was combined 1:1 with 10% Pluronic F127 and mixed thoroughly by pipetting before loading (Cohen et al. 1974). The mixture was added 1:100 to each well of a chamber slide for a final KS6 concentration of 5 µM and incubated for 30-60 minutes at 37 °C. Where indicated, cells were subsequently stained with 10 nM MitoTracker Green FM (Life Technologies, Grand Island, NY, USA). KS6 was developed in-house (Center for Biosignatures Discovery Automation, Tempe, AZ, USA).

3.2.3. Live-cell imaging

Cells seeded in an 8-chamber µ-slide (Ibidi, Verona, WI, USA) were primed with 1 µg/mL E. coli O111:B4 LPS (Sigma Aldrich, St. Louis, MO, USA) for 2-4 hours. Samples were imaged on a Nikon Ti microscope equipped with a C2si confocal scanner (Nikon Instruments, Melville, NY, USA) and Tokai Hit stage-top incubator (Tokai Hit Co., Shizuoka, Japan). Excitation laser lines were 408, 488, 561 and 639 nm and emission was collected by photomultipliers filtered for the standard DAPI, FITC, TRITC, and Cy5 bandwidths. Objectives used were 20× air 0.75 NA, 60× oil immersion 1.4 NA or 60× water immersion 1.2 NA, all from Nikon. Where indicated, cells were imaged in the presence of 5 µM TO-PRO-3 (Life Technologies, Grand Island, NY, USA). For calcium imaging, cells were loaded with 1× Fluo-4 DIRECT solution (Life Technologies, Grand Island, NY, USA) and incubated for 30-60 minutes prior to imaging.

3.2.4. Immunofluorescence

Cells seeded in an 8-chamber µ-slide were primed for 4 hours with 1 µg/mL E. coli O111:B4 LPS. Cells were additionally treated with the caspase-1 inhibitor ac-YVAD-CHO (50 µM) for the last 30 minutes of priming to inhibit cell detachment downstream of inflammasome assembly. For inflammasome stimulation, cells were treated with 3 mM ATP for 1 hour. Cells were fixed with 4% formaldehyde solution prepared in PBS from powdered paraformaldehyde, permeabilized in

0.25% Triton X-100 in PBS and blocked in 0.25% Triton X-100 in PBS containing 5% BSA at room temperature. Polyclonal rabbit Caspase-1 p10 antibody (#SC-514, Santa Cruz Biotechnology, Dallas, TX) was added 1:100 overnight at 4 °C. Secondary antibody, AlexaFluor 488-conjugated goat-anti-rabbit secondary antibody (Life Technologies, Grand Island, NY, USA), was added 1:1000 at room temperature and for 1 hour. DAPI solution was added using NucBlue Fixed (Life Technologies, Grand Island, NY, USA) according to manufacturer's instructions in PBS. Samples were covered with 150 µL mounting medium (90% glycerol, 10% (10X) PBS with 0.01% NaN_3) and kept at 4 °C until imaging. Inflammasome images were obtained as 0.5-1 µm z-stacks and presented as maximum intensity projections. Samples were prepared with assistance from Mounica Rao.

3.2.5. Caspase-1 FLICA Assay

J774A.1 were seeded at a density of 1-2 x 10^5 per well in 200 µL of complete DMEM and grown overnight. The following day cells were primed for 4 hours with 1 µg/mL E. coli O111:B4 LPS. During the last hour of priming cells were loaded with 1× FAM-YVAD-FMK (Caspase-1 FLICA; Immunochemistry Technologies, Bloomington, MN, USA) and 10 µg/mL Hoechst 33342 in complete medium. Additional inhibitors as indicated were added during the last 15-20 minutes of priming. Cells were stimulated with 3 mM ATP for 30 minutes, subsequently washed 2× with warm DMEM and fixed in 2% formaldehyde solution for 10 minutes at room temperature. Cells were washed 1× with PBS and submerged in 200 µL mounting medium (90% glycerol in PBS and 0.1% NaN_3). Samples were imaged by laser-scanning confocal microscopy as a series of 0.5 µm z-stacks on a Nikon Ti microscope equipped with a Nikon C2si confocal scanner controlled by the Nikon Elements AR software. Stacks were prepared as maximum intensity projections using ImageJ/FIJI. Caspase-1 FLICA was excited at 488 nm and emission was collected in the FITC channel while Hoechst 33342 was excited at 408 nm and emission was collected in the DAPI channel. Samples were prepared with assistance from Mounica Rao.

3.2.6. Lysate and supernatant protein collection

Cells were seeded in 6-well plates (10^6 cells/well) and primed for 4 hours with 1 µg/mL E. coli O111:B4 LPS in complete DMEM containing 10% FBS. After priming, cells were washed 1× with serum-free DMEM and 1.1 mL of warm serum-free DMEM was added to each well. Where noted, cells were treated with inhibitors for 15-30 minutes. Inflammasome activation was triggered by application of freshly prepared 3 mM ATP solution in serum-free DMEM for 30 minutes. After stimulation, supernatants were collected and spun at 14,000 g for 15 minutes at 4 °C to remove cellular debris and approximately 1 mL was transferred to fresh 1.5 mL tubes. Ten µL of StrataClean resin (Agilent, Santa Clara, CA) was added to each supernatant, mixed well and placed on a rotator in a 4 °C refrigerator for 1 hour. Concentrated supernatant protein was collected by pelleting the StrataClean resin, removing the supernatant and heating the resin resuspended in 50 µL 1× Laemmli buffer at 95 °C for 5 minutes. Cell lysates were prepared by addition of 100 µL hot 1× Laemmli buffer to each well for 5-10 minutes, scraping and transferring samples to 1.5 mL tubes and heating at 95 °C for 5 minutes. Samples were prepared with assistance from Mounica Rao.

3.2.7. Immunoblotting

Twelve µL of concentrated supernatant or lysate was separated on 4-12% Mini-Protean TGX gels (Bio-Rad, Hercules, CA) at 100V for 1 hour. Proteins were transferred to 0.2 µm nitrocellulose membranes (LiCor, Lincoln, NE) at 100V for 1 hour, and subsequently blocked in 5% non-fat dry milk in PBS containing 0.2% Tween-20 for 1 hour. Blocked membranes were incubated in 5% BSA in PBS containing 0.2% Tween-20 and either 1:500 rabbit polyclonal against Caspase-1 p10 (#SC-514, Santa Cruz) or 1:1000 goat polyclonal against IL-1β (#AF-401-NA, R&D Systems, Minneapolis, MN) and rotated overnight at 4 °C. The following day, donkey anti-goat IRDye® 800CW and goat anti-rabbit IRDye® 680RD secondary antibodies (Li-Cor, Lincoln, NE) were applied at a dilution of 1:15000 with rocking for 1 hour at room temperature. Membranes were

imaged on a Li-Cor Odyssey CLx on auto exposure with high quality setting. Samples were prepared with assistance from Mounica Rao.

3.2.8. Lactate Dehydrogenase release assay

Cells were seeded in 96-well plates and primed for 4 hours with 1 µg/mL E. coli O111:B4 LPS. Cells were treated for the last 15-30 minutes with 500 µM MitoTEMPO and stimulated for 30 minutes with 3 mM ATP. Fifty µL of supernatant was used for LDH activity assay with the CytoTox96 Non-Radioactive Cytotoxicity Kit (Promega, Madison, WI) according to manufacturer's instructions.

3.2.9. ELISA

J774A.1 cells were seeded in 96 well plates at a concentration of 10^5 cells/well and incubated overnight. Cells were primed for 4 hours with 1 µg/mL E. coli O111:B4 LPS and subsequently stimulated for 30 minutes with 3 mM ATP in 100 µL medium. Where indicated, cells were treated with 100 µM BAPTA-AM (Tocris, Minneapolis, MN, USA) for 15 minutes prior to ATP treatment. Supernatants were collected and released IL-1β was evaluated with ELISA using the R&D Systems DuoSet kit according to the manufacturer's protocol. Developed plates were read on a Biotek Synergy H4 mutli-mode plate reader with Gen5 software.

3.2.10. Statistical analysis

Statistics were performed where indicated with GraphPad Prizm version 6.05 (GraphPad, La Jolla, CA, USA) and procedures for each analysis are described in the figure captions.

3.3. RESULTS

3.3.1. $P2X_7$ receptor-dependent potassium efflux induces the inflammasome in J774A.1 macrophages

The response of the J774A.1 mouse monocyte/macrophage cell line to extracellular ATP was determined first. As expected, immunoblotting indicated that untreated J774A.1 lack proIL-1β while maintaining constitutive levels of procaspase-1 (**Figure 3-1A**). Upon priming with E. coli LPS, proIL-1β protein becomes highly expressed. Release of active caspase-1 p10 and mature IL-1β p17 was detected in concentrated supernatants of LPS-primed J774A.1 after treatment with 3 mM extracellular ATP. The release of both active components was abolished in the presence of high extracellular potassium (to suppress the intracellular-extracellular concentration gradient) as well as the selective, competitive, $P2X_7$ receptor antagonist A438079 (D.W. Nelson et al. 2006). The requirement for potassium efflux in inflammasome-mediated pyroptotic cell death was confirmed by propidium iodide staining and live cell imaging (**Figure 3-1B**). Combined LPS and ATP treatment resulted in a time-dependent accumulation of cells positive for propidium iodide that was inhibited in the presence of 130 mM extracellular potassium. Further, immunofluorescence revealed the assembly of the inflammasome as indicated by the presence of classical perinuclear caspase-1 specks that were suppressed by high extracellular potassium and treatment with A438079 (**Figure 3-1C**). Thus, J774A.1 exhibit the 1st/2nd signal (LPS priming and ATP stimulation, respectively) behavior representative of the potassium efflux-dependent inflammasome pathway in macrophages.

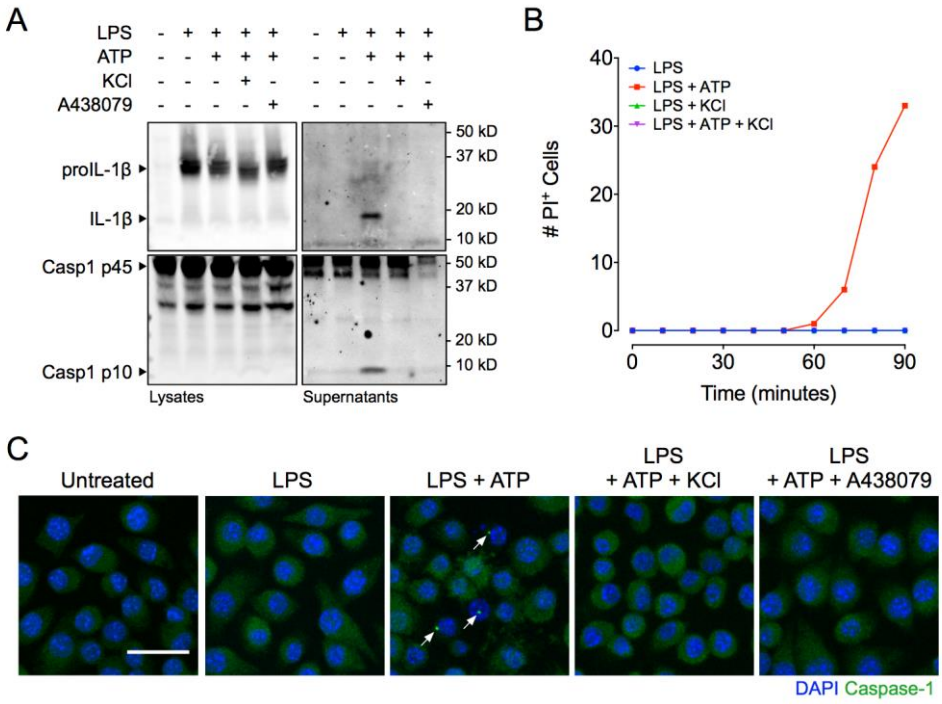

Figure 3-1. P2X$_7$-induced potassium efflux regulates NLRP3 inflammasome assembly and pyroptotic cell death. (A) Immunoblot analysis of procaspase-1 p45 and activated p10 fragments, and proIL-1β (34 kD) and mature (17 kD) fragments in the lysates and concentrated supernatants of J774A.1 primed for 4 hours with 1 µg/mL LPS and stimulated with 3 mM ATP for 30 minutes with or without addition of 130 mM extracellular KCl or 25 µM of the P2X$_7$ antagonist A438079. (B) Time-resolved uptake of propidium iodide in J774A.1 primed with LPS for 4 hours and stimulated with ATP in the presence or absence of 130 mM extracellular KCl. (C) Immunofluorescence for caspase-1 (green) in J774A.1 untreated or primed for 4 hours with 1 µg/mL LPS and subsequently stimulated with 3 mM ATP for 30 minutes with or without 130 mM extracellular KCl or 25 µM A438079. Arrows: caspase-1 specks indicative of inflammasome assembly. Scale bar represents 50 µm. Nuclei are stained with NucBlue Fixed DAPI solution (blue).

3.3.2. ATP-induced calcium influx regulates the NLRP3 inflammasome

The role of ATP-induced calcium influx on inflammasome activation was determined next. Previous study has shown that intracellular calcium chelation with BAPTA-AM suppresses IL-1β processing and release upon ATP-induced inflammasome activation (Lee et al. 2012). In agreement with this observation, it was found that BAPTA-AM significantly suppressed ATP-induced IL-1β processing and release as indicated by ELISA in J774A.1 cell supernatants (**Figure 3-2A**). It has not yet been reported whether calcium chelation suppresses IL-1β processing and release upstream or downstream of inflammasome assembly, though some reports propose a possible calcium influx-dependent lysosomal exocytosis pathway for IL-1β

release (Bergsbaken et al. 2011). The caspase-1-specific fluorescent inhibitor of caspase activation (FLICA; FAM-YVAD-fmk) was used to observe ATP-induced inflammasome assembly as indicated by perinuclear caspase-1 specks (**Figure 3-2B**). While stimulation with 3 mM ATP resulted in substantial perinuclear caspase-1 speck appearance indicative of inflammasome assembly, chelation with BAPTA-AM completely inhibited any indication of inflammasome formation. These results suggest that calcium influx regulates ATP-induced NLRP3 activation upstream of inflammasome formation.

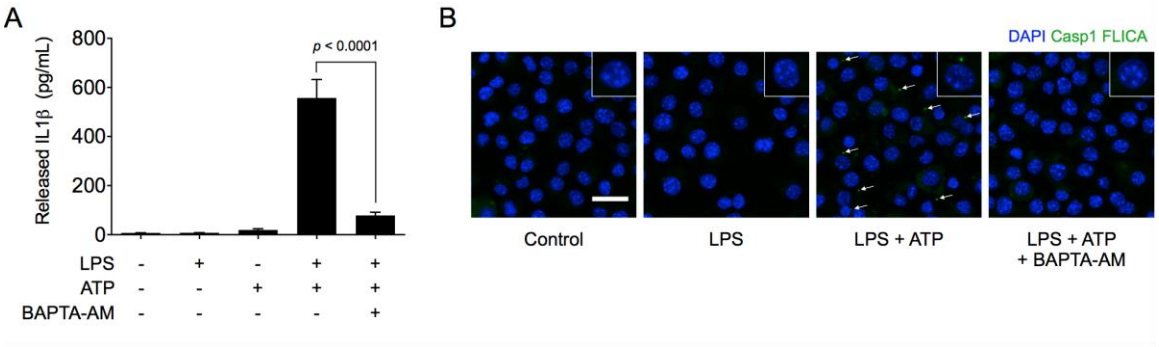

Figure 3-2. Calcium influx is an upstream regulator of IL-1β release and NLRP3 inflammasome assembly. (A) ELISA analysis of released IL-1β from J774A.1 primed with 1 µg/mL LPS for 4 hours and stimulated with 3 mM ATP for 30 minutes. Where indicated, cells were pretreated with 100 µM BAPTA-AM prior to addition of ATP. Statistics were calculated by one-way ANOVA with Tukey's post-hoc and represent the mean and standard error of two independent experiments. (B) Cells were prepared as in (A), except for the addition of caspase-1 FLICA 1 hour prior to the addition of ATP. Arrows point to perinuclear caspase-1 specks. Green fluorescence indicates caspase-1 FLICA signal and blue fluorescence indicates Hoechst 33342 stained DNA. Scale bar represents 25 µm. Results are representative of two independent experiments.

3.3.3. Direct visualization of potassium mobilization in macrophages with a novel intracellular sensor

In order to better understand the intracellular potassium dynamics triggered by ATP-induced NLRP3 inflammasome activation, KS6, a novel intracellular potassium sensor was used (**Figure 3-3A**). As briefly described in Chapter 2, KS6 has improved sensitivity and selectivity compared to PBFI, the only currently, commercially available potassium sensor **(Figure 3-3B**). As KS6 is functionalized with a triphenylphosphonium group for enrichment in the mitochondria, we first

confirmed the sensor localization in J774A.1 cells. Live-cell imaging revealed a strongly enriched signal from KS6 in the mitochondrial matrix as verified by co-staining with MitoTracker Green FM (**Figure 3-3C-F**). As observed for other cell lines, a portion of KS6 signal was localized to the cytosol (approximately 20% by co-localization analysis). Thus, KS6 enriches in the mitochondria as expected and is available for detection of cytosolic and mitochondrial potassium content.

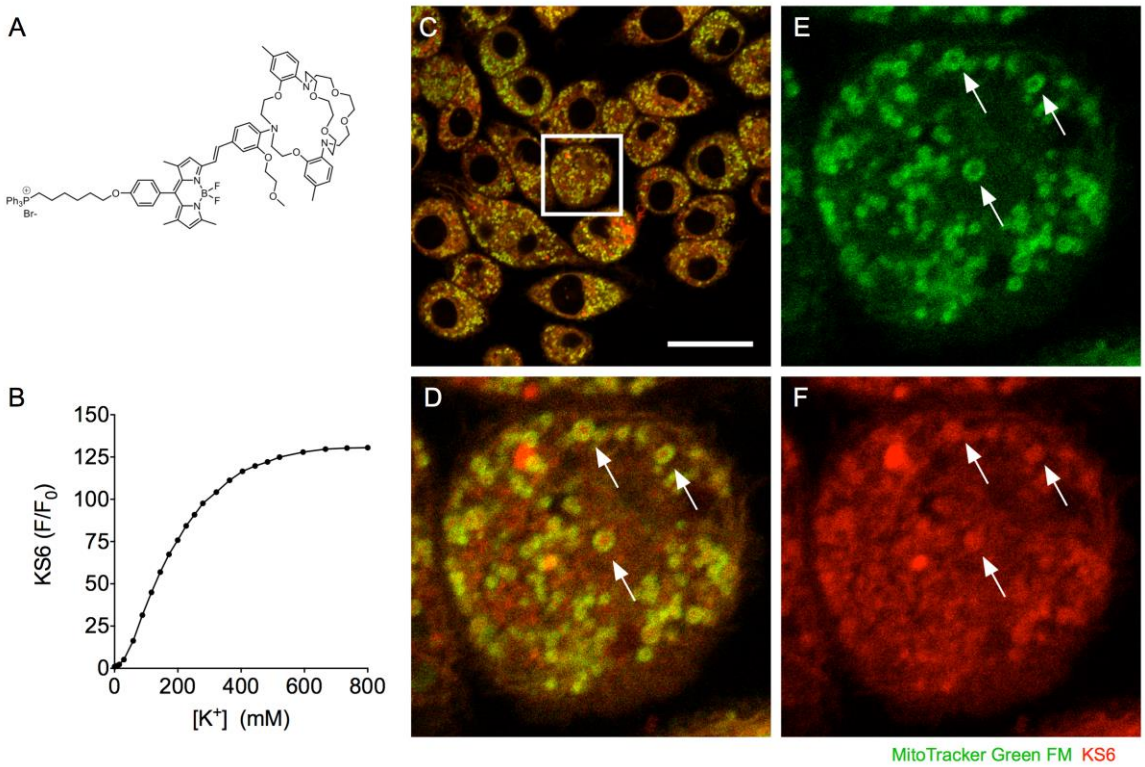

Figure 3-3. KS6 localizes to the mitochondria and the cytosol in live cells. (A) Chemical structure of the intracellular potassium sensor KS6. (B) Spectrofluorophotometric characterization of KS6 signal response to potassium titration in solution. (C) J774A.1 were stained with KS6 intracellular potassium sensor and MitoTracker Green FM prior to imaging by confocal microscopy. (D) Inset of boxed region from (C) displaying the overlap of MitoTracker Green FM and KS6. (E) Signal from MitoTracker Green FM. (F) Signal from KS6. Arrows indicate discrete mitochondria clearly stained for both probes. Scale bar represents 25 µm. KS6 structure and titration were provided by Xiangxing Kong.

It was next confirmed that whole-cell KS6 signal responds to ATP-induced $P2X_7$ activation. $P2X_7$ engagement results in the opening of a non-specific cation pore and potassium efflux across the intracellular-extracellular potassium concentration gradient (Yan et al. 2008). This response was probed by demonstrating a live cell titration between physiologically normal (130 mM) and intermediate (50 mM) concentrations of additional extracellular potassium (**Figure**

3-4A). Next, whether differing concentrations of extracellular ATP would result in a dose-dependent opening of the $P2X_7$ pore and concomitant potassium efflux was tested, as recently reported for membrane permeability (Ursu et al. 2014). A dose-dependence of both potassium efflux and membrane permeability was observed as indicated by the response of KS6 and uptake of the membrane impermeable DNA dye TO-PRO-3, respectively (**Figure 3-4B and C**). Both events were dependent on $P2X_7$ activity as inhibition with A438079 suppressed both events (**Figure 3-5**). Importantly, the single cell microscopic data confirm previous reports that the approximate threshold for potassium concentration required for ATP-induced inflammasome activity is approximately 50-60% of basal levels, corresponding to a total cellular potassium concentration of about 60-80 mM. Taken together, these experiments confirm that KS6 is an effective sensor for direct visualization of $P2X_7$-dependent intracellular potassium dynamics in live macrophages.

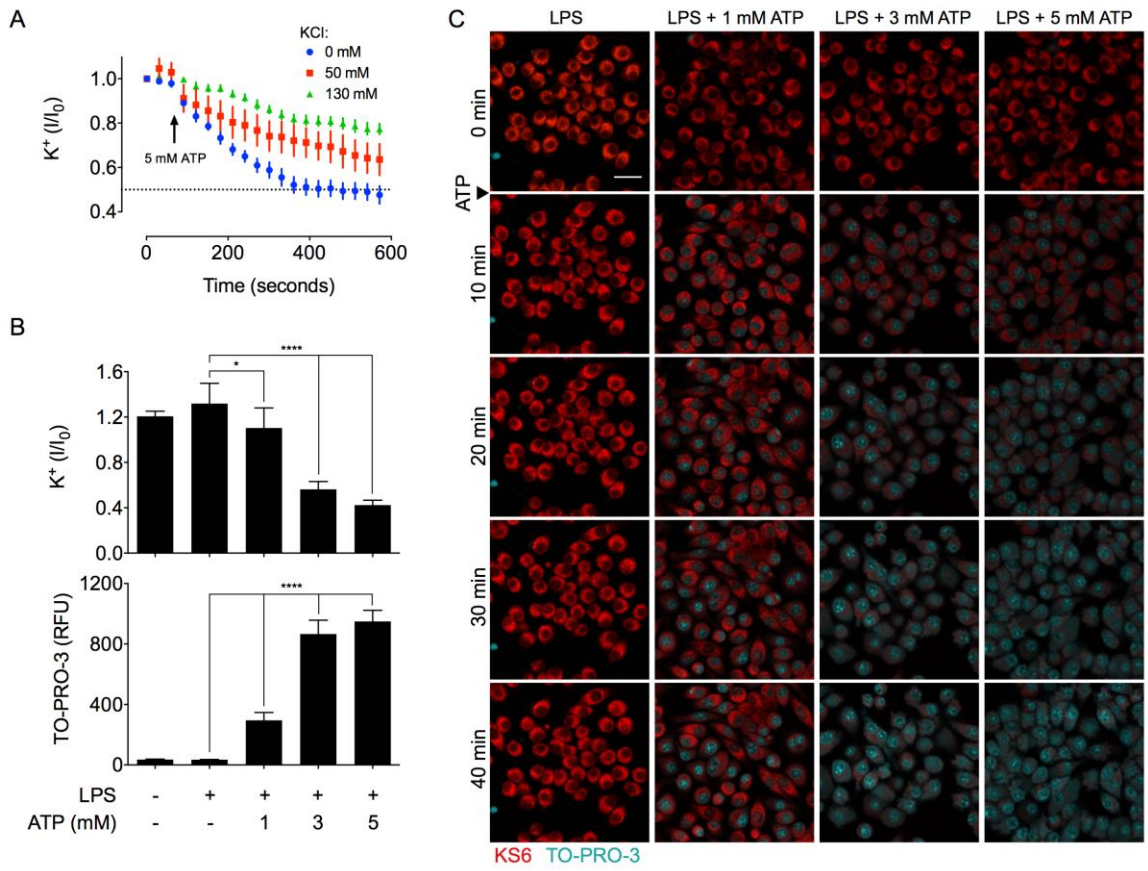

Figure 3-4. Real-time intracellular potassium dynamics observed with KS6. (A) Kinetic trace of potassium efflux from J774A.1 cells stimulated with 5 mM ATP at the indicated time point in the presence of 0 mM additional KCl (normal DMEM medium), 50 or 130 mM additional extracellular KCl. Traces represent the mean and standard deviation of 10-20 cells in each field. (B) Response at 40 minutes of potassium efflux (top panel) or TO-PRO-3 uptake (bottom panel) of J774A.1 primed for 4 hours with 1 µg/mL LPS and treated with 1, 3 or 5 mM extracellular ATP. Bars represent mean and standard deviation of 20 cells in each condition. Statistics were performed by one-way ANOVA with Fischer's LSD comparison test. *p<0.05 and ****p<0.0001 (C) Representative fields at the indicated time-points of LPS-primed J774A.1 loaded with KS6 (red) and treated with 1, 3 or 5 mM extracellular ATP in the presence of TO-PRO-3 (cyan). Scale bar represents 50 µm.

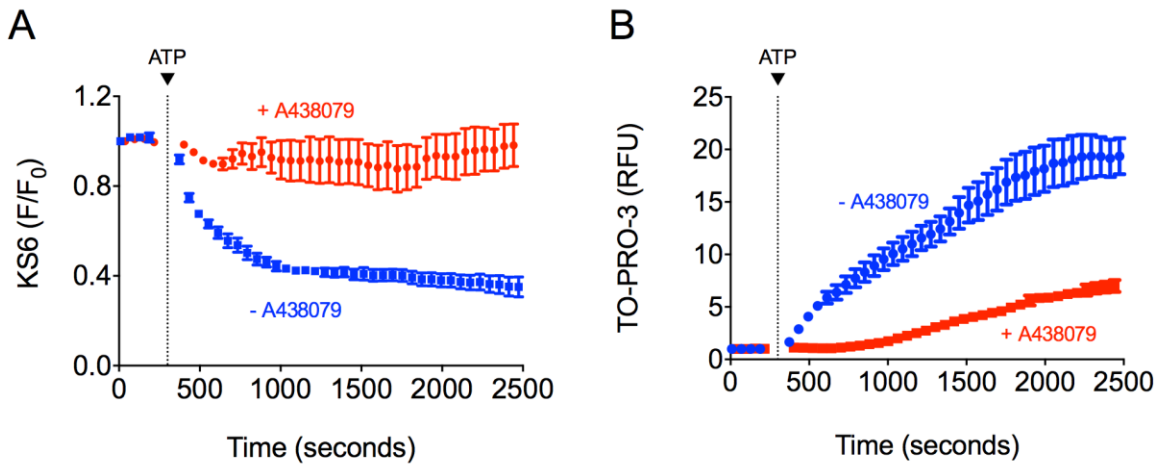

Figure 3-5. ATP-induced potassium efflux and membrane permeability are $P2X_7$-dependent. Potassium efflux visualized using KS6 (A) or membrane permeability as indicated by the uptake of membrane-impermeant TO-PRO-3 (B) are inhibited in LPS-primed, ATP-stimulated J774A.1 macrophages when treated with the $P2X_7$ inhibitor A438079. Traces represent mean and standard error for 5 representative cells.

3.3.4. Extracellular ATP mobilizes mitochondrial potassium downstream of $P2X_7$ engagement

Mitochondrial potassium represents a significant portion of total cellular potassium, as its concentration is nearly twice (200-300 mM) that of the cytosol (100-150 mM) (Nolin et al. 2013). Because extracellular ATP is detected at plasma membrane-localized $P2X_7$ receptors resulting in cytosolic potassium efflux, it was next determined if the mitochondrial potassium pool was mobilized by macrophage purinergic signaling. KS6 was co-localized with MitoTracker Green FM to observe the kinetics of mitochondrial potassium in live J774A.1 cells (**Figure 3-6**). Real-time monitoring of KS6 signal during $P2X_7$ engagement with 3 mM extracellular ATP revealed both cytosolic and mitochondrial potassium depletion. The depletion of cytosolic and mitochondrial potassium was suppressed by 130 mM extracellular potassium or by inhibition of $P2X_7$ with A438079. Notably, the loss of potassium occurred prior to the shrinking and disintegration morphology indicative of mitochondrial damage.

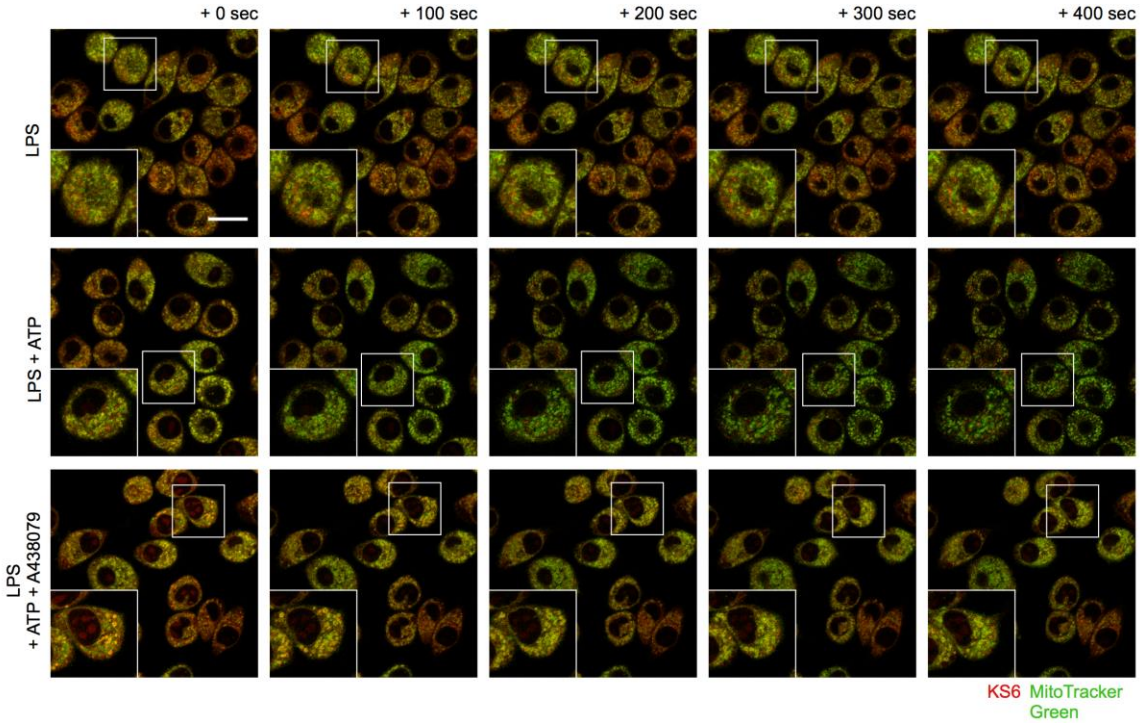

Figure 3-6. $P2X_7$ activation results in mitochondrial potassium mobilization. J774A.1 cells were primed for 4 hours with 1 µg/mL LPS and loaded with 5 µM KS6 (red) and 10 nM MitoTracker Green FM (green). Real-time confocal microscopy was performed to track the potassium dynamics after stimulation with 3 mM extracellular ATP with or without the $P2X_7$ inhibitor A438079. Results revealed a rapid, receptor-dependent mobilization of potassium as indicated by a reduction in KS6 signal in the co-localized space with MitoTracker Green FM that was sensitive to inhibition with A438079. Subsequent to the mobilization, mitochondria appeared to fragment. Fields are representative of at least 3-5 experiments. Scale bar represents 20 µm.

3.3.5. Mitochondrial reactive oxygen species are essential for pyroptosis in J774A.1 macrophages

It was next determined if mitochondrial ROS (mROS) was necessary for the assembly and function of the inflammasome. LPS-primed J774A.1 were treated with ATP with and without pre-treatment with the mitochondria-localized reactive oxygen scavenger MitoTEMPO. Previous studies have shown that MitoTEMPO is effective in inhibiting pyroptosis and release of IL-1β (Heid et al. 2013). Here, it is shown that the assembly of the inflammasome speck, as indicated by immunofluorescence for caspase-1, is strongly inhibited in the presence of MitoTEMPO (**Figure 3-7A**). The role of mROS in inflammasome function was further validated by demonstrating an inhibition of caspase-1 p10 and IL-1β p17 processing and release when cells are treated with ATP in the presence of MitoTEMPO as detected by immunoblotting (**Figure 3-**

7B). Lastly, it was demonstrated that pyroptotic cell death requires mROS by measurement of lactate dehydrogenase activity in cell supernatants (**Figure 3-7C**). These results demonstrate the need for mROS in the assembly and activity of the inflammasome.

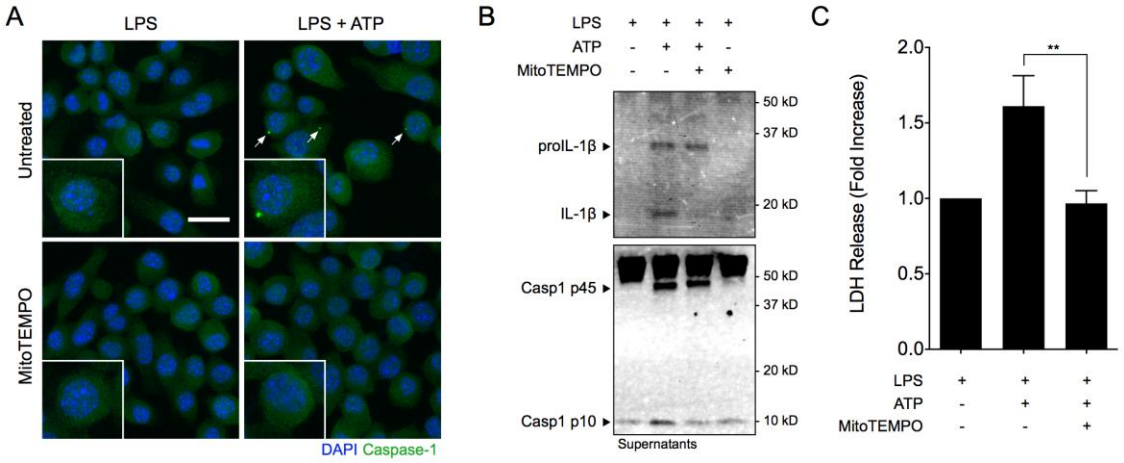

Figure 3-7. Mitochondrial ROS is essential for ATP-evoked inflammasome activity in J774A.1 cells. (A) Immunofluorescence for caspase-1 (green) in J774A.1 primed for 4 hours with 1 µg/mL LPS and subsequently stimulated with 3 mM ATP for 30 minutes with or without 500 µM MitoTEMPO treatment. Arrows point to caspase-1 specks indicative of inflammasome assembly. Scale bar represents 20 µm. Nuclei are stained with NucBlue Fixed DAPI solution (blue). (B) Immunoblot analysis of pro-caspase-1 p45 and activated p10 fragments, and proIL-1β (34 kD) and mature (17 kD) fragments in the lysates and concentrated supernatants of J774A.1 primed for 4 hours with 1 µg/mL LPS and stimulated with 3 mM ATP for 30 minutes with or without pretreatment with 500 µM MitoTEMPO. (C) Assessment of lactate dehydrogenase (LDH) activity in the supernatants of J774A.1 primed with 1 µg/mL LPS and stimulated with ATP for 30 minutes with or without pretreatment with 500 µM MitoTEMPO. Results are fold-change versus LPS primed cells and error bars represent standard error of two independent experiments. ***p*<0.01 by one-way ANOVA with Tukey's post-hoc comparison.

3.3.6. $P2X_7$-dependent potassium and calcium ion flux is essential for mitochondrial mROS production

As direct visualization revealed that the mitochondrial potassium pool responds to receptor-mediated changes in intracellular potassium, it was next determined if ion flux had an effect on pro-inflammatory mitochondrial signaling. Using the mitochondria-targeted reactive oxygen species probe MitoSOX whether potassium efflux and calcium influx had an effect on ROS production was investigated (**Figure 3-8**). Results indicated a substantial increase in MitoSOX signal when LPS-primed cells were stimulated with ATP. In support of a role for $P2X_7$ signaling in

this response, inhibition of the channel with A438079 reduced levels of mROS production to that of basal levels seen in LPS-primed J774A.1. Importantly, both potassium efflux and calcium influx were necessary for the generation of mROS as treatment with 130 mM extracellular KCl (**Figure 3-8A**) or BAPTA-AM (**Figure 3-8B**) resulted in strong suppression of MitoSOX oxidation.

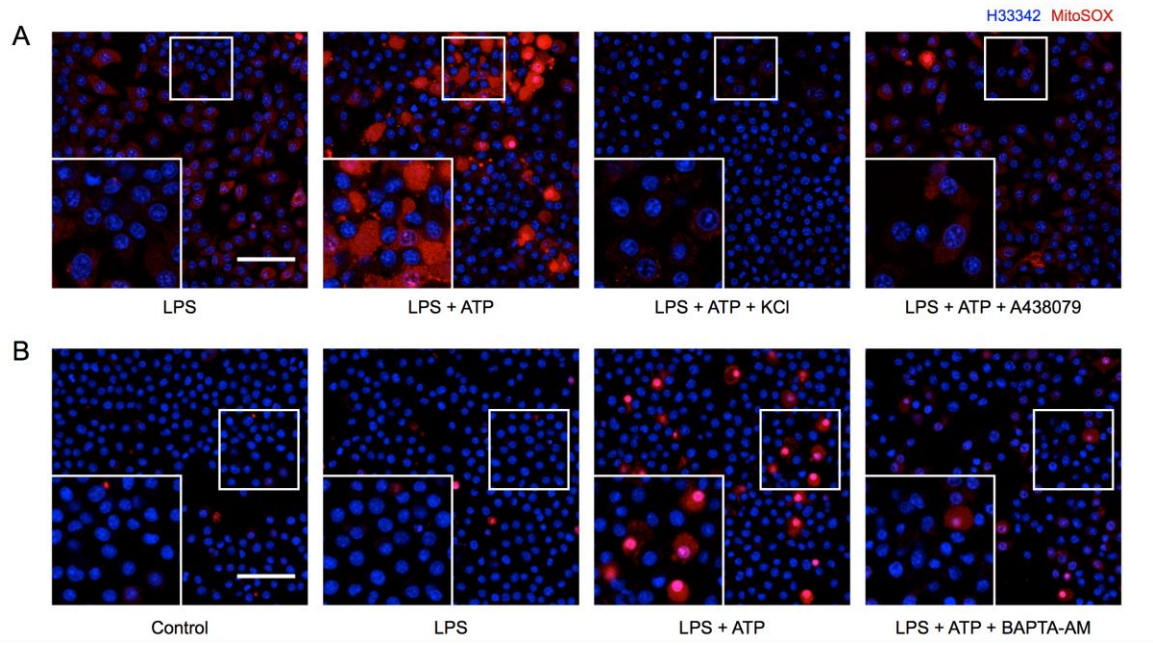

Figure 3-8. Potassium and calcium flux are necessary for $P2X_7$-dependent mROS generation. J774A.1 cells were left untreated, primed with LPS for 4 hours, or primed with LPS and treated with 3 mM ATP as indicated. MitoSOX (red) was added to all samples 15 minutes after ATP addition and incubated for an additional 15 minutes prior to imaging. (A) Evaluation of the role of $P2X_7$ and potassium efflux in mROS generation. 130 mM KCl and 25 µM A438079 were added 15-20 minutes prior to ATP addition. (B) Evaluation of the role of calcium influx in mROS generation. 100 µM BAPTA-AM was added 15-20 minutes prior to ATP addition. Nuclei are stained with Hoechst 33342 (blue). Scale bar is 50 µm. Results are representative of at least 2 independent experiments.

Comparing the kinetics of MitoSOX oxidation and potassium efflux in the mitochondria it was find that potassium mobilization is a rapid event and likely occurs upstream of ROS generation. While this is difficult to directly correlate due to KS6 exhibiting rapid response dynamics while MitoSOX converts by a comparatively slow process, the seconds-scale response of potassium efflux is notable quicker than the apparent minutes-scale generation of ROS. These results taken together, suggest that calcium and potassium flux triggered by $P2X_7$ activation result in mitochondrial ion imbalance and mROS generation upstream of NLRP3 inflammasome activation.

3.3.7. ATP-induced potassium efflux is required for calcium influx

While both potassium and calcium are implicated in ATP-induced inflammasome activation, it is unclear if there is a relationship between them (Sutterwala, Haasken, and Cassel 2014). To investigate the dynamics of ATP-induced ion flux, multiplexed imaging of potassium and calcium was performed by combining the KS6 intracellular potassium sensor with Fluo-4, a commercially available calcium indicator (**Figure 3-9**). Results showed that LPS priming alone had no dramatic effect on ion content; calcium transients were apparent but overall signal was stable for both calcium and potassium. Upon ATP stimulation, a rapid calcium signal spike occurred, followed by a second, more sustained increase in calcium signal. This bi-phasic calcium response is indicative of the kinetics associated with rapid, endoplasmic reticulum-stored calcium ahead of plasma membrane-localized calcium entry from the extra-cellular environment (Murakami, Ockinger, Yu, and Byles 2012). Importantly, potassium flux occurred concurrently with the second phase of calcium influx, but was stable through the initial calcium spike. Calcium chelation with BAPTA-AM resulted in a suppression of calcium dynamics, but had no effect on the ability for ATP to induce potassium depletion. This suggests that potassium flux may be upstream of calcium flux. Addition of extracellular potassium had no effect on the initial calcium spike after ATP addition, but suppressed the second, sustained calcium rise. Together, these results suggest that ATP-induced potassium efflux is upstream and necessary for plasma membrane-associated calcium influx, but not transient store-associated calcium spikes.

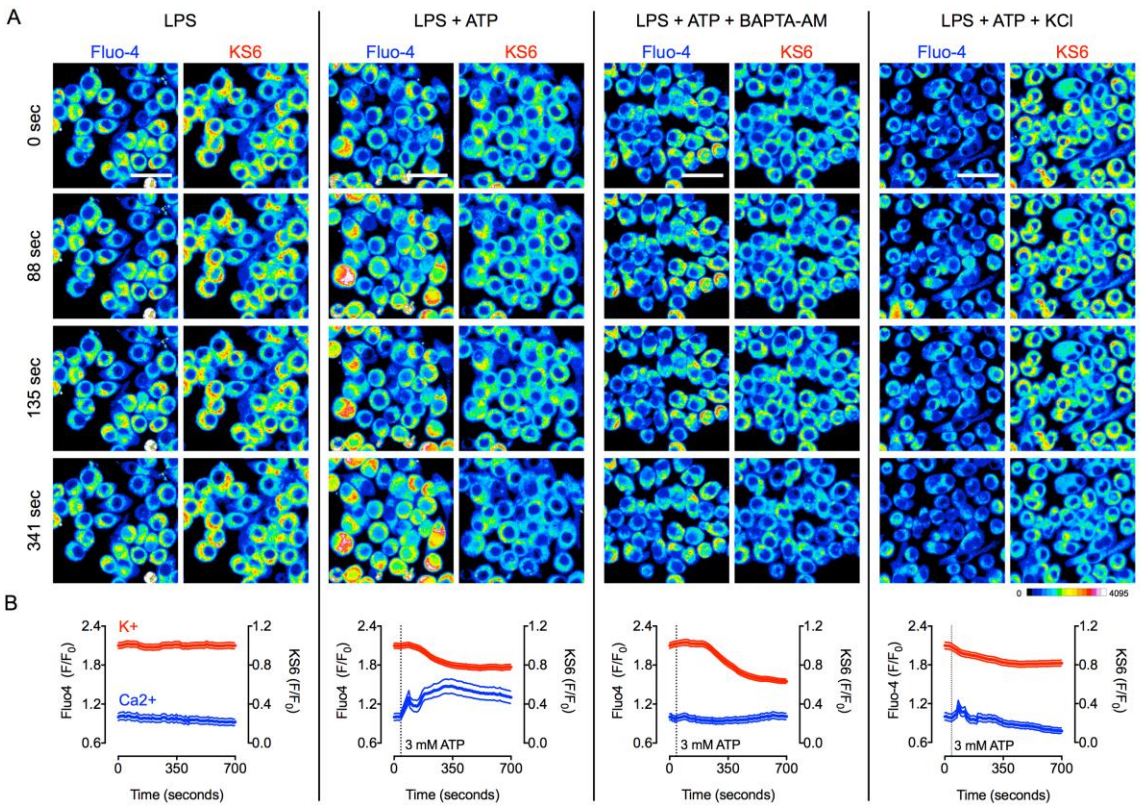

Figure 3-9. Real-time, multiplexed visualization of ATP-induced potassium and calcium dynamics. J774A.1 cells were primed for 4 hours with 1 µg/mL LPS, stained with KS6 and Fluo-4 DIRECT and both fluorophores were imaged simultaneously by confocal microscopy. (A) Representative fields for each condition showing Fluo-4 and KS6 signal responses. 16-color pseudocolor look-up tables were used for visualization. Blue indicates low signal intensity and red indicates high signal intensity. Scale bar represents 25 µm. (B) Mean and standard error for 30 representative cells in each condition. Where indicated cells were stimulated with 3 mM ATP. Inhibitors were added 15-20 minutes prior to imaging. Results are representative of at least 2 experiments.

3.4. DISCUSSION

In this study the question of how ion flux and mitochondrial reactive oxygen interact upstream of inflammasome assembly was investigated. Both of these phenomena are recognized as key mediators of inflammasome regulation and have been separately suggested as the common induction mechanism for inflammasome assembly. Despite the proposal that there is a link between potassium efflux and mitochondrial signaling resulting in inflammasome assembly, this association has yet to be observed (Petrilli et al. 2007; Martinon 2010; Tschopp 2011; Sutterwala, Haasken, and Cassel 2014). Further, no direct evidence regarding the relationship between

calcium and potassium has been described. Thus, it has been unclear how ion flux and oxidative signaling contribute to inflammasome regulation.

Because of its long-standing and apparently ubiquitous participation in linking stimulus detection and inflammasome assembly, potassium is often used as a metric of basic characterization for both new activators and inhibitors of the inflammasome. Details of how potassium affects the inflammasome have not been adequately described, however, because of technical limitations in potassium measurement. The most common methods for determining the role of potassium in various aspects of the inflammasome pathway are either blockade with high extracellular potassium or quantitation of potassium content by spectroscopy or photometry of bulk populations lysed in nitric acid (Franchi et al. 2007; Petrilli et al. 2007; Muñoz-Planillo et al. 2013). While high extracellular potassium is effective for determining how blockade of potassium efflux affects downstream phenotypes, which we have also used in this study, it is obscures intermediate responses and is unable to reveal cellular kinetics. Likewise, bulk cell potassium determination can provide only low-resolution kinetic details and completely obscures the contribution of individual cells or subpopulations in the response to stimuli. The latter point was recently identified to be an essential character of inflammasome-associated response by macrophages. Specifically, it was observed by single cell analysis that IL-1β was released in a bursting fashion only from cells dying by pyroptosis (Liu et al. 2014). This opposes the long-standing paradigm of secretion by various controversial pathways (Piccioli and Rubartelli 2013). This observation highlights the importance of investigating inflammasome-associated cellular processes at the single cell level and avoiding reliance on bulk cell determination methods.

While calcium indicators are well established and extensively used, existing methods for probing potassium are lacking. To date, Arlehamn et al. have reported the only live cell imaging experiments on potassium in macrophages stimulated to undergo inflammasome assembly by infection with Pseudomonas (Arlehamn et al. 2010). A major limitation to this study, however, is their application of PBFI for live cell potassium readout. PBFI is a potassium sensor that exhibits nearly equivalent sensitivity to sodium ions as it does to potassium ions, which makes its readout difficult to interpret (Minta and Tsien 1989). Further, PBFI has a Kd <10 mM and its response

saturates at approximately 50 mM, a concentration lower than the threshold for inflammasome activation as reported by others and reaffirmed in this study. Accordingly, upstream dynamics are obscured by a saturated sensor response and a depletion of cellular potassium can only be detected upon cell death with PBFI. Lastly, PBFI is necessarily excited with UV light and therefore induces phototoxic damage to cells under observation, potentially obscuring the effects of stimulus-induced cell death. For the current studied KS6, an improved intracellular potassium sensor, which addresses the drawbacks of PBFI, was applied (publication in revision). KS6 is excited by visible light, is strongly selective for potassium against sodium and other monovalent and divalent ions, readily taken up by live cells, and is sensitive to potassium across a supraphysiological range. An additional feature of KS6 is its enrichment in mitochondria due to the presence of a triphenylphosphonium group, thereby localizing it to both the cytosol and mitochondria of cells. Here it is shown that KS6 can be effectively used for observing dynamic responses of potassium in live cells and, further, that it can be multiplexed with other intracellular indicators for analytes such as calcium.

Detection of extracellular ATP by the $P2X_7$ purinergic receptor is a prototypical stimulus for NLRP3 inflammasome activation (Perregaux and Gabel 1994; Franchi et al. 2007). Potassium efflux and ROS generation have independently been proposed as downstream effects of $P2X_7$ activation (Bartlett, Yerbury, and Sluyter 2013). By live cell imaging and direct visualization a rapid and robust mitochondrial potassium mobilization associated with $P2X_7$ engagement was identified. $P2X_7$ is expressed on the plasma membrane and its sensing activity is therefore localized distally to mitochondrial responses (Di Virgilio et al. 1998). It is proposed that mitochondria mobilize their potassium pool as a response to changes in cytosolic potassium levels, which is directly responsive to $P2X_7$ activity by proximity. This provides additional support for the observation that mitochondria respond to cytosolic potassium levels, as it was previously shown that mitochondria are capable of sequestering and buffering cytosolic potassium (Kozoriz et al. 2010). A mitochondrial potassium buffering mechanism is further supported by the finding that efflux is ATP dose-dependent. $P2X_7$ has multiple ATP-sensing sites that have been shown to dose-dependently affect the level of pore dilation permission to ion flux (Yan et al. 2010). Our

data suggest that the magnitude of $P2X_7$ activation dictates the degree of potassium efflux, and therefore inflammasome assembly responses.

Intracellular ion homeostasis is essential for maintenance of mitochondrial integrity as mitochondrial membrane potential is heavily dependent on charge distribution (Garlid and Paucek 2003; Dubyak 2004). It was hypothesized that the mitochondrial potassium loss we observed would be correlated with mitochondrial reactive oxygen production. In support of this, it was found that blockade with high extracellular potassium or the $P2X_7$ inhibitor A438079 suppressed the elevated levels of mitochondrial ROS observed with ATP treatment. Likewise, it was found that potassium blockade and calcium chelation suppressed mROS generation. By performing the first-ever multiplexed imaging of potassium and calcium in live cells, it was found that potassium efflux was necessary for calcium influx downstream of ATP treatment. These results suggest a mechanism whereby potassium efflux triggered by $P2X_7$ activation regulates calcium influx, ultimately resulting in calcium overload-induced mROS generation leading to NLRP3 inflammasome activation (**Figure 3-10**).

This study establishes a previously unknown relationship between potassium and calcium during purinergic receptor-dependent activation of the NLRP3 inflammasome. Namely, potassium efflux is the dominant regulatory ion upstream of calcium influx, both of which are required for mitochondrial oxidative signaling leading to NLRP3 inflammasome activation. This finding reconciles the observation that intervention in calcium signaling can modulate inflammasome signaling, but treatment with calcium ionophores are insufficient for stimulating IL-1β processing and release (Perregaux and Gabel 1994; Murakami, Ockinger, Yu, Byles, et al. 2012). This study also provides the first highly selective, real-time observation of ATP-induced potassium dynamics as well as the first multiplexed imaging of calcium and potassium in live cells. Future work towards elucidating the NLRP3 inflammasome pathway may benefit from application of real-time visualization of potassium and calcium ion dynamics.

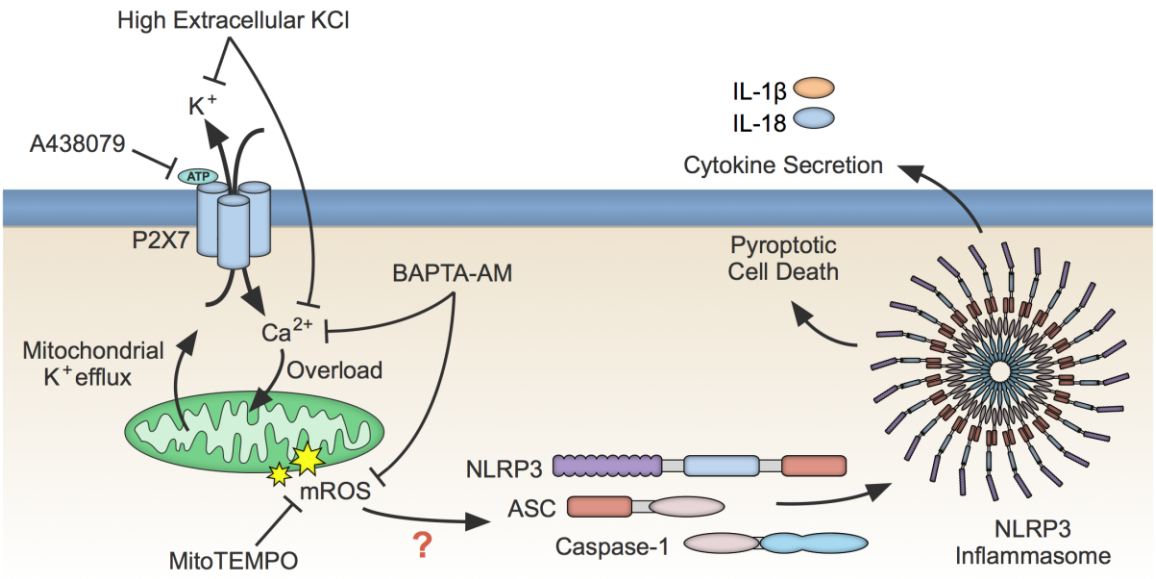

Figure 3-10. Proposed mechanism for ion flux-dependent regulation of the NLRP3 inflammasome. Activation of the $P2X_7$ receptor pathway with extracellular ATP results in the exchange of potassium and calcium across the plasma membrane, dominantly regulated by efflux of potassium from the cytosol to the extracellular space. Influx of calcium causes a mitochondrial calcium overload resulting in mitochondrial destabilization and mROS generation, which activates the NLRP3 inflammasome through an unknown mechanism, but possibly by involvement of TXNIP (Zhou et al. 2010; Horng 2014). $P2X_7$ receptor activation also results in a mitochondrial potassium efflux that may be involved in mitochondrial destabilization and mROS generation. Inhibition of potassium efflux prevents calcium influx and downstream mROS generation. Likewise, chelation of intracellular calcium prevents mROS generation.

CHAPTER 4: ADDITIONAL DEVELOPED METHODS: SINGLE CELL RT-qPCR

4.1 INTRODUCTION AND BACKGROUND

It is known that cellular heterogeneity is present even in seemingly homogenous, isogenic populations. This heterogeneity is observed in cell size, function and growth stage, and at both protein and gene transcript levels (Klein et al. 2002; Pardal, M.F. Clarke, and Morrison 2003; Johnson and Newby 2009). Despite the potential impact of investigating this heterogeneity, most of our understanding of disease pathology has been informed by bulk measurements made on cellular populations (Levsky and R.H. Singer 2003). This approach is not optimal because population-averaged measurements are not always representative of the actual biological state or response. For example, multimodal responses become obscured and the contributions of rare, but important cells can be diluted beyond detection. Therefore, for many biologically and medically relevant questions, single cell resolution techniques are required (Lidstrom and Meldrum 2003; de Souza 2012; Ståhlberg et al. 2012).

Our lab and others have shown that performing gene expression analyses at the single cell level reveals useful information about disease states and conditional responses of both mammalian and bacterial cells (Ginsberg et al. 2004; Gao, W. Zhang, and Meldrum 2011; Narsinh et al. 2011; Zeng et al. 2011). However, these approaches rely on expensive, specialized equipment for automated cell sorting, or complicated and methodologically difficult manipulation tools. As a result, single cell gene expression experiments are often inaccessible to research labs with limited resources or expertise (Ståhlberg and Bengtsson 2010; Zeng et al. 2011). An additional limitation of existing methods is that chemical dissociation of samples is usually used to harvest cells for end-point analysis. This treatment has the potential to introduce physiological perturbations that may be reflected in variations in RNA species of interest. Further, during dissociation from an adherent population and processing by methods such as microcapillary aspiration or flow sorting, individual cells cannot be easily tracked. As a result, analyses done on live, adherent cells cannot be directly correlated with subsequent gene expression data for

individual cells. Finally, custom-developed instrumentation, while enabling an individual lab to perform single cell experiments, may not be reproducible in other venues due to differences in protocols and sample handling. A comparison of the available methods for single cell isolation is given in **Table 4-1**. To address these challenges, an adaptable pipeline for performing correlated live cell imaging and single cell reverse transcription quantitative polymerase chain reaction (RT-qPCR) was optimized which requires only broadly available equipment, minimal investment in consumables and minimal cell perturbation. The presented method was characterized for optimal single cell isolation and demonstrate its application by identification of GFP-expressing cells from among a mixed population with non-expressing cells both microscopically and by molecular detection using RT-qPCR on the same single cells.

Table 4-1. Comparison of current methods for single cell isolation

Method	Advantages	Disadvantages
Fluorescence-activated Cell Sorting	- High throughput - Single cell resolution - Fluorescence-compatible - Specific cell isolation - Live cell compatible	- High cost - Specialized technical expertise needed - Suspended cells only - No cell-cell interaction capability - Variable performance
Laser Capture Microdissection	- Single cell resolution - Fluorescence-compatible - Specific cell isolation - Compatible with tissue samples - Capable of cell-cell interaction studies	- Low throughput - High cost - Specialized technical expertise needed - Infrequently compatible with live cells - Potential neighbouring cell contamination - Need to identify cell of interest - Adhered cells only - Variable performance
Microcapillary aspiration	- Single cell resolution - Fluorescence-compatible - Live cell compatible - Capable of cell-cell interaction studies	- Low throughput - High cost - Necessary technical expertise - Suspended cells only - Variable performance
Microfluidics	- Variable throughput - Variable cost - Single cell resolution - Fluorescence-compatible - Live cell compatible - Adherent or suspended cells - Capable of cell-cell interaction studies	- Specialized technical expertise needed - Generally specialized per experiment - Random cell isolation - Variable performance
Terasaki plate and dilution	- Low cost - Low technical complexity - Single cell resolution - Fluorescence-compatible - Live cell compatible - Adherent or suspended cells - Capable of cell-cell interaction studies - Consistent performance	- Mid to low throughput - Random cell selection

Terasaki-style microtest assays were developed in the 1960s by Paul Terasaki for tissue-typing microcytotoxicity tests on human leukocyte antigens with only one microliter of patient antiserum (Terasaki and McClelland 1964). Modern Terasaki plates are generally made of optically clear polystyrene with flat-bottomed wells accommodating approximately 20 µL volumes each. While still used for their original intended microcytotoxicity purposes, Terasaki plates have also been used for isolation cloning, because, after plasma treatment to promote cell adhesion, they provide a small, fluid-isolated culture environment for growth (Bishop 1981). Because of the small volumes, ability to support adherent cell culture and compatibility with microscopic observation, Terasaki plates are excellent candidate substrates for designing a single cell RT-qPCR assay. These commonly available substrates are underutilized in the literature for single cell RT-qPCR analysis and have only been demonstrated for single-plex identification of gene expression (Smith, Malley, and Schechter 2000). Further, the previously published, and rarely reported, application of this substrate for single cell RT-qPCR is non-optimized and only briefly described thereby requiring substantial preliminary work for groups wanting to use this technique.

Here, the optimized application of Terasaki plates for single cell RT-qPCR is described, an expansion of the pipeline to include correlated molecular analysis with fluorescence microscopy, and a step-wise protocol with troubleshooting guidelines. Major advantages of the method described here versus existing methods include low method adoption cost and learning curve, broad compatibility with various detection chemistries and microscopic methods, and multiplexing analysis of visual observations and molecular detection in the same single cells. The presented pipeline was designed by combining and characterizing simple, inexpensive and reliable methods to reduce costs and maximize broad applicability (**Figure 4-1**). Briefly, single cells are isolated by the following steps: 1) establish cell density using a cell counter, 2) determine the optimal cell density required to achieve one single cell per well in a Terasaki plate, 3) homogenize the suspension and dispense 10 µL into each well using a standard hand-held micropipette, 4) incubate cells for approximately 10–20 minutes in either a tissue culture hood or a 37ºC incubator, 5) verify and score positive single cells in each well. As demonstrated, the

resulting single cells can be used for a number of downstream applications including experimental treatments, fluorescence microscopy and RT-qPCR analysis.

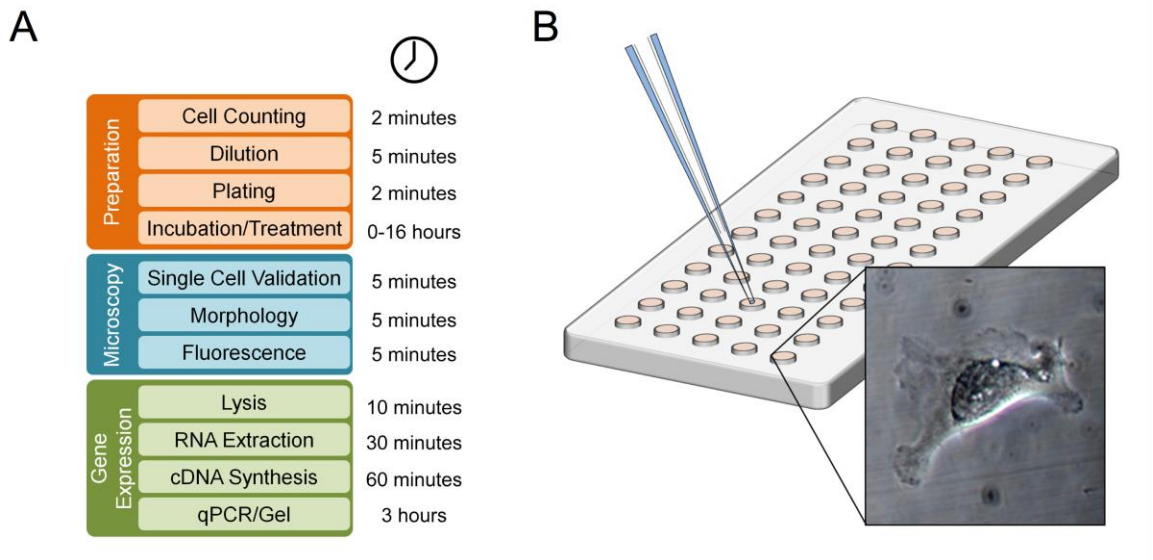

Figure 4-1. Schematic overview of the single cell RT-qPCR pipeline. (A) Succinct overview of the pipeline, sectioned into three main processes: preparation, microscopy, and gene expression. Approximate time per plate for each step in the procedure is shown. (B) Diagram of the cell isolation process. Diluted solutions of cells are dispensed into fluidically isolated wells of a Terasaki plate. Inset illustrates the spreading morphology of a single adherent cell on the plate.

4.2 METHODS

4.2.1. Cell culture

CP-A (ATCC® CRL-4027™, Manassas, VA, USA) and TurboGFP-expressing CP-D cells (ATCC® CRL-4030™, Manassas, VA, USA) transduced with MISSION® pLKO.1-puro-UbC-TurboGFP™ (Sigma Aldrich, St. Louis MO, USA) were maintained in serum-free Keratinocyte medium modified with 20 ng/mL epidermal growth factor, 140 µg/mL bovine pituitary extract, 100 U/mL penicillin and 100 µg/mL streptomycin (Gibco, Grand Island, NY, USA). Cells were maintained at 37°C under 5% CO_2 in a humidified atmosphere. Cells were trypsinized with 0.05% Trypsin-EDTA for 10 minutes, centrifuged at 900 rpm for 3 minutes and counted using the Trypan Blue assay on a Countess® automated cell counter (Life Technologies, Grand Island, NY, USA); only passages identified as greater than or equal to 95% viable were utilized in experiments. Cells were resuspended at 200–300 cells/mL or in a 1:1 mixture unless otherwise noted. THP-1

(ATCC® TIB-202™, Manassas, VA, USA) cells were cultured per ATCC instructions and used for determining well occupancy in preliminary concentration curve experiments as well as the three-color fluorescence data. MDA-MB-231 (ATCC® HTB-26™, Manassas, VA, USA) cells were cultured at 37°C under 5% CO_2 in a humidified atmosphere in complete DMEM supplemented with 10% FBS, 100U/mL penicillin and 100 µg/mL streptomycin (Gibco, Grand Island, NY, USA) and subcultured as described for the CP-A and CP-D cells. MDA-MB-231 cells were used for determining well occupancy in preliminary concentration curve experiments.

4.2.2. Preparation of Terasaki plates

Terasaki-style microtest plates (#470378, Thermo Scientific, Pittsburgh, PA, USA) were briefly cleaned using pressurized nitrogen gas to remove particulate from the well area. The plates were then exposed to air plasma in a plasma cleaner (PDC-001, Harrick Plasma, Ithaca, NY, USA) for 1 minute under 500 mTorr vacuum with 10.15 W RF-power; a decrease in the time necessary for cell spreading after plasma treating was observed, but this step is not required. The outer surfaces of the plates were sprayed with 70% ethanol and allowed to dry in a sterile, laminar flow hood prior to cell seeding.

4.2.3. Cell isolation

Cells were counted on the Countess® automated cell counter as described in section 4.2.1.1 and resuspended at the desired density in 1 mL of culture medium (200-300 cells/mL for single cell isolation experiments, variable for tunable occupancy experiments). Cells were seeded in 10 µL volumes in each well of a Terasaki plate and placed in a 37 °C incubator for 2-24 hours. Experiments were performed with Colleen Ziegler.

4.2.4. Microscopy

Plates were briefly observed by phase contrast microscopy on a Nikon TS-100 microscope with 10× and 20× objectives and scored for viability as “live” or “dead” based on spreading morphology and phase contrast characteristics. Wells identified as containing a live single cell were further

observed for fluorescence on an EVOS® FLoid® Cell Imaging Station (Life Technologies, Grand Island, NY, USA) using the white and green light detection options. For testing three-color fluorescence compatibility, live THP-1 cells were loaded with 10 µg/mL Hoechst 33342, 500 nM MitoTracker CMXRos and 2 µM Calcein AM (Life Technologies, Grand Island, NY, USA) and imaged on a Nikon TE2000 inverted microscope with a C2 confocal scanner (Nikon Instruments, Melville, NY, USA).

4.2.5. RNA isolation and purification

Samples were harvested from individual wells containing single cells using RNA lysis buffer (Zymo Research, Irvine, CA, USA) by three repeated applications of 10 µL to an individual well. All three volumes of RNA lysis buffer containing lysate from an individual cell were transferred to a PCR tube and kept at -80°C until further use (less than one week) and subsequently processed for RNA extraction and purification using the Quick-RNA™ MicroPrep kit (Zymo Research, Irvine, CA, USA). Briefly, the complete volume of cell lysate was transferred directly to the provided spin columns and purified according to manufacturer's instructions. Total RNA was eluted to a final volume of 9 µL in DEPC-treated water. Purified total RNA was used immediately or stored at -80 °C for less than one week. Experiments were performed with Colleen Ziegler.

4.2.6. Reverse transcription

First-strand cDNA synthesis was performed in a Veriti thermal cycler (Life Technologies, Grand Island, NY, USA) using the qScript™ cDNA SuperMix reagent (Quanta Biosciences, Gaithersburg, MD, USA). Briefly, 7 µL of total RNA, 2 µL of qScript™ cDNA SuperMix and 1 µL of DEPC-treated water was added to a PCR tube. Samples were kept at 25 °C for 5 minutes, 42 °C for 30 minutes, 85 °C for 5 minutes and held at 4 °C until retrieval. Synthesized cDNA was stored at -20°C until further use. Experiments were performed with Colleen Ziegler.

4.2.7. qPCR and results validation

qPCR was performed using the SYBR Premix Ex Taq™ II reagent (TaKaRa, Mountain View, CA, USA). Briefly, a master mix was prepared for each reaction containing 5 µL SYBR Premix Ex Taq™ II (2×), 0.4 µL each of 4 µM forward and reverse primers, 0.2 µL ROX reference dye and 2.0 µL DEPC-treated water. Once master mix was dispensed into PCR tubes or wells of a PCR plate, 2 µL of cDNA were added to each reaction (or 2 µL DEPC-treated water for no-template controls) and qPCR cycling was performed. Primers used are described in **Table 4-2**. Three technical replicates and a no-template control reaction were performed for each gene in each sample. A StepOnePlus™ Real-Time PCR System (Life Technologies, Grand Island, NY, USA) was used for thermal cycling according to the following conditions: 1 cycle at 95 °C for 30 seconds, 40 cycles 95 °C for 5 seconds then 60 °C for 30 seconds with data collection, followed by a melt curve analysis. Data was analyzed using StepOne™ Software version 2.1 (Life Technologies, Grand Island, NY, USA). Results were confirmed via 1% agarose gel electrophoresis using Lonza SeaKEM LE (Lonza, Basel, Switzerland) with 1× TAE buffer and SYBR safe dye (Life Technologies, Grand Island, NY, USA). Additional confirmation was evaluated by melting curve analysis. Primers were validated by band extraction from the agarose gel (QIAquick Gel Extraction kit, Qiagen, Germantown, MD, USA) followed by sequencing. Experiments were performed with Colleen Ziegler.

Table 4-2. RT-qPCR primers

Gene target	Accession #	Forward Sequence	Reverse Sequences	Size (bp)
Beta-actin (human)	NM_001101.3	5′-ctggaacggtgaaggtgaca	5′-aagggacttcctgtaacaacgca	140
GFP (TurboGFP)	GU452685.1	5′-aggacagcgtgatcttcacc	5′-cttgaagtgcatgtggctgt	164

4.3. RESULTS

4.3.1. Tunable single cell isolation on small-volume Terasaki plates

Optimization of cell seeding density is essential for obtaining single cell occupancy in Terasaki microtest plates. A dilution series was performed in order to determine the effective cell occupancy distribution as a function of stock cell density prior to seeding. The occupancy of wells obtained by various densities of initial cells is shown in **Figure 4-2**. By performing a statistical fit, it was found that isolation of cells by this method results in a tight correlation to a Poisson distribution. Accordingly, the maximum frequency for a single cell well obtained by random seeding in Terasaki plates is approximately 35%, which may be obtained with an initial cell density of 250-350 cells/mL.

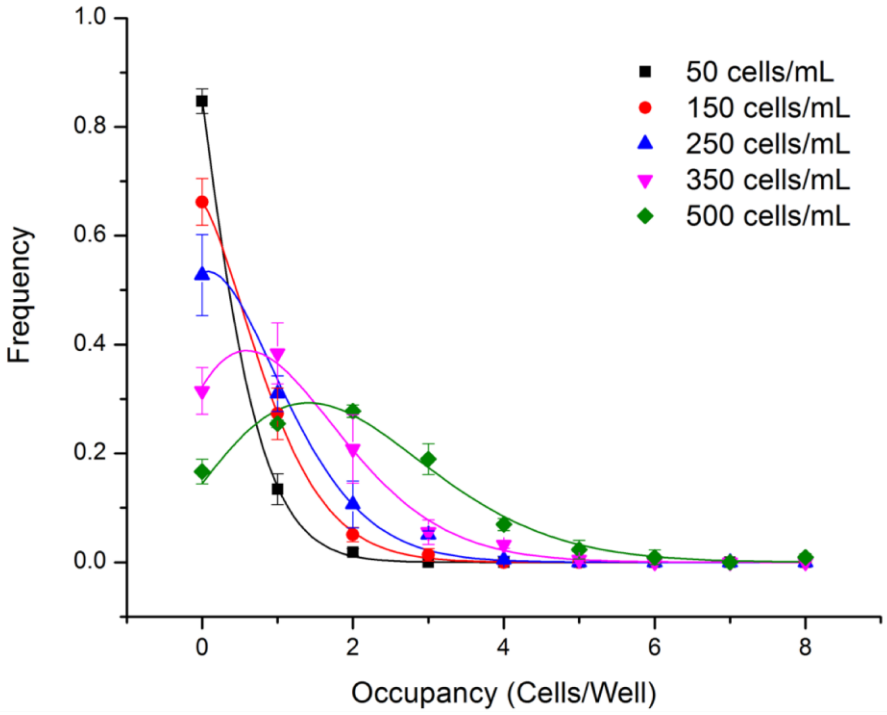

Figure 4-2. Tunability of single cell isolation. Concentration curve experiments with MDA-MB-231 cells demonstrating the ability to tune the well occupancy by altering initial seeding concentration according to Poisson statistics. Approximately 250–350 cells/mL was identified as the optimal concentration for obtaining single cells. Error bars represent standard deviation and curves represent Poisson fit.

4.3.2. Multi-color fluorescence microscopy of isolated single cells

The application of fluorescent vital dyes provides functional information on the cells under observation. Therefore, the use of fluorescent dyes on isolated single cells upstream of molecular analysis can provide a convenient route for multiplexing functional, live-cell information with molecular analysis. A point to note, regarding fluorescent staining in an isolated setting, is the viability of the cell. Fluorescent dye signals can relocalize or be lost during changes in viability. To determine whether isolated single cells on Terasaki plates are compatible with multicolor fluorescence microscopy, single THP-1 cells were stained with Hoechst 33342, MitoTracker Red CMXRos and Calcein AM (**Figure 4-3**). Imaging with laser scanning confocal microscopy revealed expected localization and signal intensities for all three fluorescent vital stains, indicating that cell viability is maintained throughout the isolation procedure, and that the substrate used for isolation and culture is compatible with imaging sufficient for functional multiplexing across the commonly used DAPI, FITC and TRITC spectral channels.

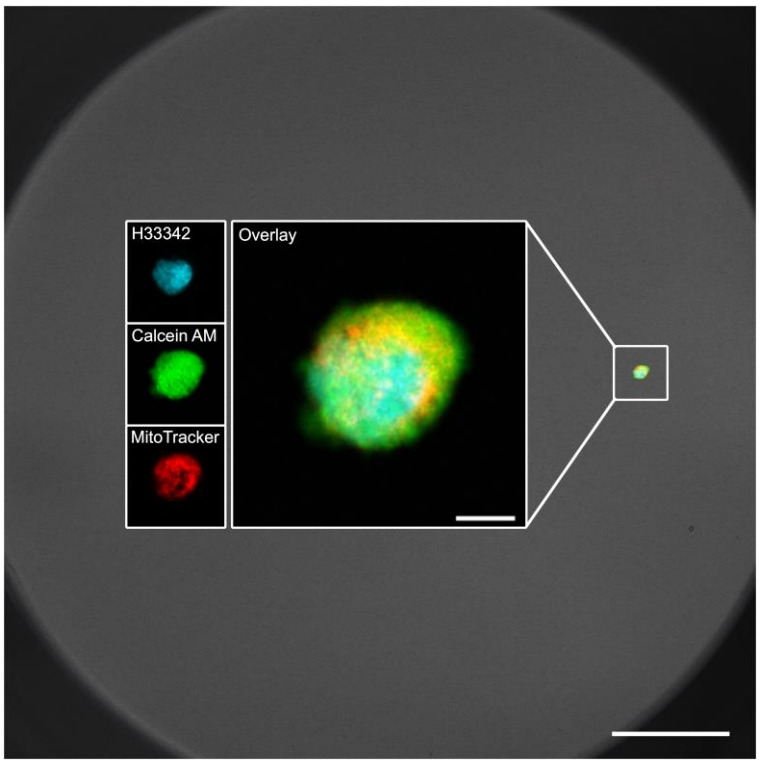

Figure 4-3. Demonstration of three-color fluorescence on Terasaki plates. An isolated THP-1 cell is stained with Hoechst 33342 (DNA; blue), Calcein AM (cell membrane integrity; green) and MitoTracker CMXRos (mitochondria; red). Main scale bar represents 100 μm and inset scale bar represents 5 μm.

4.3.3. Multiplexed single cell gene expression analysis and fluorescence microscopy of the same single cells

To demonstrate the ability of the pipeline to identify specific signatures of single cells, the presence of GFP transcripts was measured in isolated cells from a population containing a mixture of GFP-positive and GFP-negative cells. It was sought to determine whether the volumes attainable in the Terasaki plates would allow detection of GFP transcripts from GFP-positive cells that could be correlated with fluorescence observations from the same sample. The GFP-positive cells used in these experiments were CP-D cells (ATCC® CRL-4030™), an hTERT-immortalized cell line representing high-grade dysplasia in Barrett's esophagus that was stably transfected with a plasmid containing the GFP coding sequence. The GFP-negative cells were CP-A cells (ATCC® CRL-4027™) a related hTERT-immortalized cell line representing non-dysplastic metaplasia in Barrett's esophagus. Both of these cell lines were mixed 1:1 prior to being seeded

on a Terasaki plate for single cell isolation. Single cells were scored and GFP-positive and –negative cells were identified by fluorescence microscopy and subsequently isolated for gene expression analysis (**Figure 4-4**).

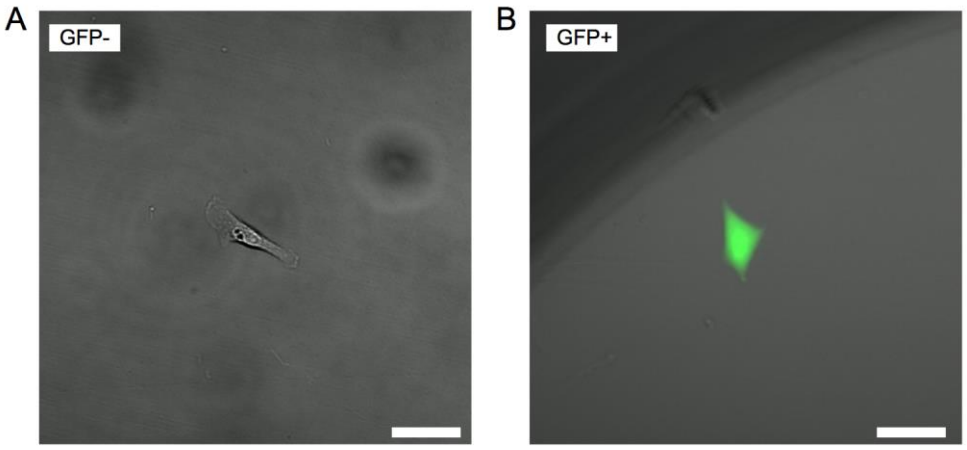

Figure 4-4. Visual identification of fluorescence in isolated single cells. Adherent GFP-negative (A) and GFP-positive (B) cells obtained by the described method on Terasaki plates and observed by fluorescence microscopy. Scale bars represent 50 µm.

Total RNA was purified from each collected single cell and the entire collected eluate was used in independent reverse transcription reactions to produce cDNA. Subsequently, the cDNA was divided into three replicates for the target gene, GFP, and three replicates for the control gene, beta-actin. Simultaneous no template controls were run in parallel. Reproducibility of this method was good, as representatively indicated by the tight distribution of the amplification curves in **Figure 4-5A** and the height of the peaks in the melt curves in **Figure 4-5B**. As is commonly observed in RT-qPCR using intercalating chemistries (e.g., SYBR), occasional primer dimer amplification occurred, as seen in the late-rising dotted green amplification curve in the lower panel of **Figure 4-5A**. Primer dimer amplification is identified and distinguished from sample amplification by the characteristically late C_q value, lack of expected melt curve peak and small band size (**Figure 4-5A and B and Figure 4-5D**).

A challenge in single cell analysis is the ability to discriminate between variability due to error in a method and real differences due to biological heterogeneity and gene expression stochasticity. Using the presented pipeline, the data collected by RT-qPCR and melt curve

analyses illustrated marked differences in GFP mRNA levels between isolated cells from a mixed population that corresponded to positive and negative fluorescence observations (**Figure 4-5A and B**). Normalized C_q analysis ($C_{q,GFP}$ - $C_{q,ACTB}$) demonstrated a significant difference in signal between GFP-positive and negative cells as determined by *T*-test with $p < 0.05$ (**Figure 4-5C**) (Livak and Schmittgen 2001). A gel electrophoresis analysis was performed to validate the qPCR data according to expected amplicon sizes, which are described in the Methods section (**Figure 4-5D**). The results were further confirmed by band extraction and DNA sequencing, resulting in nucleotide sequences corresponding to the two expected gene targets. These results show that the volumes attainable in the Terasaki plate yield sufficient sample concentration to quantify gene expression of single cells for the purpose of population discrimination despite the inherent difficult in identifying variability due to error or endogenous heterogeneity and stochasticity.

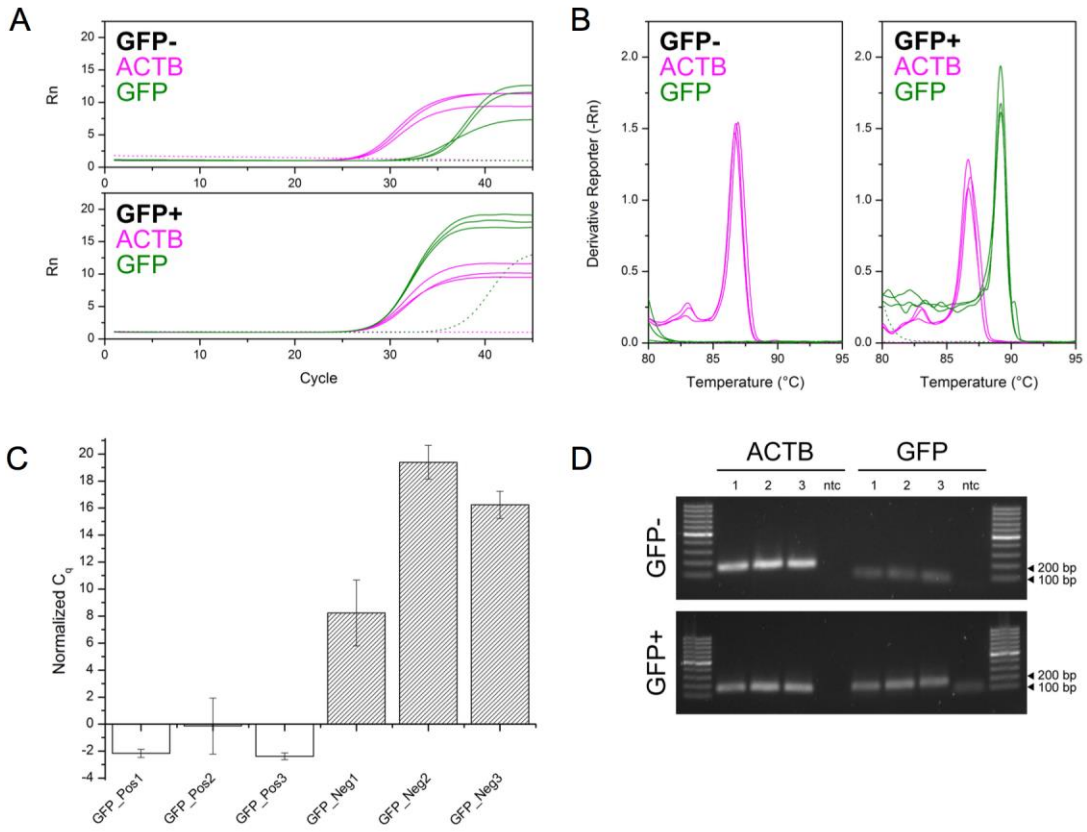

Figure 4-5. Molecular analysis of GFP positive and negative single cells. A) qPCR curves demonstrating the ability to differentiate between GFP-negative (top) and GFP-positive (bottom) cells without pre-amplification. Two gene targets were identified in each single cell: beta-actin (magenta) and GFP (green). The delayed amplification shown in the GFP-negative curves are caused by primer dimers, as supported by melt curve analysis, agarose gel electrophoresis and DNA sequencing. B) Melt curve analysis showing the identification of individual peaks corresponding to the presence or absence of GFP (green), while beta-actin is observed at similar levels in both samples (magenta). C) Analyzed data for three GFP-positive (left group) and three GFP-negative (right group) cells isolated from a mixed population of cells. Results for each single cell were normalized to expression of beta-actin (ACTB) and reported as normalized C_q, which is defined as $C_{q,\,GFP} - C_{q,\,ACTB}$. Error bars represent standard deviation of 3 technical replicates of divided samples from individual cells. The difference between normalized C_q from GFP+/- is significant as determined by T-test with $p < 0.05$. D) Validation gel illustrating the presence of beta-actin in both cells, but a differential presence of GFP amplification in cells that were observed to be GFP-positive versus GFP-negative. Off-target bands in the negative control are primer dimers as confirmed by melt-curve analysis.

4.4. DISCUSSION

While single cell studies have the potential to reveal important heterogeneity in a wide variety of biological systems, the ability to perform the techniques required for single cell analysis are commonly limited by a laboratory's technical expertise and available instrumentation. It was sought to develop a simple protocol for performing single cell gene expression studies that is accessible to any lab already performing similar studies on bulk samples.

A simple and effective method is demonstrated for isolating live single cells for microscopic imaging and gene expression analysis by RT-qPCR. The major advantages of our method over previous approaches include: 1) the use of commonly available consumables circumventing the need for expensive equipment, 2) improved throughput of single cell selection compared to other manual methods due to random seeding and direct verification of well occupancy and viability, 3) a simplified single cell isolation procedure with minimal physical and chemical manipulation of cells, 4) total RNA extraction compatible with detection of multiple gene targets, and 5) multiplexed single cell imaging and gene expression analysis. Further, the method is compatible with a wide range of chemistries, allowing integration into experimental protocols that include various drug treatments or fluorescent indicators. All steps can be carried out under standard aseptic cell culture conditions and cell viability is not compromised. Suggested improvements to the presented protocol such as electronic repeating pipettes or fluid handling robots may require additional purchases, but will improve throughput; the time to seed one plate was reduced from approximately 5 minutes to less than 45 seconds with an electronic repeating pipette. Also, RNA isolation and purification may be avoided by using one-step RT-qPCR reagents, though this comes at the cost of reducing the number of gene targets per single cell sample. Additionally, the use of Taqman or other hydrolysis probe chemistries can improve the amplification specificity, but may result in considerably more expensive up-front costs per reaction.

The ability to multiplex visual observations of cells with molecular analysis is essential to understanding dynamic responses of cells to external perturbation. The method reported here

provides a straightforward and effective procedure for achieving multiplexed visual and molecular analysis at the single cell level. It is anticipated that this method will be extensible to the analysis other biomolecules (e.g., proteins) at the single cell level using assays such as proximity ligation assay-qPCR (Ståhlberg et al. 2012). Further, the use of live-cell fluorescent reporters can facilitate the tracking of intracellular events for improved temporal correlation with molecular analysis.

With respect to inflammasome biology, this method may be particularly useful for studying heterogeneity in IL-1β upregulation. One possible application is tracking the oscillatory nuclear translocation of a fluorescently tagged NF-κB then correlating those dynamics to the production of IL-1β mRNA transcripts (D.E. Nelson et al. 2004). It would, for example, be interesting to determine if transcriptional priming by LPS was correlated with readiness to assemble the inflammasome driven by gene expression upregulation of inflammasome-related components such as NLRP3 or IL-1β. Recent evidence suggests that single cell responses may be critical for systemic responses mediated by inflammasome activity (Liu et al. 2014). The method presented in this study may allow an additional level of multiplexing by correlating fluorescently tracked events with molecular analysis.

CHAPTER 5: ADDITIONAL DEVELOPED METHODS: LIVE-CELL INTRACELLULAR ATP VISUALIZATION

5.1. INTRODUCTION AND BACKGROUND

Adenosine-5'-triphosphate (ATP) is the predominant energy currency of the cell and is a substrate for most energy-required pathways. Aside from its role in enzymatic processes, ATP is also involved in purinergic intercellular signaling cascades in a variety of tissues (Fields 2000; Bodin and Burnstock 2001; Novak, Amstrup, and Henriksen 2003; Schwiebert and Zsembery 2003). As described in Chapters 1 and 3, ATP plays a crucial and prototypical role in activating the NLRP3 inflammasome by activation of $P2X_7$ purinergic receptors (Perregaux and Gabel 1994; Mariathasan et al. 2006). Additionally, the ATP-release channel Pannexin-1 has been implicated in regulating the activity of the NLRP3 inflammasome through autocrine and paracrine activation pathways (Pelegrin and Surprenant 2006; Latz, Xiao, and Stutz 2013). There is also evidence that maintenance of intracellular ATP content may play a role in IL-1β signaling. Metabolic blockade with a glucose analog, 2-deoxyglucose, or mitochondrial electron transport disruption with sodium azide cause an ATP depletion-dependent activation of the NLRP1b inflammasome (Liao and Mogridge 2013).

Elucidation of ATP signaling dynamics in the inflammasome pathway has been difficult to achieve due to limitations in existing methodology. Previous reports have interrogated ATP content in the context of the inflammasome by apyrase-mediate inhibition of autocrine and paracrine signaling or luciferase assays of intracellular content (Riteau et al. 2012; Liao and Mogridge 2013). Both of these approaches are end-point, bulk cell assays that prohibit visualization of single cell dynamics. As shown in Chapters 2 and 3, real-time dynamics of intracellular processes may be crucial for understanding specific mechanisms upstream of inflammasome activation.

Here, a mouse macrophage cell line stably expressing a genetically encoded intracellular ATP sensor was developed. The sensor, ATeam (Adenosine 5'-Triphosphate indicator based on Epsilon subunit for Analytical Measurements) is composed of cyan fluorescent protein (CFP)

fused with yellow fluorescent protein (YFP) via a linker from the *Bacillus subtilis* F_0F_1 ATP synthase epsilon subunit that confers highly selective and sensitive binding to free ATP (**Figure 5-1**) (Imamura et al. 2009; Kotera et al. 2010). When ATP is detected by the ATeam linker, the CFP and YFP proteins come within Fluorescence Resonance Energy Transfer (FRET) distance from one another and a ratiometric change in fluorescence emission wavelength is observed. This chapter describes the generation and characterization of the ATeam-expressing macrophage cell line and proposes possible uses for its future application.

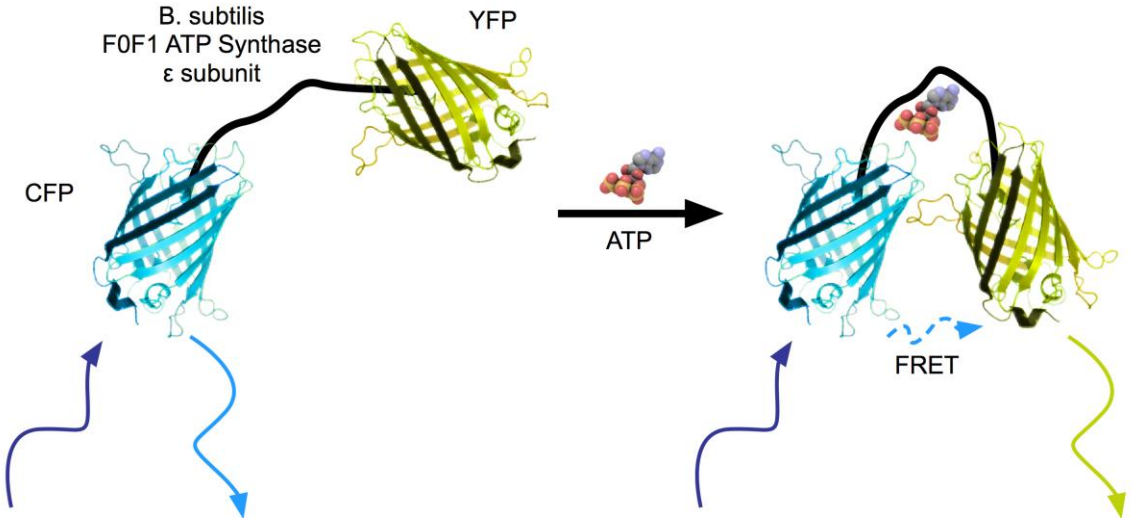

Figure 5-1. Overview of ATeam ATP sensor function. ATeam consists of cyan fluorescent protein (CFP) fused to yellow fluorescent protein (YFP) linked by the epsilon subunit of a bacterial F_0F_1 ATP synthase. Upon detection of ATP, CFP and YFP come are brought within FRET-compatible distance from each other and a shift in emission wavelength is observed.

5.2. METHODS

5.2.1. Cell culture

The murine macrophage cell line RAW 264.7 (ATCC® TIB-71™, Manassas, VA, USA) were maintained in complete DMEM supplemented with 10% fetal bovine serum, 100 U/mL penicillin and 100 µg/mL streptomycin. Cells were maintained at 37 °C under 5% CO_2 in a humidified atmosphere. Cells were passaged by scraping and viability was assessed using the Trypan Blue assay on a Countess® automated cell counter (Life Technologies, Grand Island, NY, USA).

5.2.2. ATeam plasmid preparation

ATeam1.03-nD/nA/pcDNA3 was a gift from Takeharu Nagai (Addgene plasmid # 51958). E. coli DH5α stab cultures obtained from Addgene were streaked on 1× ampicillin agar plates. Plasmids were prepared from single clones by MiniPrep (Qiagen, Valencia, CA, USA) and were verified by sequencing using primers CMV-Forward (5'- CGCAAATGGGCGGTAGGCGTG) and BGH-Reverse (5'- TAGAAGGCACAGTCGAGG) at the DNASU sequencing core (Tempe, AZ, USA). A verified clone was grown overnight in 1 L of Terrific Broth and endotoxin-free plasmid was prepared using MaxiPrep (Clontech, Mountain View, CA, USA).

5.2.3. Cell transfections and stabilization

Three million RAW 264.7 cells were seeded in a 60 mm dish and incubated overnight. The following day FuGENE® HD:DNA complexes (Promega, Madison, WI, USA) were formed at a ratio of 3.5:1 in OptiMEM medium (Life Technologies, Grand Island, NY, USA) and added to the cells in 6 mL of complete DMEM. Transfected cells were grown for 2 days in the transfection medium. On the third day, cells were washed 1× in fresh DMEM and 5 mL of DMEM containing 500 µg/mL G418 selective antibiotic was added to the cells. Cells were transferred to a T25 flask and continuously grown in DMEM containing 500 µg/mL G418 for 2 weeks, washing and exchanging medium every 2 days. Expression was evaluated on the EVOS FLoid cell imaging station using the FITC channel (exciting the YFP portion of ATeam). Cells were frozen down and stored under liquid nitrogen.

5.2.4. Spectral confocal microscopy and ratiometric analysis

Transiently transfected RAW 264.7 cells were seeded in an 8-chamber µSlide (Ibidi) and imaged by spectral microscopy on a Nikon Ti microscope equipped with a C2si confocal scanner with spectral detector. The excitation wavelength was 408 nm and collected spectrum (453 nm – 608 nm with 5 nm grating resolution) was selected to overlap both CFP (475 nm) and YFP (527 nm) peaks. After a baseline measurement was taken, 50 mM 2-deoxyglucose (2-DG) and 10 mM sodium azide (NaN_3) were applied to cells. Imaging was continued for 60 minutes.

To determine the intracellular ATP content, mean intensities of each cell were collected at 527 nm and 475 nm emission wavelengths. The 527/475 nm ratio value is directly proportional to the intracellular ATP content where a value of 1 is considered ATP-depleted.

5.2. RESULTS

5.3.1. Generation of a mouse macrophage cell line stably expressing intracellular ATP sensor

Generation of transfected cell lines without viral delivery is challenging in macrophage-type cells as they are highly sensitivity to endotoxic components of plasmid preparation and recognize double stranded DNA in the cytosol. Specifically, the HIN200 domain of the AIM2 inflammasome binds transfected double stranded DNA, resulting in inflammasome assembly and pyroptosis (Hornung et al. 2009). The RAW 264.7 macrophage cell line is suitable for non-viral transfection as it does not express the inflammasome adapter protein ASC, making it less sensitive to both endotoxic components and cytosolic double stranded DNA. Successful transfection was achieved using the non-lipid cationic polymer reagent FuGENE® HD (Promega). Use of the popular reagent Lipofectamine LTX (Life Technologies), despite its low toxicity formulation, resulted in a large amount of cell death, likely due to the toxic nature of cationic lipids.

5.3.2. Spectral characterization of ATeam and real-time detection of intracellular ATP in live cells

Confocal microscopy with spectral detection was used to characterize the ATeam sensor *in situ* in live, expressing RAW 264.7 cells. Due to the limited availability of optimal, 435 nm laser wavelength for excitation of the FRET sensor, 408 nm light was used to excite the CFP donor, with emission wavelengths collected across both CFP and YFP peaks. Additionally, blockade of both the glycolytic and oxidative phosphorylation pathways was used to assess the responsiveness of ATeam to ATP depletion. Spectral kinetic responses are given in **Figure 5-2**. Demonstration of real-time imaging in order to isolate specific single cell responses is provided in

Figure 5-3. Emission ratio results to visualize the magnitude of ATP depletion are given in **Figure 5-4**.

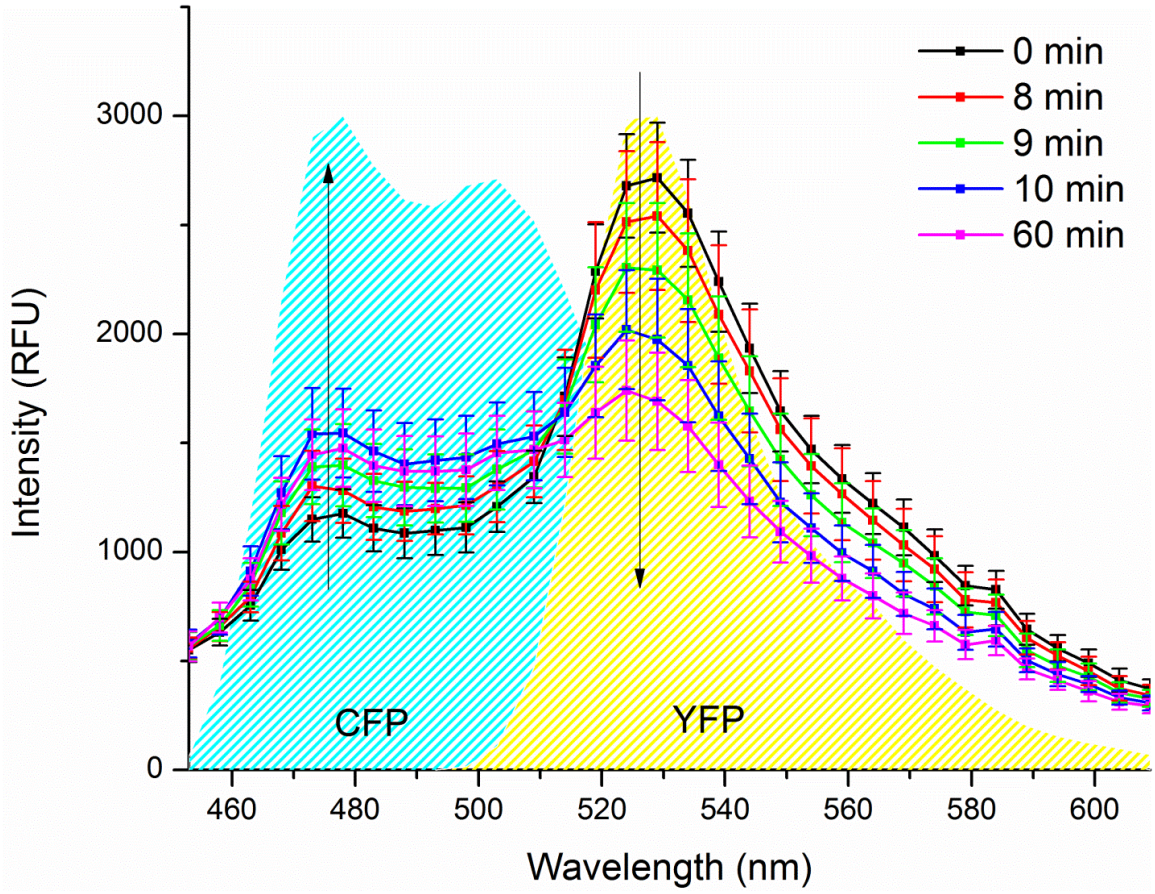

Figure 5-2. FRET-induced spectral shift of ATeam during ATP depletion. RAW 264.7 cells expressing ATeam were imaged by spectral confocal microscopy. At approximately 5 minutes cells were treated with 50 mM 2DG and 10 mM NaN_3 and continuously imaged for 60 minutes. Traces are the full emission spectrum mean and standard deviation for 6 cells from a representative field overlaid over reference spectra for CFP and YFP. A drop in the YFP peak concomitant with a rise in the CFP peak is observed over time. Results are representative of at least 2 independent experiments.

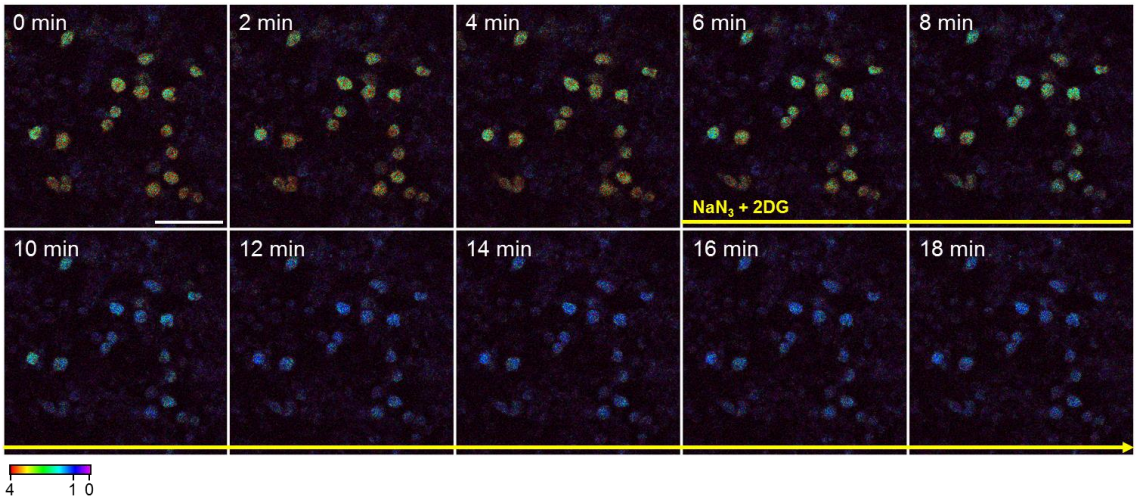

Figure 5-3. Real-time visualization of ATP depletion in live macrophages. RAW 264.7 cells expressing ATeam were imaged by spectral confocal microscopy. Where indicated (yellow line), cells were treated with 50 mM 2DG and 10 mM NaN_3 and continuously imaged. Signal represents the ratio of emission at 527 nm over the emission at 475 nm when ATeam is excited with 408 nm light. Scale bar represents 50 µm. Results are representative of at least 2 independent experiments.

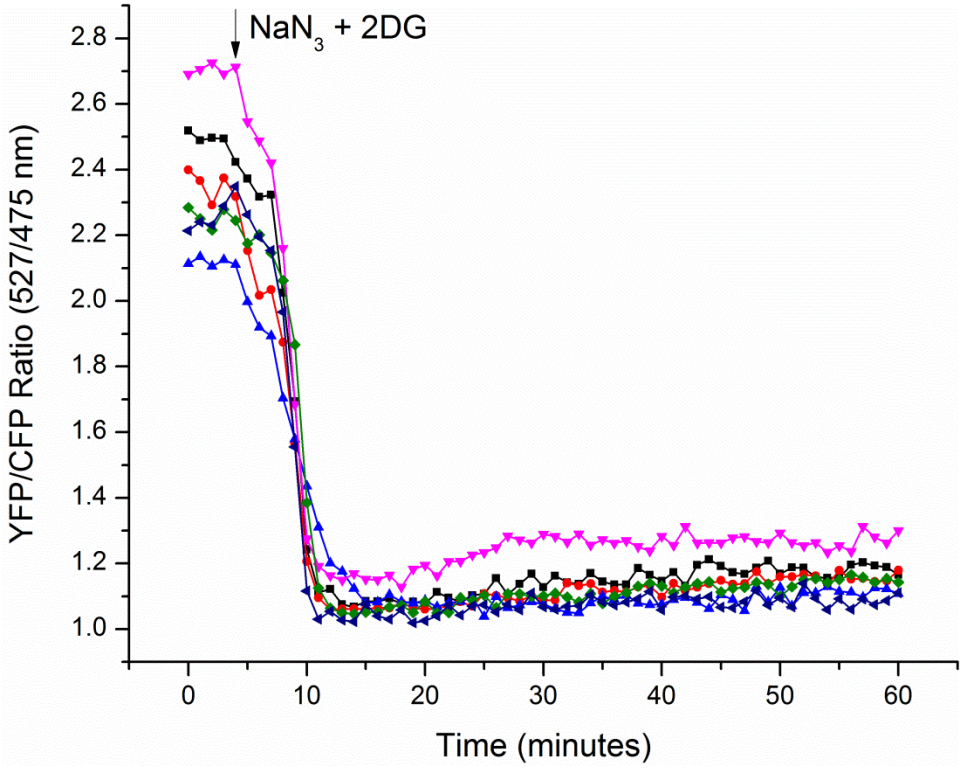

Figure 5-4. Ratiometric detection of ATP depletion. Traces represent the YFP/CFP ratio of ATeam signal from single cells after treatment with 2DG and NaN_3 at the indicated time. Results are representative of at least 2 independent experiments.

5.4. DISCUSSION

As described in Chapters 2 and 3 of this dissertation, tracking molecular concentration and localization in real-time is crucial for elucidating the dynamics of signaling pathways. This is supported by recent reports showing the identification of an all-or-none activation of caspase-1 downstream of inflammasome-activating stimuli by expression of a genetically encoded biosensor for caspase-1 activation (Liu et al. 2014).

Because ATP is closely related to cellular metabolism and signaling associated with many events in the immune system, interrogation of intracellular ATP in live immune cells is crucially important. Current efforts to perform such analyses rely in bulk cell determination or inhibition of ATP-dependent events. Here, a macrophage cell line was developed that stably expresses the genetically encoded intracellular ATP sensor ATeam. This tool will be helpful for studying events related to metabolic responses to macrophage perturbation.

It should be noted that while the RAW 264.7 macrophage cell line exhibits many characteristics related to primary macrophages, such as phagocytosis and TLR4/NF-κB signaling, they are deficient in the adapter protein ASC (Pelegrin, Barroso-Gutierrez, and Surprenant 2008). As such, RAW 264.7 cannot, by default, be used for investigating the NLRP3 inflammasome pathway and will require reconstitution of ASC expression in order to perform such studies. This is difficult to achieve while maintaining expression of a second transfected protein, as ASC overexpression heightens cellular sensitivity to stress and cells non-virally transfected with ASC rapidly die (unpublished observations). An alternative approach, unavailable during the course of this dissertation work, would be to virally transduce ATeam into either a primary macrophage cell line or another cell line that contains the full NLRP3 pathway, such as THP-1 or J774A.1. Viral transduction of ASC into the RAW 264.7 cell line may achieve the same goal. In this way, expression of the inflammasome pathway is available, and ratiometric ATP determination can be used for studying metabolic events related to inflammasome activity.

CHAPTER 6: CONCLUSIONS AND FUTURE PERSPECTIVES

6.1. SUMMARY AND INTERPRETATION OF BIOLOGICAL FINDINGS

The ability for the NLRP3 inflammasome to respond to diverse stimuli is essential for its role in mediating innate immune responses to damage and infection (Martinon, Mayor, and Tschopp 2009). Despite intensive study on the mechanisms of inflammasome regulation, it is still unclear how structurally and functionally dissimilar triggers all converge on the same signaling pathway (Sutterwala, Haasken, and Cassel 2014). The issue of dissimilar activating stimuli was addressed by using extracellular ATP to induce an active, receptor-dependent signaling event and nigericin to induce a passive, receptor-independent perturbation to ion flux converging on the NLRP3 inflammasome pathway. This dissertation work focused on the role of ion flux in regulating events leading to NLRP3 inflammasome assembly and pyroptotic cell death.

The results of Chapter 2 define a connection between potassium efflux and Syk tyrosine kinase activation. While recent work has shown that Syk is required for phosphorylation of ASC as a molecular switch leading to inflammasome activation, little has been reported on how Syk is regulated in the inflammasome pathway (Hara et al. 2013; Neumann and Ruland 2013; Laudisi, Viganò, and Mortellaro 2014; Lin et al. 2015). The position of Syk in the inflammasome pathway was defined as downstream of nigericin-induced potassium efflux and upstream of mitochondrial oxidative signaling. Further, the first evidence that Syk regulates pyroptosis is described (Laudisi, Viganò, and Mortellaro 2014). This is the first example of an intermediate regulator of inflammasome activation displaying sensitivity to potassium efflux. Potassium-dependent regulation of Syk is important because potassium efflux is a difficult mechanism to directly control. While potassium channel inhibitors have been postulated to suppress inflammasome activity by prohibiting potassium efflux, no data has been reported to demonstrate the inhibition of potassium efflux using these drugs. Indeed, the effects of potassium channel inhibitors have been reported as independent of their effect on their respective target channels (Petrilli et al. 2007). As such, how potassium channel inhibitors such as glyburide suppress inflammasome activity is currently unclear. Further, while addition of KCl to the medium is a convenient method for inhibiting

potassium efflux *in vitro*, this is not feasible *in vivo* as effects on bystander cell populations would be detrimental. Thus, an intermediate signal that mediates the effects of potassium flux upstream of inflammasome assembly may be a more appropriate pharmaceutical target. Indeed, Syk inhibitors are already under investigation as potential treatments for inflammatory pathologies (Weinblatt et al. 2008; Bajpai 2009; Podolanczuk et al. 2009; Genovese et al. 2011).

The results of Chapter 3 address the open question of ion flux dynamics upstream of inflammasome assembly. As described, potassium has been a broadly investigated inflammasome-regulating ion for decades (Perregaux and Gabel 1994; Muñoz-Planillo et al. 2013). Recently, additional evidence suggests that calcium may also be a critical regulator of inflammasome assembly (Lee et al. 2012; Murakami, Ockinger, Yu, and Byles 2012; Horng 2014). The role of each of these ions upstream of inflammasome assembly has been unclear. It was identified that both potassium efflux and calcium influx are necessary for mitochondrial oxidative signaling upstream of NLRP3 inflammasome assembly. Further investigation revealed that potassium efflux appears to regulate calcium influx. Abrogation of potassium concentration gradients prohibits the secondary, sustained calcium influx that occurs downstream of $P2X_7$ activation by extracellular ATP. This is significant, as it may explain why inhibiting potassium or calcium independently both affect inflammasome activation, since these results indicate that they are part of a sequentially coordinated cation flux. A compiled overview of the biological findings from this dissertation is given in **Figure 6-1**.

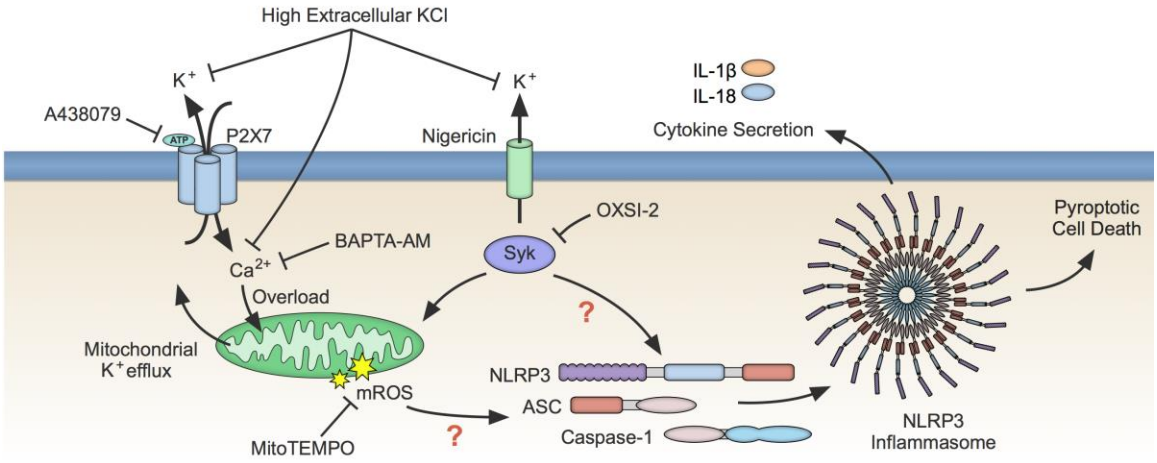

Figure 6-1. Overview of biological findings. This dissertation addressed both active and passive mechanisms for inducing potassium efflux upstream of the NLRP3 inflammasome. Passive, nigericin-induced potassium efflux results in downstream Syk activation and Syk-dependent oxidative signaling. Additionally, Syk activation regulates inflammasome assembly, cytokine secretion and pyroptotic cell death. Active, $P2X_7$ purinergic receptor activation results in potassium efflux-dependent calcium influx and mitochondrial potassium mobilization. Further, ATP-induced potassium efflux results in a potassium and calcium-dependent mROS generation that was required for inflammasome assembly, cytokine secretion and pyroptotic cell death.

6.2. DEVELOPED METHODS

Three methods were developed during this dissertation: (1) the application of a novel intracellular potassium sensor for dynamic visualization of potassium flux in live cells; (2) an optimized pipeline for single cell isolation, fluorescence microscopy and correlated molecular analysis by RT-qPCR; (3) a macrophage cell line expressing an intracellular ATP sensor. These methods provide a new set of tools for investigation of inflammasome biology that will contribute to future studies by facilitating analysis of dynamic, difficult-to-measure events with single cell resolution.

The ability to visualize potassium dynamics in live cells is a powerful advance. Existing methods for performing potassium measurements in the inflammasome pathway have predominantly involved potassium blockade (which we also use) and ion spectroscopy (Franchi et al. 2007; Petrilli et al. 2007; Muñoz-Planillo et al. 2013). These methods lack the ability to determine dynamics with high spatial or temporal resolution as they require bulk sample

processing. The only reported example of potassium imaging in the inflammasome pathway uses the sensor PBFI, which as limitations related to dynamic range and ion selectivity. As such, no group has sufficiently reported the character of potassium dynamics in cells stimulated within the inflammasome signaling pathway (Minta and Tsien 1989; Arlehamn et al. 2010). The novel intracellular potassium sensor described here allowed identification of rapid potassium flux dynamics with unmatched selectivity. Further, as the sensor is also enriched in the mitochondria, it provided the first descriptions of mitochondrial potassium mobilization in response to purinergic receptor activation. This is significant and may help to explain oxidative signaling as an upstream trigger of inflammasome activation (Tschopp 2011).

The optimized single cell pipeline contributes an inexpensive approach for addressing transcriptional heterogeneity in cellular populations. Importantly, the described method allows for correlation of fluorescence microscopy with molecular analysis at the single cell level. This is critical for investigating the inflammasome pathway as heterogeneous response is plainly apparent by fluorescence microscopy and recent reports have shown that IL-1β release may be performed only by sub-populations of pyroptotic cells downstream of inflammasome activation (Liu et al. 2014). The procedure reported by Liu et al interrogates protein release in isolated single cells, but is not readily adaptable to investigations of gene expression heterogeneity, and thus the priming response in the inflammasome pathway. Therefore, the single cell pipeline developed during this dissertation work addresses a technical need for a method capable of integrating fluorescence microscopy with same-cell correlations to gene expression analysis.

While the role of ATP as an external stimulus is universally accepted in the field of inflammasome biology, little attention has been paid to intracellular ATP content. One reason for this is the end-point nature of available methods for ATP determination. The development of a macrophage cell line expressing an intracellular ATP sensor provides a first-ever proof-of-principle for the real-time interrogation of ATP content in live immune cells (Imamura et al. 2009; Kotera et al. 2010). While the RAW 264.7 cell line used for this study is incapable of engaging the NLRP3 inflammasome pathway due to a deletion of the adapter protein ASC, the ability for ATeam to be expressed in immune cells is promising for future work (Pelegrin, Barroso-Gutierrez,

and Surprenant 2008). This method will prove useful for investigating metabolic responses to pro-inflammatory stimuli.

6.3. FUTURE PERSPECTIVES

This work establishes a relationship between cation flux, kinase activation and oxidative signaling upstream of the NLRP3 inflammasome. However, there are a number of compelling open questions that warrant further study:

1. **How is Syk activated by potassium efflux?** While this work establishes a novel and relevant relationship between potassium ion efflux and Syk activation upstream of oxidative signaling and inflammasome activation, it is unclear how nigericin-induced efflux results in Syk phosphorylation. It will be important to determine if global phosphatase and kinase activity is affected by sudden changes in cellular ion content. Additionally, it is unclear whether Syk phosphorylation and activation is sufficient for Syk-mediate ASC phosphorylation upstream of inflammasome assembly (Hara et al. 2013; Lin et al. 2015). For example, it may be possible that ion content induces conformational changes in Syk, ASC, or some other intermediate that facilitates phosphorylation-dependent inflammasome assembly. Biochemical analysis of ion effects on protein conformation assisted by FRET tagging of protein domains will be helpful in testing this possibility.
2. **Is mitochondrial potassium mobilization essential for NLRP3 inflammasome assembly?** Identification of the specific mechanism by which mitochondrial potassium mobilization occurs will be helpful in determining whether this phenomena is linked to oxidative signaling and inflammasome activation. A broad screen of mitochondrial ion channel deletions or mutants will rapidly identify whether this phenomenon is a channel-mediated event, or whether it is a passive process mediated by changes in membrane integrity.
3. **Is potassium efflux-dependent regulation of calcium influx due to ionic pressure or channel activation?** Because potassium and calcium are both

positively charged, it is possible that the potassium-dependent regulation of calcium influx observed in this work is related to passive, charge-passed inhibition. However, there is also a possibility that this effect may be due to activation of gated ion channels. A broad screen of membrane-expressed ion channel deletions or mutants will help to identify whether this process is active or passive.

The further elucidation of mechanisms regulating the NLRP3 inflammasome is crucial to identifying targets for modulating innate immune system-driven inflammation. The identification of ion flux and kinase signaling as upstream regulators further justifies the development of inhibitors against relevant ion channels and protein kinases as therapeutic tools to ameliorate inflammatory pathologies.

6.4. THESIS CONTRIBUTIONS

This dissertation addresses a number of fundamental gaps in understanding NLRP3 inflammasome regulation with a focus on the role of cation flux. The primary contributions of this dissertation to the field of inflammasome biology are:

8. The first demonstration of real-time potassium flux measurements downstream of $P2X_7$ receptor activation and nigericin treatment with high spatiotemporal resolution and analyte specificity.
9. The first measurements of correlated, live-cell dynamics of potassium and calcium flux.
10. The identification of Syk tyrosine kinase as a downstream effector of potassium efflux during nigericin-induced inflammasome assembly and pyroptotic cell death.
11. The implication of Syk kinase activity in the generation of mitochondrial reactive oxygen species upstream of NLRP3 inflammasome assembly.

12. The identification of a dose-dependent relationship between $P2X_7$ purinergic receptor activation, intracellular potassium efflux and plasma membrane permeability.
13. The identification of a mitochondrial potassium pool mobilization downstream of $P2X_7$ purinergic receptor activation.
14. Establishment of potassium efflux as a regulating step for NLRP3 inflammasome-activating calcium influx during $P2X_7$ purinergic receptor activation.

In addition to clarifying the role for cation flux upstream of NLRP3 activation, this dissertation also describes the development of two methods relevant to the study of single cell signatures of cellular and macrophage heterogeneity:

3. A method for correlated fluorescence microscopy and molecular analysis of live single cells was developed. The method allows for the isolation and observation by fluorescence microscopy of live single cells, coupled with downstream processing and multi-target gene expression analysis by RT-qPCR.
4. A mouse macrophage cell line was generated and characterized expressing a protein-based biosensor for live, kinetic analysis of intracellular ATP.

6.5. FUNDING SOURCES

Funding for this work was provided by the Microscale Life Sciences Center, an NIH NHGRI Center of Excellence in Genomic Science (5P50 HG002360 to Dr. Deirdre Meldrum), and the NIH Common Fund LINCS (Library of Integrated Network-Based Cellular Signatures) program (U01CA164250 to Dr. Deirdre Meldrum). Additionally, I received a fellowship from the Science Foundation Arizona and travel funding from the Biological Design Graduate Program and Arizona State University Graduate and Professional Students Association.

REFERENCES

Abrams ST, Zhang N, Manson J, Liu T, Dart C, Baluwa F, Wang SS, Brohi K, Kipar A, Yu W, et al. 2013. Circulating Histones Are Mediators of Trauma-associated Lung Injury. Am J Respir Crit Care Med 187:160–169.

Akira S, Takeda K. 2004. Toll-like receptor signalling. Nature Reviews Immunology 4:499–511.

Aksentijevich I, D Putnam C, Remmers EF, Mueller JL, Le J, Kolodner RD, Moak Z, Chuang M, Austin F, Goldbach-Mansky R, et al. 2007. The clinical continuum of cryopyrinopathies: Novel CIAS1 mutations in North American patients and a new cryopyrin model. Arthritis Rheum 56:1273–1285.

Allam R, Darisipudi MN, Tschopp J, Anders H-J. 2013. Histones trigger sterile inflammation by activating the NLRP3 inflammasome. Eur. J. Immunol. 43:3336–3342.

Allen IC, Scull MA, Moore CB, Holl EK, McElvania-TeKippe E, Taxman DJ, Guthrie EH, Pickles RJ, Ting JP-Y. 2009. The NLRP3 Inflammasome Mediates In Vivo Innate Immunity to Influenza A Virus through Recognition of Viral RNA. Immunity 30:556–565.

Alnemri ES, Livingston DJ, Nicholson DW, Salvesen G, Thornberry NA, Wong WW, Yuan J. 1996. Human ICE/CED-3 protease nomenclature. Cell 87:171.

Arlehamn CSL, Petrilli V, Gross O, Tschopp J, Evans TJ. 2010. The Role of Potassium in Inflammasome Activation by Bacteria. J. Biol. Chem. 285:10508–10518.

Auron PE, Webb AC, Rosenwasser LJ, Mucci SF, Rich A, Wolff SM, Dinarello CA. 1984. Nucleotide-Sequence of Human Monocyte Interleukin-1 Precursor cDNA. Proceedings of the National Academy of Sciences 81:7907–7911.

Babelova A, Moreth K, Tsalastra-Greul W, Zeng-Brouwers J, Eickelberg O, Young MF, Bruckner P, Pfeilschifter J, Schaefer RM, Grone HJ, et al. 2009. Biglycan, a Danger Signal That Activates the NLRP3 Inflammasome via Toll-like and P2X Receptors. J. Biol. Chem. 284:24035–24048.

Bajpai M. 2009. Fostamatinib, a Syk inhibitor prodrug for the treatment of inflammatory diseases. IDrugs 12:174–185.

Baroja-Mazo A, Martín-Sánchez F, Gomez AI, Martínez CM, Amores-Iniesta J, Compan V, Barberà-Cremades M, Yagüe J, Ruiz-Ortiz E, Antón J, et al. 2014. The NLRP3 inflammasome is released as a particulate danger signal that amplifies the inflammatory response. Nat. Immunol. 15:738–748.

Bartlett R, Yerbury JJ, Sluyter R. 2013. P2X7 Receptor Activation Induces Reactive Oxygen Species Formation and Cell Death in Murine EOC13 Microglia. Mediators of Inflammation 2013:1–18.

Bauernfeind FG, Horvath G, Stutz A, Alnemri ES, MacDonald K, Speert D, Fernandes-Alnemri T, Wu J, Monks BG, Fitzgerald KA, et al. 2009. Cutting Edge: NF- B Activating Pattern Recognition and Cytokine Receptors License NLRP3 Inflammasome Activation by Regulating NLRP3 Expression. The Journal of Immunology 183:787–791.

Ben Lu, Nakamura T, Inouye K, Li J, Tang Y, Lundbäck P, Valdes-Ferrer SI, Olofsson PS, Kalb T, Roth J, et al. 2012. Novel role of PKR in inflammasome activation and HMGB1 release. Nature

488:670–674.

Bergsbaken T, Fink SL, Hartigh den AB, Loomis WP, Cookson BT. 2011. Coordinated Host Responses during Pyroptosis: Caspase-1-Dependent Lysosome Exocytosis and Inflammatory Cytokine Maturation. The Journal of Immunology 187:2748–2754.

Bertin J, DiStefano PS. 2000. The PYRIN domain: a novel motif found in apoptosis and inflammation proteins. Cell Death Differ 7:1273–1274.

Bishop CE. 1981. A miniaturised single-step method of cell cloning. J. Immunol. Methods 46:47–51.

Black RA, Kronheim SR, Cantrell M, Deeley MC, March CJ, Prickett KS, Wignall J, Conlon PJ, Cosman D, Hopp TP. 1988. Generation of biologically active interleukin-1 beta by proteolytic cleavage of the inactive precursor. J. Biol. Chem. 263:9437–9442.

Black RA, Kronheim SR, Sleath PR. 1989. Activation of interleukin- 1β by a co-induced protease. FEBS Letters 247:386–390.

Bodin P, Burnstock G. 2001. Purinergic Signalling: ATP Release. Neurochem. Res. 26:959–969.

Brennan MA, Cookson BT. 2000. Salmonella induces macrophage death by caspase-1-dependent necrosis. Mol. Microbiol. 38:31–40.

Brodsky IE, Medzhitov R. 2011. Pyroptosis: Macrophage Suicide Exposes Hidden Invaders. Curr. Biol. 21:R72–R75.

Brookes PS, Yoon Y, Robotham JL, Anders MW, Sheu S-S. 2004. Calcium, ATP, and ROS: a mitochondrial love-hate triangle. AJP: Cell Physiology 287:C817–33.

Brough D, Le Feuvre RA, Wheeler RD, Solovyova N, Hilfiker S, Rothwell NJ, Verkhratsky A. 2003. Ca2+ Stores and Ca2+ Entry Differentially Contribute to the Release of IL-1β and IL-1α from Murine Macrophages. The Journal of Immunology 170:3029–3036.

Broz P, Newton K, Lamkanfi M, Mariathasan S, Dixit VM, Monack DM. 2010. Redundant roles for inflammasome receptors NLRP3 and NLRC4 in host defense against Salmonella. J Exp Med 207:1745–1755.

Cai X, Chen J, Xu H, Liu S, Jiang Q-X, Halfmann R, Chen ZJ. 2014. Prion-like Polymerization Underlies Signal Transduction in Antiviral Immune Defense and Inflammasome Activation. Cell 156:1207–1222.

Calligaris L, Marchetti F, Tommasini A, Ventura A. 2007. The efficacy of anakinra in an adolescent with colchicine-resistant familial Mediterranean fever. Eur J Pediatr 167:695–696.

Cerretti D, Kozlosky C, Mosley B, Nelson N, Van Ness K, Greenstreet T, March C, Kronheim, Druck T, Cannizzaro L, et al. 1992. Molecular cloning of the interleukin-1 beta converting enzyme. Science 256:97–100.

Chen C-J, Kono H, Golenbock D, Reed G, Akira S, Rock KL. 2007. Identification of a key pathway required for the sterile inflammatory response triggered by dying cells. Nat. Med. 13:851–856.

Chen G, Shaw MH, Kim Y-G, Núñez G. 2009. NOD-Like Receptors: Role in Innate Immunity and Inflammatory Disease. Annu. Rev. Pathol. Mech. Dis. 4:365–398.

Chen GY, Núñez G. 2010. Sterile inflammation: sensing and reacting to damage. Nature Publishing Group 10:826–837.

Chen R, Kang R, Fan X-G, Tang D. 2014. Release and activity of histone in diseases. Cell Death Dis 5:e1370–9.

Chu J, Thomas LM, Watkins SC, Franchi L, Núñez G, Salter RD. 2009. Cholesterol-dependent cytolysins induce rapid release of mature IL-1β from murine macrophages in a NLRP3 inflammasome and cathepsin B-dependent manner. Journal of Leukocyte Biology 86:1227–1238.

Chu ZL, Pio F, Xie Z, Welsh K, Krajewska M, Krajewski S, Godzik A, Reed JC. 2001. A novel enhancer of the Apaf1 apoptosome involved in cytochrome c-dependent caspase activation and apoptosis. J. Biol. Chem. 276:9239–9245.

Cogswell JP, Godlevski MM, Wisely GB, Clay WC, Leesnitzer LM, Ways JP, Gray JG. 1994. NF-kappa B regulates IL-1 beta transcription through a consensus NF-kappa B binding site and a nonconsensus CRE-like site. The Journal of Immunology 153:712–723.

Cohen LB, Salzberg BM, Davila HV, Ross WN, Landowne D, Waggoner AS, Wang CH. 1974. Changes in axon fluorescence during activity: molecular probes of membrane potential. J. Membr. Biol. 19:1–36.

Colombini M. 2004. VDAC: the channel at the interface between mitochondria and the cytosol. Mol. Cell. Biochem. 256-257:107–115.

Compan V, Baroja-Mazo A, Lopez-Castejon G, Gomez AI, Martínez CM, Angosto D, Montero MT, Herranz AS, Bazán E, Reimers D, et al. 2012. Cell volume regulation modulates NLRP3 inflammasome activation. Immunity 37:487–500.

Cookson BT, Brennan MA. 2001. Pro-inflammatory programmed cell death. Trends Microbiol. 9:113–114.

Cruz CM, Rinna A, Forman HJ, Ventura ALM, Persechini PM, Ojcius DM. 2007. ATP activates a reactive oxygen species-dependent oxidative stress response and secretion of proinflammatory cytokines in macrophages. J. Biol. Chem. 282:2871–2879.

de Souza N. 2012. Single-cell methods. Nature Methods 9:35–35.

Di Virgilio F, Chiozzi P, Falzoni S, Ferrari D, Sanz JM, Venketaraman V, Baricordi OR. 1998. Cytolytic P2X purinoceptors. Cell Death Differ 5:191–199.

Dinarello CA. 1984. Interleukin-1. Review of infectious diseases.

Dinarello CA. 2013. The C3a receptor, caspase-1, and release of IL-1β. Blood.

Dolinay T, Kim YS, Howrylak J, Hunninghake GM, An CH, Fredenburgh L, Massaro AF, Rogers A, Gazourian L, Nakahira K, et al. 2012. Inflammasome-regulated cytokines are critical mediators of acute lung injury. Am J Respir Crit Care Med 185:1225–1234.

Dostert C, Pétrilli V, Van Bruggen R, Steele C, Mossman BT, Tschopp J. 2008. Innate immune activation through Nalp3 inflammasome sensing of asbestos and silica. Science 320:674–677.

Dubyak GR. 2004. Ion homeostasis, channels, and transporters: an update on cellular mechanisms. AJP: Advances in Physiology Education 28:143–154.

Duewell P, Kono H, Rayner KJ, Sirois CM, Vladimer G, Bauernfeind FG, Abela GS, Franchi L, Núñez G, Schnurr M, et al. 2010. NLRP3 inflammasomes are required for atherogenesis and activated by cholesterol crystals. Nature 464:1357–1361.

Duncan JA, Gao X, Huang MTH, O'Connor BP, Thomas CE, Willingham SB, Bergstralh DT, Jarvis GA, Sparling PF, Ting JPY. 2009. Neisseria gonorrhoeae Activates the Proteinase Cathepsin B to Mediate the Signaling Activities of the NLRP3 and ASC-Containing Inflammasome. The Journal of Immunology 182:6460–6469.

Engström L, Ruud J, Eskilsson A, Larsson A, Mackerlova L, Kugelberg U, Qian H, Vasilache AM, Larsson P, Engblom D, et al. 2012. Lipopolysaccharide-Induced Fever Depends on Prostaglandin E2 Production Specifically in Brain Endothelial Cells. Endocrinology 153:4849–4861.

Faires JS, Mccarty DJ. 1962. Acute arthritis in man and dog after intrasynovial injection of sodium urate crystals. The Lancet.

Feldmeyer L, Keller M, Niklaus G, Hohl D, Werner S, Beer H-D. 2007. The inflammasome mediates UVB-induced activation and secretion of interleukin-1beta by keratinocytes. Curr. Biol. 17:1140–1145.

Fields R. 2000. ATP: an extracellular signaling molecule between neurons and glia. Trends in Neurosciences 23:625–633.

Franchi L, Amer A, Body-Malapel M, Kanneganti T-D, Özören N, Jagirdar R, Inohara N, Vandenabeele P, Bertin J, Coyle A, et al. 2006. Cytosolic flagellin requires Ipaf for activation of caspase-1 and interleukin 1β in salmonella-infected macrophages. Nat. Immunol. 7:576–582.

Franchi L, Kanneganti T-D, Dubyak GR, Núñez G. 2007. Differential requirement of P2X7 receptor and intracellular K+ for caspase-1 activation induced by intracellular and extracellular bacteria. J. Biol. Chem. 282:18810–18818.

French FMF Consortium. 1997. A candidate gene for familial Mediterranean fever. Nature Genetics 17:25–31.

Gao W, Zhang W, Meldrum DR. 2011. RT-qPCR based quantitative analysis of gene expression in single bacterial cells. J. Microbiol. Methods 85:221–227.

Garlid KD, Paucek P. 2003. Mitochondrial potassium transport: the K+ cycle. Biochimica et Biophysica Acta (BBA) - Bioenergetics 1606:23–41.

Genovese MC, Kavanaugh A, Weinblatt ME, Peterfy C, DiCarlo J, White ML, O'Brien M, Grossbard EB, Magilavy DB. 2011. An oral Syk kinase inhibitor in the treatment of rheumatoid arthritis: A three- month randomized, placebo- controlled, phase II study in patients with active rheumatoid arthritis that did not respond to biologic agents. Arthritis Rheum 63:337–345.

Ghonime MG, Shamaa OR, Das S, Eldomany RA, Fernandes-Alnemri T, Alnemri ES, Gavrilin MA, Wewers MD. 2014. Inflammasome Priming by Lipopolysaccharide Is Dependent upon ERK Signaling and Proteasome Function. The Journal of Immunology 192:3881–3888.

Ginsberg SD, Elarova I, Ruben M, Tan F, Counts SE, Eberwine JH, Trojanowski JQ, Hemby SE, Mufson EJ, Che S. 2004. Single-cell gene expression analysis: implications for neurodegenerative and neuropsychiatric disorders. Neurochem. Res. 29:1053–1064.

Giri JG, Lomedico PT, Mizel SB. 1985. Studies on the synthesis and secretion of interleukin 1. I. A 33,000 molecular weight precursor for interleukin 1. The Journal of Immunology 134:343–349.

Gombault A, Baron L, Couillin I. 2012. ATP release and purinergic signaling in NLRP3 inflammasome activation. Front Immunol 3:414.

Goss CH, Brower RG, Hudson LD, Rubenfeld GD, ARDS Network. 2003. Incidence of acute lung injury in the United States. Crit. Care Med. 31:1607–1611.

Grabarek J, Amstad P, Darzynkiewicz Z. 2002. Use of fluorescently labeled caspase inhibitors as affinity labels to detect activated caspases. Hum. Cell 15:1–12.

Gross O, Poeck H, Bscheider M, Dostert C, Hannesschläger N, Endres S, Hartmann G, Tardivel A, Schweighoffer E, Tybulewicz V, et al. 2009. Syk kinase signalling couples to the Nlrp3 inflammasome for anti-fungal host defence. Nature 459:433–436.

Gu Y, Kuida K, Tsutsui H, Ku G, Hsiao K, Fleming MA, Hayashi N, Higashino K, Okamura H, Nakanishi K, et al. 1997. Activation of interferon-gamma inducing factor mediated by interleukin-1beta converting enzyme. Science 275:206–209.

Guarda G, Zenger M, Yazdi AS, Schroder K, Ferrero I, Menu P, Tardivel A, Mattmann C, Tschopp J. 2011. Differential Expression of NLRP3 among Hematopoietic Cells. The Journal of Immunology 186:2529–2534.

Halle A, Hornung V, Petzold GC, Stewart CR, Monks BG, Reinheckel T, Fitzgerald KA, Latz E, Moore KJ, Golenbock DT. 2008. The NALP3 inflammasome is involved in the innate immune response to amyloid-β. Nat. Immunol. 9:857–865.

Hara H, Tsuchiya K, Kawamura I, Fang R, Hernandez-Cuellar E, Shen Y, Mizuguchi J, Schweighoffer E, Tybulewicz V, Mitsuyama M. 2013. Phosphorylation of the adaptor ASC acts as a molecular switch that controls the formation of speck-like aggregates and inflammasome activity. Nature Publishing Group 14:1247–1255.

Hari A, Zhang Y, Tu Z, Detampel P, Stenner M, Ganguly A, Shi Y. 2014. Activation of NLRP3 inflammasome by crystalline structures via cell surface contact. Sci. Rep. 4:7281–8.

Harijith A, Ebenezer DL, Natarajan V. 2014. Reactive oxygen species at the crossroads of inflammasome and inflammation. Front Physiol 5:352.

Heid ME, Keyel PA, Kamga C, Shiva S, Watkins SC, Salter RD. 2013. Mitochondrial Reactive Oxygen Species Induces NLRP3-Dependent Lysosomal Damage and Inflammasome Activation. The Journal of Immunology 191:5230–5238.

Heneka MT, Kummer MP, Stutz A, Delekate A, Schwartz S, Vieira-Saecker A, Griep A, Axt D, Remus A, Tzeng T-C, et al. 2013. NLRP3 is activated in Alzheimer's disease and contributes to pathology in APP/PS1 mice. Nature 493:674–678.

Hlaing T, Guo RF, Dilley KA, Loussia JM, Morrish TA, Shi MM, Vincenz C, Ward PA. 2001. Molecular cloning and characterization of DEFCAP-L and -S, two isoforms of a novel member of the mammalian Ced-4 family of apoptosis proteins. J. Biol. Chem. 276:9230–9238.

Hoffman HM, Throne ML, Amar NJ, Sebai M, Kivitz AJ, Kavanaugh A, Weinstein SP, Belomestnov P, Yancopoulos GD, Stahl N, et al. 2008. Efficacy and safety of rilonacept (interleukin-1 trap) in patients with cryopyrin-associated periodic syndromes: Results from two sequential placebo-controlled studies. Arthritis Rheum 58:2443–2452.

Hofmann K, Bucher P, Tschopp J. 1997. The CARD domain: a new apoptotic signalling motif. Trends Biochem. Sci. 22:155–156.

Hogquist KA, Nett MA, Unanue ER, Chaplin DD. 1991. Interleukin 1 is processed and released during apoptosis. Proceedings of the National Academy of Sciences 88:8485–8489.

Horng T. 2014. Calcium signaling and mitochondrial destabilization in the triggering of the NLRP3 inflammasome. Trends in Immunology 35:253–261.

Hornung V, Ablasser A, Charrel-Dennis M, Bauernfeind F, Horvath G, Caffrey DR, Latz E, Fitzgerald KA. 2009. AIM2 recognizes cytosolic dsDNA and forms a caspase-1-activating inflammasome with ASC. Nature 458:514–518.

Hornung V, Bauernfeind F, Halle A, Samstad EO, Kono H, Rock KL, Fitzgerald KA, Latz E. 2008. Silica crystals and aluminum salts activate the NALP3 inflammasome through phagosomal destabilization. Nat. Immunol. 9:847–856.

Huang H, Evankovich J, Yan W, Nace G, Zhang L, Ross M, Liao X, Billiar T, Xu J, Esmon CT, et al. 2011. Endogenous histones function as alarmins in sterile inflammatory liver injury through Toll-like receptor 9 in mice. Hepatology 54:999–1008.

Ichinohe T, Pang IK, Iwasaki A. 2010. Influenza virus activates inflammasomes via its intracellular M2 ion channel. Nat. Immunol. 11:404–410.

Imamura H, Nhat KPH, Togawa H, Saito K, Iino R, Kato-Yamada Y, Nagai T, Noji H. 2009. Visualization of ATP levels inside single living cells with fluorescence resonance energy transfer-based genetically encoded indicators. Proceedings of the National Academy of Sciences 106:15651–15656.

Jin C, Flavell RA. 2010. Molecular mechanism of NLRP3 inflammasome activation. J. Clin. Immunol. 30:628–631.

Johnson JL, Newby AC. 2009. Macrophage heterogeneity in atherosclerotic plaques. Curr. Opin. Lipidol. 20:370–378.

Kang R, Zhang Q, Hou W, Yan Z, Chen R, Bonaroti J, Bansal P, Billiar TR, Tsung A, Wang Q, et al. 2014. Intracellular Hmgb1 inhibits inflammatory nucleosome release and limits acute pancreatitis in mice. Gastroenterology 146:1097–1107.

Kankkunen P, Teirila L, Rintahaka J, Alenius H, Wolff H, Matikainen S. 2010. (1,3)- -Glucans Activate Both Dectin-1 and NLRP3 Inflammasome in Human Macrophages. The Journal of Immunology 184:6335–6342.

Katnelson MA, Rucker LG, Russo HM, Dubyak GR. 2015. K+ Efflux Agonists Induce NLRP3 Inflammasome Activation Independently of Ca2+ Signaling. :1–19.

Kerr JF, Wyllie AH, Currie AR. 1972. Apoptosis: a basic biological phenomenon with wide-ranging implications in tissue kinetics. Br. J. Cancer 26:239–257.

Klein CA, Blankenstein TJF, Schmidt-Kittler O, Petronio M, Polzer B, Stoecklein NH, Riethmüller G. 2002. Genetic heterogeneity of single disseminated tumour cells in minimal residual cancer. Lancet 360:683–689.

Koonin EV, Aravind L. 2000. The NACHT family - a new group of predicted NTPases implicated in apoptosis and MHC transcription activation. Trends Biochem. Sci. 25:223–224.

Kostura MJ, Tocci MJ, Limjuco G, Chin J, Cameron P, Hillman AG, Chartrain NA, Schmidt JA. 1989. Identification of a monocyte specific pre-interleukin 1 beta convertase activity. Proceedings

of the National Academy of Sciences 86:5227–5231.

Kotera I, Iwasaki T, Imamura H, Noji H, Nagai T. 2010. Reversible Dimerization of Aequorea victoriaFluorescent Proteins Increases the Dynamic Range of FRET-Based Indicators. ACS Chem. Biol. 5:215–222.

Kozoriz MG, Church J, Ozog MA, Naus CC, Krebs C. 2010. Temporary sequestration of potassium by mitochondria in astrocytes. J. Biol. Chem. 285:31107–31119.

Laliberte RE, Eggler J, Gabel CA. 1999. ATP treatment of human monocytes promotes caspase-1 maturation and externalization. J. Biol. Chem. 274:36944–36951.

Lamkanfi M, Dixit VM. 2014. Mechanisms and functions of inflammasomes. Cell 157:1013–1022.

Lamkanfi M, Mueller JL, Vitari AC, Misaghi S, Fedorova A, Deshayes K, Lee WP, Hoffman HM, Dixit VM. 2009. Glyburide inhibits the Cryopyrin/Nalp3 inflammasome. The Journal of Cell Biology 187:61–70.

Lamkanfi M, Sarkar A, Vande Walle L, Vitari AC, Amer AO, Wewers MD, Tracey KJ, Kanneganti TD, Dixit VM. 2010. Inflammasome-Dependent Release of the Alarmin HMGB1 in Endotoxemia. The Journal of Immunology 185:4385–4392.

Latz E, Xiao TS, Stutz A. 2013. Activation and regulation of the inflammasomes. Nature Reviews Immunology 13:397–411.

Laudisi F, Viganò E, Mortellaro A. 2014. Tyrosine kinases: the molecular switch for inflammasome activation. Cell Mol Immunol 11:129–131.

Lee G-S, Subramanian N, Kim AI, Aksentijevich I, Goldbach-Mansky R, Sacks DB, Germain RN, Kastner DL, Chae JJ. 2012. The calcium-sensing receptor regulates the NLRP3 inflammasome through Ca2+ and cAMP. Nature 492:123–127.

Lepore L, Paloni G, Caorsi R, Alessio M, Rigante D, Ruperto N, Cattalini M, Tommasini A, Zulian F, Ventura A, et al. 2010. Follow-up and quality of life of patients with cryopyrin-associated periodic syndromes treated with Anakinra. J. Pediatr. 157:310–315.e1.

Levsky JM, Singer RH. 2003. Gene expression and the myth of the average cell. Trends Cell Biol. 13:4–6.

Li H, Willingham SB, Ting JPY, Re F. 2008. Cutting Edge: Inflammasome Activation by Alum and Alum's Adjuvant Effect Are Mediated by NLRP3. The Journal of Immunology 181:17–21.

Li P, Allen H, Banerjee S, Franklin S, Herzog L, Johnston C, McDowell J, Paskind M, Rodman L, Salfeild J, et al. 1995. Mice deficient in IL-1 beta-converting enzyme are defective in production of mature IL-1 beta and resistant to endotoxic shock. Cell 80:401–411.

Li P, Nijhawan D, Budihardjo I, Srinivasula SM, Ahmad M, Alnemri ES, Wang X. 1997. Cytochrome c and dATP-dependent formation of Apaf-1/caspase-9 complex initiates an apoptotic protease cascade. Cell 91:479–489.

Liao KC, Mogridge J. 2013. Activation of the Nlrp1b Inflammasome by Reduction of Cytosolic ATP. Infection and Immunity 81:570–579.

Lidstrom ME, Meldrum DR. 2003. Life-on-a-chip. Nat. Rev. Microbiol. 1:158–164.

Lin Y-C, Huang D-Y, Wang J-S, Lin Y-L, Hsieh S-L, Huang K-C, Lin W-W. 2015. Syk is involved in NLRP3 inflammasome-mediated caspase-1 activation through adaptor ASC phosphorylation and enhanced oligomerization. Journal of Leukocyte Biology:1–11.

Liu T, Yamaguchi Y, Shirasaki Y, Shikada K, Yamagishi M, Hoshino K, Kaisho T, Takemoto K, Suzuki T, Kuranaga E, et al. 2014. Single-Cell Imaging of Caspase-1 Dynamics Reveals an All-or-None Inflammasome Signaling Response. Cell Rep 8:974–982.

Livak KJ, Schmittgen TD. 2001. Analysis of relative gene expression data using real-time quantitative PCR and the 2(-Delta Delta C(T)) Method. Methods 25:402–408.

Lopez-Castejon G, Brough D. 2011. Understanding the mechanism of IL-1β secretion. Cytokine & growth factor reviews.

Lu A, Magupalli VG, Ruan J, Yin Q, Atianand MK, Vos MR, Schröder GF, Fitzgerald KA, Wu H, Egelman EH. 2014. Unified Polymerization Mechanism for the Assembly of ASC-Dependent Inflammasomes. Cell 156:1193–1206.

Luan Z-G, Zhang X-J, Yin X-H, Ma X-C, Zhang H, Zhang C, Guo R-X. 2013. Downregulation of HMGB1 protects against the development of acute lung injury after severe acute pancreatitis. Immunobiology 218:1261–1270.

Lupfer C, Kanneganti T-D. 2013. Unsolved Mysteries in NLR Biology. Front Immunol 4:285.

MacKenzie A, Wilson HL, Kiss-Toth E, Dower SK, North RA, Surprenant A. 2001. Rapid secretion of interleukin-1beta by microvesicle shedding. Immunity 15:825–835.

Man SM, Hopkins LJ, Nugent E, Cox S, Gluck IM, Tourlomousis P, Wright JA, Cicuta P, Monie TP, Bryant CE. 2014. Inflammasome activation causes dual recruitment of NLRC4 and NLRP3 to the same macromolecular complex. Proceedings of the National Academy of Sciences 111:7403–7408.

Manji GA, Wang L, Geddes BJ, Brown M, Merriam S, Al-Garawi A, Mak S, Lora JM, Briskin M, Jurman M, et al. 2002. PYPAF1, a PYRIN-containing Apaf1-like Protein That Assembles with ASC and Regulates Activation of NF-κB. J. Biol. Chem. 277:11570–11575.

March CJ, Mosley B, Larsen A, Cerretti DP, Braedt G, Price V, Gillis S, Henney CS, Kronheim SR, Grabstein K. 1985. Cloning, sequence and expression of two distinct human interleukin-1 complementary DNAs. Nature 315:641–647.

Marchetti C, Chojnacki J, Toldo S, Mezzaroma E, Tranchida N, Rose SW, Federici M, Van Tassell BW, Zhang S, Abbate A. 2014. A novel pharmacologic inhibitor of the NLRP3 inflammasome limits myocardial injury after ischemia-reperfusion in the mouse. J. Cardiovasc. Pharmacol. 63:316–322.

Mariathasan S, Newton K, Monack DM, Vucic D, French DM, Lee WP, Roose-Girma M, Erickson S, Dixit VM. 2004. Differential activation of the inflammasome by caspase-1 adaptors ASC and Ipaf. Nature 430:213–218.

Mariathasan S, Weiss DS, Newton K, McBride J, O'Rourke K, Roose-Girma M, Lee WP, Weinrauch Y, Monack DM, Dixit VM. 2006. Cryopyrin activates the inflammasome in response to toxins and ATP. Nature 440:228–232.

Marichal T, Ohata K, Bedoret D, Mesnil C, Sabatel C, Kobiyama K, Lekeux P, Coban C, Akira S, Ishii KJ, et al. 2011. DNA released from dying host cells mediates aluminum adjuvant activity.

Nat. Med. 17:996–1002.

Martinon F, Burns K, Tschopp J. 2002. The inflammasome: a molecular platform triggering activation of inflammatory caspases and processing of proIL-beta. Mol. Cell 10:417–426.

Martinon F, Hofmann K, Tschopp J. 2001. The pyrin domain: a possible member of the death domain-fold family implicated in apoptosis and inflammation. Curr. Biol. 11:R118–20.

Martinon F, Mayor A, Tschopp J. 2009. The inflammasomes: guardians of the body. Annu. Rev. Immunol. 27:229–265.

Martinon F, Pétrilli V, Mayor A, Tardivel A, Tschopp J. 2006. Gout-associated uric acid crystals activate the NALP3 inflammasome. Nature 440:237–241.

Martinon F. 2010. Signaling by ROS drives inflammasome activation. Eur. J. Immunol. 40:616–619.

Masumoto J, Taniguchi S, Ayukawa K, Sarvotham H, Kishino T, Niikawa N, Hidaka E, Katsuyama T, Higuchi T, Sagara J. 1999. ASC, a novel 22-kDa protein, aggregates during apoptosis of human promyelocytic leukemia HL-60 cells. J. Biol. Chem. 274:33835–33838.

McNeela EA, Burke Á, Neill DR, Baxter C, Fernandes VE, Ferreira D, Smeaton S, El-Rachkidy R, McLoughlin RM, Mori A, et al. 2010. Pneumolysin Activates the NLRP3 Inflammasome and Promotes Proinflammatory Cytokines Independently of TLR4.Philpott DJ, editor. PLoS Pathog 6:e1001191–16.

Medzhitov R. 2010. Inflammation 2010: New Adventures of an Old Flame. Cell 140:771–776.

Meissner F, Seger RA, Moshous D, Fischer A, Reichenbach J, Zychlinsky A. 2010. Inflammasome activation in NADPH oxidase defective mononuclear phagocytes from patients with chronic granulomatous disease. Blood 116:1570–1573.

Meixenberger K, Pache F, Eitel J, Schmeck B, Hippenstiel S, Slevogt H, N'Guessan P, Witzenrath M, Netea MG, Chakraborty T, et al. 2010. Listeria monocytogenes-Infected Human Peripheral Blood Mononuclear Cells Produce IL-1 , Depending on Listeriolysin O and NLRP3. The Journal of Immunology 184:922–930.

Miao EA, Alpuche-Aranda CM, Dors M, Clark AE, Bader MW, Miller SI, Aderem A. 2006. Cytoplasmic flagellin activates caspase-1 and secretion of interleukin 1β via Ipaf. Nat. Immunol. 7:569–575.

Minta A, Tsien RY. 1989. Fluorescent indicators for cytosolic sodium. J. Biol. Chem. 264:19449–19457.

Mirault T, Launay D, Cuisset L, Hachulla E, Lambert M, Queyrel V, Quemeneur T, Morell-Dubois S, Hatron P-Y. 2006. Recovery from deafness in a patient with Muckle-Wells syndrome treated with anakinra. Arthritis Rheum 54:1697–1700.

Morales-Torres J. 2010. R788 (fostamatinib disodium): a novel approach for the treatment of rheumatoid arthritis. International Journal of Clinical Rheumatology 5:9–15.

Mosser DM, Edwards JP. 2008. Exploring the full spectrum of macrophage activation. Nature Reviews Immunology 8:958–969.

Mukhopadhyay P, Rajesh M, Haskó G, Hawkins BJ, Madesh M, Pacher P. 2007. Simultaneous

detection of apoptosis and mitochondrial superoxide production in live cells by flow cytometry and confocal microscopy. Nat Protoc 2:2295–2301.

Muñoz-Planillo R, Kuffa P, Martínez-Colón G, Smith BL, Rajendiran TM, Núñez G. 2013. K^+ efflux is the common trigger of NLRP3 inflammasome activation by bacterial toxins and particulate matter. Immunity 38:1142–1153.

Murakami T, Ockinger J, Yu J, Byles V, McColl A, Hofer AM, Horng T. 2012. Critical role for calcium mobilization in activation of the NLRP3 inflammasome. Proc. Natl. Acad. Sci. U.S.A. 109:11282–11287.

Murakami T, Ockinger J, Yu J, Byles V. 2012. Critical role for calcium mobilization in activation of the NLRP3 inflammasome.

Muta T, Takeshige K. 2001. Essential roles of CD14 and lipopolysaccharide-binding protein for activation of toll-like receptor (TLR)2 as well as TLR4 Reconstitution of TLR2- and TLR4-activation by distinguishable ligands in LPS preparations. Eur. J. Biochem. 268:4580–4589.

Nakahira K, Haspel JA, Rathinam VAK, Lee S-J, Dolinay T, Lam HC, Englert JA, Rabinovitch M, Cernadas M, Kim HP, et al. 2010. Autophagy proteins regulate innate immune responses by inhibiting the release of mitochondrial DNA mediated by the NALP3 inflammasome. Nature Publishing Group 12:222–230.

Narsinh KH, Sun N, Sanchez-Freire V, Lee AS, Almeida P, Hu S, Jan T, Wilson KD, Leong D, Rosenberg J, et al. 2011. Single cell transcriptional profiling reveals heterogeneity of human induced pluripotent stem cells. J. Clin. Invest. 121:1217–1221.

Nelson DE, Ihekwaba AEC, Elliott M, Johnson JR, Gibney CA, Foreman BE, Nelson G, See V, Horton CA, Spiller DG, et al. 2004. Oscillations in NF-kappaB signaling control the dynamics of gene expression. Science 306:704–708.

Nelson DW, Gregg RJ, Kort ME, Perez-Medrano A, Voight EA, Wang Y, Grayson G, Namovic MT, Donnelly-Roberts DL, Niforatos W, et al. 2006. Structure-activity relationship studies on a series of novel, substituted 1-benzyl-5-phenyltetrazole P2X7 antagonists. J. Med. Chem. 49:3659–3666.

Nencioni L, Villa L, Tagliabue A, Antoni G, Presentini R, Perin F, Silvestri S, Boraschi D. 1987. In vivo immunostimulating activity of the 163-171 peptide of human IL-1 beta. The Journal of Immunology 139:800–804.

Neumann K, Ruland J. 2013. Kinases conquer the inflammasomes. Nature Publishing Group 14:1207–1208.

Nicholson DW, Ali A, Thornberry NA, Vaillancourt JP, Ding CK, Gallant M, Gareau Y, Griffin PR, Labelle M, Lazebnik YA. 1995. Identification and inhibition of the ICE/CED-3 protease necessary for mammalian apoptosis. Nature 376:37–43.

Nickel W, Rabouille C. 2009. Mechanisms of regulated unconventional protein secretion. Nat. Rev. Mol. Cell Biol. 10:148–155.

Nolin F, Michel J, Wortham L, Tchelidze P, Balossier G, Banchet V, Bobichon H, Lalun N, Terryn C, Ploton D. 2013. Changes to cellular water and element content induced by nucleolar stress: investigation by a cryo-correlative nano-imaging approach. Cell. Mol. Life Sci. 70:2383–2394.

Novak I, Amstrup J, Henriksen KL. 2003. ATP release and effects in pancreas. Drug development

….

Okamura H, Tsutsi H, Komatsu T, Yutsudo M, Hakura A, Tanimoto T, Torigoe K, Okura T, Nukada Y, Hattori K. 1995. Cloning of a new cytokine that induces IFN-gamma production by T cells. Nature 378:88–91.

Palomäki J, Välimäki E, Sund J, Vippola M, Clausen PA, Jensen KA, Savolainen K, Matikainen S, Alenius H. 2011. Long, Needle-like Carbon Nanotubes and Asbestos Activate the NLRP3 Inflammasome through a Similar Mechanism. ACS Nano 5:6861–6870.

Papin S, Cuenin S, Agostini L, Martinon F, Werner S, Beer H-D, Grütter C, Grütter M, Tschopp J. 2007. The SPRY domain of Pyrin, mutated in familial Mediterranean fever patients, interacts with inflammasome components and inhibits proIL-1β processing. Cell Death Differ 14:1457–1466.

Pardal R, Clarke MF, Morrison SJ. 2003. Applying the principles of stem-cell biology to cancer. Nat. Rev. Cancer 3:895–902.

Pelegrin P, Barroso-Gutierrez C, Surprenant A. 2008. P2X7 Receptor Differentially Couples to Distinct Release Pathways for IL-1 in Mouse Macrophage. The Journal of Immunology 180:7147–7157.

Pelegrin P, Surprenant A. 2006. Pannexin-1 mediates large pore formation and interleukin-1 beta release by the ATP-gated P2X(7) receptor. EMBO J. 25:5071–5082.

Perregaux D, Gabel CA. 1994. Interleukin-1 beta maturation and release in response to ATP and nigericin. Evidence that potassium depletion mediated by these agents is a necessary and common feature of their activity. J. Biol. Chem. 269:15195–15203.

Petrilli V, Papin S, Dostert C, Mayor A, Martinon F, Tschopp J. 2007. Activation of the NALP3 inflammasome is triggered by low intracellular potassium concentration. Cell Death Differ 14:1583–1589.

Piccini A, Carta S, Tassi S, Lasiglie D, Fossati G, Rubartelli A. 2008. ATP is released by monocytes stimulated with pathogen-sensing receptor ligands and induces IL-1 beta and IL-18 secretion in an autocrine way. Proceedings of the National Academy of Sciences 105:8067–8072.

Piccioli P, Rubartelli A. 2013. The secretion of IL-1β and options for release. Semin. Immunol. 25:425–429.

Podolanczuk A, Lazarus AH, Crow AR, Grossbard E, Bussel JB. 2009. Of mice and men: an open-label pilot study for treatment of immune thrombocytopenic purpura by an inhibitor of Syk. Blood 113:3154–3160.

Poyet JL, Srinivasula SM, Tnani M, Razmara M, Fernandes-Alnemri T, Alnemri ES. 2001. Identification of Ipaf, a human caspase-1-activating protein related to Apaf-1. J. Biol. Chem. 276:28309–28313.

Puren AJ, Fantuzzi G, Dinarello CA. 1999. Gene expression, synthesis, and secretion of interleukin 18 and interleukin 1beta are differentially regulated in human blood mononuclear cells and mouse spleen cells. Proceedings of the National Academy of Sciences 96:2256–2261.

Rathinam VAK, Vanaja SK, Fitzgerald KA. 2012. Regulation of inflammasome signaling. Nat. Immunol. 13:333–332.

Riteau N, Baron L, Villeret B, Guillou N, Savigny F, Ryffel B, Rassendren F, Le Bert M, Gombault

A, Couillin I. 2012. ATP release and purinergic signaling: a common pathway for particle-mediated inflammasome activation. Cell Death Dis 3:e403–10.

Salminen A, Ojala J, Suuronen T, Kaarniranta K, Kauppinen A. 2008. Amyloid-β oligomers set fire to inflammasomes and induce Alzheimer's pathology. Journal of Cellular and Molecular Medicine 12:2255–2262.

Sandanger O, Ranheim T, Vinge LE, Bliksoen M, Alfsnes K, Finsen AV, Dahl CP, Askevold ET, Florholmen G, Christensen G, et al. 2013. The NLRP3 inflammasome is up-regulated in cardiac fibroblasts and mediates myocardial ischaemia-reperfusion injury. Cardiovascular Research 99:164–174.

Schenk U, Westendorf AM, Radaelli E, Casati A, Ferro M, Fumagalli M, Verderio C, Buer J, Scanziani E, Grassi F. 2008. Purinergic Control of T Cell Activation by ATP Released Through Pannexin-1 Hemichannels. Sci Signal 1:–ra6.

Schroder K, Tschopp J. 2010. The Inflammasomes. Cell 140:821–832.

Schwiebert EM, Zsembery A. 2003. Extracellular ATP as a signaling molecule for epithelial cells. Biochimica et Biophysica Acta (BBA) - Biomembranes 1615:7–32.

Shi Y, Evans JE, Rock KL. 2003. Molecular identification of a danger signal that alerts the immune system to dying cells. Nature 425:516–521.

Shimada K, Crother TR, Karlin J, Dagvadorj J, Chiba N, Chen S, Ramanujan VK, Wolf AJ, Vergnes L, Ojcius DM, et al. 2012. Oxidized Mitochondrial DNA Activates the NLRP3 Inflammasome during Apoptosis. Immunity 36:401–414.

Singer II, Scott S, Chin J, Bayne EK, Limjuco G, Weidner J, Miller DK, Chapman K, Kostura MJ. 1995. The interleukin-1 beta-converting enzyme (ICE) is localized on the external cell surface membranes and in the cytoplasmic ground substance of human monocytes by immuno-electron microscopy. J Exp Med 182:1447–1459.

Smith RD, Malley JD, Schechter AN. 2000. Quantitative analysis of globin gene induction in single human erythroleukemic cells. Nucleic Acids Res. 28:4998–5004.

So A, De Smedt T, Revaz S, Tschopp J. 2007. A pilot study of IL-1 inhibition by anakinra in acute gout. Arthritis Res. Ther. 9:R28.

Srinivasula SM, Poyet J-L, Razmara M, Datta P, Zhang Z, Alnemri ES. 2002. The PYRIN-CARD protein ASC is an activating adaptor for caspase-1. J. Biol. Chem. 277:21119–21122.

Staruch MJ, Wood DD. 1983. The adjuvanticity of interleukin 1 in vivo. The Journal of Immunology 130:2191–2194.

Ståhlberg A, Bengtsson M. 2010. Single-cell gene expression profiling using reverse transcription quantitative real-time PCR. Methods 50:282–288.

Ståhlberg A, Thomsen C, Ruff D, Åman P. 2012. Quantitative PCR analysis of DNA, RNAs, and proteins in the same single cell. Clin. Chem. 58:1682–1691.

Stehlik C, Lee SH, Dorfleutner A, Stassinopoulos A, Sagara J, Reed JC. 2003. Apoptosis-associated speck-like protein containing a caspase recruitment domain is a regulator of procaspase-1 activation. The Journal of Immunology 171:6154–6163.

Steiner AA, Chakravarty S, Rudaya AY, Herkenham M. 2006. Bacterial lipopolysaccharide fever is initiated via Toll-like receptor 4 on hematopoietic cells. Blood.

Sutterwala FS, Haasken S, Cassel SL. 2014. Mechanism of NLRP3 inflammasome activation. Ann. N. Y. Acad. Sci. 1319:82–95.

Takeuchi O, Akira S. 2010. Pattern Recognition Receptors and Inflammation. Cell 140:805–820.

Tenthorey JL, Kofoed EM, Daugherty MD, Malik HS, Vance RE. 2014. Molecular Basis for Specific Recognition of Bacterial Ligands by NAIP/NLRC4 Inflammasomes. Mol. Cell 54:17–29.

Terasaki PI, McClelland JD. 1964. Microdroplet Assay of Human Serum Cytotoxins. Nature 204:998–1000.

Terkeltaub R, Sundy JS, Schumacher HR, Murphy F, Bookbinder S, Biedermann S, Wu R, Mellis S, Radin A. 2009. The interleukin 1 inhibitor rilonacept in treatment of chronic gouty arthritis: results of a placebo-controlled, monosequence crossover, non-randomised, single-blind pilot study. Annals of the Rheumatic Diseases 68:1613–1617.

Thornberry NA, Bull HG, Calaycay JR, Chapman KT, Howard AD, Kostura MJ, Miller DK, Molineaux SM, Weidner JR, Aunins J. 1992. A novel heterodimeric cysteine protease is required for interleukin-1 beta processing in monocytes. Nature 356:768–774.

Tiemi Shio M, Eisenbarth SC, Savaria M, Vinet AF, Bellemare M-J, Harder KW, Sutterwala FS, Bohle DS, Descoteaux A, Flavell RA, et al. 2009. Malarial Hemozoin Activates the NLRP3 Inflammasome through Lyn and Syk Kinases.Kazura JW, editor. PLoS Pathog 5:e1000559–14.

Ting JP-Y, Lovering RC, Alnemri ESPD, Bertin J, Boss JM, Davis B, Flavell RA, Girardin SE, Godzik A, Harton JA, et al. 2008. The NLR gene family: An official nomenclature. Immunity 28:285–287.

Toldo S, Mezzaroma E, Mauro AG, Salloum F, Van Tassell BW, Abbate A. 2014. The Inflammasome in Myocardial Injury and Cardiac Remodeling. Antioxid. Redox Signal.:150127063122000.

Tschopp J. 2011. Mitochondria: Sovereign of inflammation? Eur. J. Immunol. 41:1196–1202.

Ursu D, Ebert P, Langron E, Ruble C, Munsie L, Zou W, Fijal B, Qian Y-W, McNearney TA, Mogg A, et al. 2014. Gain and loss of function of P2X7 receptors: mechanisms, pharmacology and relevance to diabetic neuropathic pain. 10:1–11.

Vandanmagsar B, Youm Y-H, Ravussin A, Galgani JE, Stadler K, Mynatt RL, Ravussin E, Stephens JM, Dixit VD. 2011. The NLRP3 inflammasome instigates obesity-induced inflammation and insulin resistance. Nat. Med. 17:179–188.

Walev I, Reske K, Palmer M, Valeva A, Bhakdi S. 1995. Potassium-Inhibited Processing of Il-1-Beta in Human Monocytes. EMBO J. 14:1607–1614.

Weinblatt ME, Kavanaugh A, Burgos Vargas R, Dikranian AH, Medrano Ramirez G, Morales Torres JL, Murphy FT, Musser TK, Straniero N, Vicente Gonzales AV, et al. 2008. Treatment of rheumatoid arthritis with a syk kinase inhibitor: A twelve- week, randomized, placebo- controlled trial. Arthritis Rheum 58:3309–3318.

Wen H, Gris D, Lei Y, Jha S, Zhang L, Huang MT-H, Brickey WJ, Ting JP-Y. 2011. Fatty acid-induced NLRP3-ASC inflammasome activation interferes with insulin signaling. Nat. Immunol.

12:408–415.

Wong K-W, Jacobs WR Jr. 2011. Critical role for NLRP3 in necrotic death triggered by Mycobacterium tuberculosis. Cellular Microbiology 13:1371–1384.

Yan Z, Khadra A, Li S, Tomic M, Sherman A, Stojilkovic SS. 2010. Experimental Characterization and Mathematical Modeling of P2X7 Receptor Channel Gating. Journal of Neuroscience 30:14213–14224.

Yan Z, Li S, Liang Z, Tomić M, Stojilkovic SS. 2008. The P2X7 receptor channel pore dilates under physiological ion conditions. J. Gen. Physiol. 132:563–573.

Yang H, Antoine DJ, Andersson U, Tracey KJ. 2013. The many faces of HMGB1: molecular structure-functional activity in inflammation, apoptosis, and chemotaxis. Journal of Leukocyte Biology 93:865–873.

Yaron JR, Ziegler CP, Tran TH, Tian Y, Su F, Glenn HL, Meldrum DR. Single cell temporal heterogeneity in caspase-1 activation in response to NLRP3 stimuli is independent of potassium ion efflux rate. In: Vol. 24. New Orleans, LA.

Yuan X, Zhou Y, Wang W, Li J, Xie G, Zhao Y, Xu D, Shen L. 2013. Activation of TLR4 signaling promotes gastric cancer progression by inducing mitochondrial ROS production. Cell Death Dis 4:e794.

Zeng J, Wang J, Gao W, Mohammadreza A, Kelbauskas L, Zhang W, Johnson RH, Meldrum DR. 2011. Quantitative single-cell gene expression measurements of multiple genes in response to hypoxia treatment. Anal Bioanal Chem 401:3–13.

Zhang Q, Raoof M, Chen Y, Sumi Y, Sursal T, Junger W, Brohi K, Itagaki K, Hauser CJ. 2010. Circulating mitochondrial DAMPs cause inflammatory responses to injury. Nature 464:104–107.

Zheng Y, Gardner SE, Clarke MCH. 2011. Cell Death, Damage-Associated Molecular Patterns, and Sterile Inflammation in Cardiovascular Disease. Arteriosclerosis, Thrombosis, and Vascular Biology 31:2781–2786.

Zhou R, Tardivel A, Thorens B, Choi I, Tschopp J. 2010. Thioredoxin-interacting protein links oxidative stress to inflammasome activation. Nat. Immunol. 11:136–140.

Zhou R, Yazdi AS, Menu P, Tschopp J. 2011. A role for mitochondria in NLRP3 inflammasome activation. Nature 469:221–225.

Zou H, Li Y, Liu X, Wang X. 1999. An APAF-1.cytochrome c multimeric complex is a functional apoptosome that activates procaspase-9. J. Biol. Chem. 274:11549–11556.

APPENDIX A

SELECTED STEP-WISE PROTOCOLS

Protocol 1: NLRP3 Inflammasome induction

Materials (in addition to standard J774A.1 cell culture materials):

- LPS from E. coli O111:B4 (Sigma Aldrich, St. Louis, MO, USA)
- NLRP3 inducing agent
    - ATP, 3 mM final (Sigma Aldrich, St. Louis, MO, USA)
    - Nigericin, 20 µM final (Cayman Chemical, Ann Arbor, MI, USA)
- NLRP3 inhibitors
    - Potassium chloride, 130 mM final (Sigma Aldrich, St. Louis, MO, USA)
    - OXSI-2, 2 µM final (Cayman Chemical, Ann Arbor, MI, USA)
    - A438079, 25 µM final (Santa Cruz Biotechnology, Dallas, TX, USA)
    - MitoTEMPO, 500 µM final (Sigma Aldrich, St. Louis, MO, USA)
    - BAPTA-AM, 100 µM final (Tocris, Minneapolis, MN, USA)
- Culture vessels (flasks, plates, slides, etc)

Procedure:

1. Count and resuspend J774A.1 mouse macrophages to 10^6 cells/mL.
2. Seed cells according to vessel:
    a. 8-chamber slide (200 µL per well)
    b. 6-well plate (2 mL per well)
    c. T25 flask (3 mL per flask, bring to 5 mL)
    d. T75 flask (5 mL per flask, bring to 10 mL)
3. Incubate cells overnight.
4. The following day, exchange culture medium for fresh medium containing 1 µg/mL E. coli LPS. Leave appropriate non-treated controls.
5. Incubate cells for 4 hours to license the inflammasome components.
6. During the last 30 minutes of LPS priming, add appropriate NLRP3 inhibitors to final concentration listed in materials.

7. Treat cells with NLRP3-inducing agents by removing 50 µL to 1 mL of medium from each well (as appropriate), diluting the agent in the medium, and returning the medium to the well. Incubate for 30-60 minutes.
8. Assess inflammasome induction as appropriate (FLICA, Western blot, etc).

Protocol 2: FLICA Caspase-1 Assay for Inflammasome Imaging

Materials (in addition to standard J774A.1 cell culture materials):

- NLRP3-inducing chemicals (see Protocol 1)
- 150× FAM-YVAD-FMK (Immunochemistry Technologies, Bloomington, MN, USA)
- Hoechst 33342 (Immunochemistry Technologies, Bloomington, MN, USA)
- Ibidi 8-chamber µ-slide (Ibidi, Verona, WI, USA)
- 1× Phosphate-buffered saline (PBS)
- Formaldehyde solution (2% in PBS)
- Mounting medium

Equipment:

- Fluorescence-capable microscope (preferably confocal)

Procedure:

1. Count and resuspend J774A.1 mouse macrophages to 10^6 cells/mL.
2. Seed 200 µL of cell suspension in each well of an 8-chamber µ-slide and induce NLRP3 inflammasome activation according to Protocol 1. During the last 1 hour of priming add 1× FLICA reagent and 10 µg/mL Hoechst 33342.
3. Carefully remove medium from cells, avoiding aspirating potentially non-adhered cells.
4. Carefully wash each well 2× with PBS.
5. Replace medium with 2% formaldehyde solution and fix at room temperature for 10 minutes.
6. Carefully wash each well 1× with PBS.
7. Submerge each well in 200 µL mounting medium.
8. Image by fluorescence microscopy using standard DAPI and FITC excitation/emission spectra. If using confocal microscopy (preferred), prepare z-stacks throughout the imaging field and analyze by maximum intensity projection.

Protocol 3: Immunoprecipitation and Detection of phospho-Syk

Materials (in addition to standard J774A.1 cell culture materials):

- NLRP3-inducing chemicals (see Protocol 1)
- Protein A Dynabeads® (Life Technologies, Carlsbad, CA, USA)
- Antibodies (Santa Cruz Biotechnology, Dallas, TX, USA):
    - Syk (#SC-1077)
    - Phospho-Tyrosine (#SC-7020)
- BSA (Sigma Aldrich, St. Louis, MO, USA)
- RIPA lysis buffer (Santa Cruz Biotechnology, Dallas, TX, USA)
- 1× Tris-buffered saline (TBS)
- 1× TBS with 0.2% Tween (TBST)
- Phosphatase inhibitors (Biotools, Jupiter, FL, USA)
- Protease inhibitors (Pierce, Rockford, IL, USA)
- BCA assay (Pierce, Rockford, IL, USA)
- 6× denaturing Laemmli buffer (Alfa Aesar, Ward Hill, MA, USA)
- Standard Western Blotting reagents (membranes, buffers, etc)

Equipment:

- Magnetic bead stand
- Standard Western Blotting components

Procedure:

1. Prepare antibody binding solution (5% BSA in TBST) containing 1:50 Syk antibody (40 µL per condition)
2. Resuspend 1:4 volume Protein A Dynabeads® in antibody binding solution.
3. Rotate for 1-2 hours at room temperature.
4. Resuspend antibody-conjugated Protein A Dynabeads® in fresh 1× volume TBST (40 µL per condition).

5. Induce NLRP3 inflammasome activation according to Protocol 1 in 6-well plates with 1 mL treatment volumes.
6. Collect lysates by exposure to 1× RIPA with 1× protease and phosphatase inhibitors and pool with collected supernatants treated with 1× protease and phosphatase inhibitors.
7. Centrifuge at 14,000 *g*, transfer supernatants to new tubes.
8. Determine protein content by BCA assay.
9. Adjust protein content to approximately 1 mg in approximately 1.1 mL of medium with RIPA buffer. Normalize volumes and proteins across conditions.
10. Add 40 µL antibody-conjugated beads in protein samples. Supplement with BSA (10% final concentration).
11. Incubate overnight with rotation at 4 °C.
12. Wash beads 3× with cold RIPA buffer using a magnetic bead stand.
13. Transfer beads to new tubes.
14. Boil beads in 50 µL 1× Laemmli buffer at 95 °C for 10-15 minutes.
15. Separate sample by SDS-PAGE (12 µL per 15-well gel, 20 µL per 10 well gel).
16. Transfer proteins to membrane and block with 5% milk. Use TBS or TBST for all Western Blotting steps, as appropriate.
17. Develop Western Blot using the following primary antibody concentrations:
    a. Syk, 1:500
    b. Phospho-Tyrosine, 1:500
18. Divide Phospho-Tyrosine signal by total Syk signal for each condition.

Protocol 4: Preparation of proteins from NLRP3 inflammasome-induced cells

Materials (in addition to standard J774A.1 cell culture materials):

- NLRP3-inducing chemicals (see Protocol 1)
- StrataClean Resin (Agilent Technologies, Santa Clara, CA, USA)
- Protease inhibitors (Pierce, Rockford, IL, USA)
- RIPA lysis buffer (Pierce, Rockford, IL, USA)
- 6× denaturing Laemmli buffer (Alfa Aesar, Ward Hill, MA, USA)

Procedure:

1. Induce NLRP3 inflammasome activation according to Protocol 1.
2. Collect supernatants and supplement with 1× protease inhibitors. Keep on ice.
3. Add appropriately small volume of 1× hot Laemmli buffer to each well to collect protein lysates. Add only as much Laemmli as is necessary to completely cover all growth surface. (e.g., 100 µL in 6-well plates). Let sit for 15 minutes.
4. Scrape and transfer lysates to a microfuge tube and heat for 10 minutes at 95 °C.
5. Centrifuge supernatants at 5,000 *g* for 5 minutes at 4 °C. Transfer supernatants to new tube.
6. Add 1:100 StrataClean Resin to collected supernatants (e.g., 10 µL for 1 mL supernatant).
7. Rotate supernatants at 4 °C for 1 hour.
8. Centrifuge supernatant samples at 14,000 *g* for 3 minutes. Aspirate supernatant. Resuspend in 1× Laemmli (e.g., 50 µL per 10 µL StrataClean Resin). Vortex briefly, then heat at 95 °C for 10 minutes.
9. Store samples at -80 °C, or use for subsequent analysis (e.g., Western Blotting).